Studies on Electronic Properties of Organic Multi-Spin Systems

Yoshiaki Nakano

2005

Studies on Electronic Properties of Organic Multi-Spin Systems

Yoshiaki Nakano

2005

Preface

The rapid progress of molecular science in the latter half of twentieth century has enabled us to develop organic materials with the physical properties such as superconductivity and ferromagnetism which have been believed to exist only in inorganic materials before and, moreover, produced new research fields such as molecular conductor and molecule-based magnet. For example, the first organic ferromagnet was discovered in 1991. Nowadays, the relationship between molecular arrangements and physical properties on molecular assemblies has been elucidated to some extent.

The biggest advantage of organic molecules is to realize that the molecular structure can be perfectly defined as we desired by providing the desirable chemical modifications to the desirable positions of a molecule on the basis of organic synthetic methodologies, in striking contrast to the doping method utilized in the semiconductor industry, which obeys the statistical probability. In this context, thanks to the inevitable limit of the conventional downsizing in the silicon-based semiconductor device world, it has attracted considerable attention to realize a radically new class of electronics by replacing the present-day silicon-based electronic devices with the molecule-based devices making the most of the aforementioned advantage. Such an idea commenced already in 1970s, but the remarkable development of nanoscience and nanotechnology has sparked renewed interest in realization of molecule-based devices. On the other hand, we are now faced with the nascent research field known as spintronics, where an electron's spin as well as its electric charge is made use of to process information. Under the present circumstances, molecular (nano-)electronics and (nano-)spintronics are to be placed in the subject of molecular engineering.

The purpose of this thesis is to search for the possibility of controlling the spin electronic states of multi-spin systems through redox active moieties from the both experimental and theoretical points of view. This is closely related to realization of organic molecule-based spintronics. The author hopes that this thesis could contribute to the future development of science and technology of organic multi-spin systems.

Acknowledgments

The present thesis is the summary of the author's studies from 2000 to 2005 at the Department of Molecular Engineering, Graduate School of Engineering, Kyoto University.

The author would like to express his deepest gratitude to Professor Kazuyoshi Tanaka for his valuable suggestions, helpful discussions and continuous encouragement through the course of this study. He is deeply grateful to Dr. Akihiro Ito for his stimulating suggestions, informative discussions, and his kind encouragement in their collaborations.

The author wishes to express his sincere acknowledgments to Professor Tatsuhisa Kato of Josai University for his kind help in the pulsed ESR measurements.

The author also expresses his appreciation to Associate Professor Yohji Misaki for his valuable suggestions and encouragement. He wishes to thank Dr. Hiroyuki Fueno for his kind advices. Acknowledgment is also made to Associate Professor Tohru Sato for his valuable comments. He is indebted to Dr. Masashi Urabe, Mr. Takamasa Hirayama, Mr. Yohsuke Kohno, and Mr. Takuya Yagyu for their collaborations. He is also grateful to Dr. Haruhiro Ino, Mr. Hidehisa Ichiki, Mr. Tomotaka Tabuchi, Mr. Yuki Matsui, Mr. Haruya Ishizaki, Mr. Yasukazu Hirao, Mr. Tomohiro Yoshida, and Mr. Atsushi Yamamoto for their kind helps on performing his work. The author heartily thanks Dr. Kimihiro Susumu, Dr. Kazuyuki Takahashi, Dr. Takeshi Saito, Dr. Masateru Taniguchi, Dr. Takao Yoshii, and Dr. Shigekazu Ohmori for their continuous encouragement and kind experimental as well as theoretical advice. He also thanks other members of the research group of Professor Kazuyoshi Tanaka.

Finally, the author wishes to express his sincere gratitude to his friends and family, especially to his parents Akinori Nakano, Teruyo Nakano, and his grandmother the late

Tamako Kutsuna for their continuous support, understanding, and encouragement.

Yoshiaki Nakano

Kyoto, January 2005

Contents

General Introduction

1. Introduction

Magnetism is one of the phenomena which have been familiar to humankind since ancient times. The mineral lodestone, an oxide of iron that has the property of attracting iron objects, was known to the Greeks and Chinese. As is uncertain, it would seem that magnetite (lodestone, Fe_3O_4) was mined in the Magnesia region, Greece, and the word "magnet" in English has been derived from the Greek in which it means "magnesian stone". In Europe, the exploitation of magnets dates back to the period of great voyages where primitive compasses were devised on the basis of the property that a freely suspended magnet orients itself north-to-south, and they were put to practical use. In the present daily life, we are benefited immensely from various products equipped with magnets, and the discovery and development of novel, improved magnetic materials are still continuing all over the world. The modern world cannot work without magnets.

Generally speaking, when we hear the word "magnet", we usually imagine some kinds of metals, their alloys, or metal oxide materials. However, the intensive synthetic studies over the past forty years brought several families of molecule-based magnetic materials, which show several advantages unavailable in conventional

inorganic magnetic materials, e.g., low density, mechanical flexibility, tuning of properties by chemical modifications, solubility, transparency, and so on.

2. Magnetic Properties of Materials

The essence of magnetic materials is that an electron has characteristic angular momentum "spin", and these spins are represented by arrows, ↑ or ↓, in this thesis. The electron density, the distance and coupling between electron spins determine the magnetic behavior of all the materials. All the materials show a magnetic moment M upon application of a magnetic field H, so that the magnetic property is often measured in terms of the response (referred to as magnetic susceptibility χ) of the material to a magnet such as attraction or repulsion. The equation (1) holds upon the application of sufficiently weak magnetic field.

$$M = \chi H \tag{1}$$

As is often the case of organic materials, a magnet repels the substances without any unpaired electrons, and the magnetic susceptibility exhibits negative value, i.e., $\chi < 0$, being temperature independent. Such a magnetic property is called as diamagnetism.

If the unpaired electrons exist and the spins do not interact with each other in the material, they exhibit paramagnetic behavior (Figure 4(a)), where the magnetic susceptibility of the material decreases smoothly with increasing temperature T due to the thermal randomization of the magnetic moments, which obeys the Curie law (eq. 2):

$$\chi = \frac{C}{T} \tag{2}$$

where C stands for the Curie constant. The Curie constant is represented as follows:

$$C = \frac{N_A g^2 \mu_B^2 S(S+1)}{3k_B} \tag{3}$$

N_A being the Avogadro number, g the Landé g-factor, μ_B the Bohr magneton, S the spin quantum number, and k_B the Boltzmann constant. For an assembly of the species with $S = 1/2$ and $g = 2$ (e.g., organic monoradical), the Curie constant is

$$C = 0.375 \text{ emu K mol}^{-1} \tag{4}$$

As the spins get closer, they start interacting more with each other, leading to local parallel (↑↑) and antiparallel (↑↓) spin alignment. Two kinds of interaction causing these spin alignments are termed as ferromagnetic and antiferromagnetic interaction,

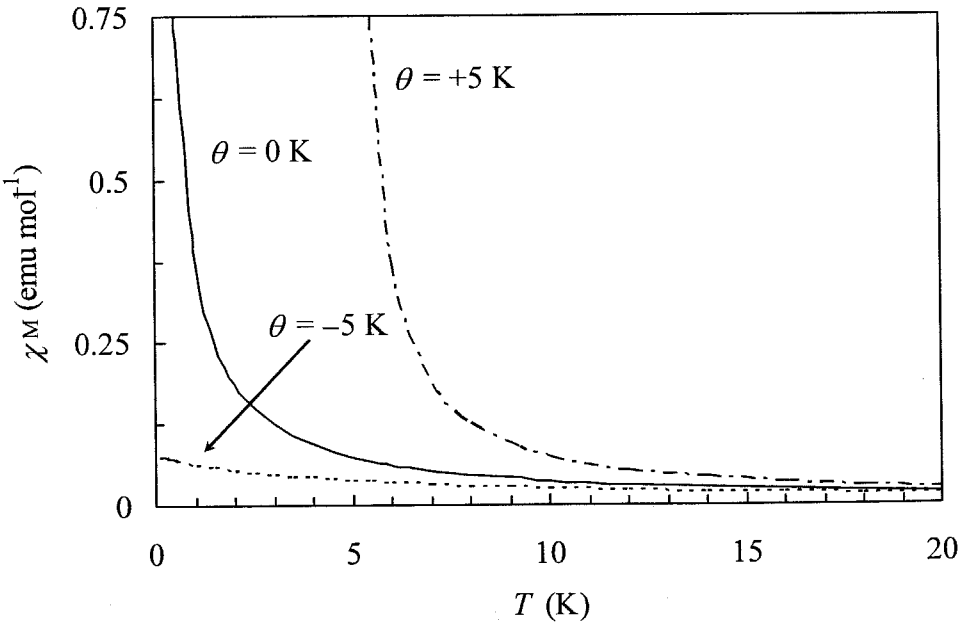

Figure 1. χ_M versus T plot for an assembly of 1 mol of species with C = 0.375 emu K mol^{-1} obeying the Curie–Weiss law.

respectively, enhancing/suppressing the magnetic susceptibility. As the result, the magnetic susceptibility of the material obeys the Curie–Weiss law (eq. 5),

$$\chi = \frac{C}{T - \theta} \tag{5}$$

where θ is denoted as the Weiss constant determined from the interception of the extrapolated slope of the χ^{-1} vs. T plot in the high temperature region. When the spins do not interact with each other (pure paramagnetic material), θ becomes zero, and the positive and negative θ indicate ferromagnetic and antiferromagnetic interactions, respectively. For $\theta > 0$, the Curie–Weiss law is obviously limited to the temperature range of $T > \theta$. Figures 1-3 show various plots of the Curie–Weiss law.

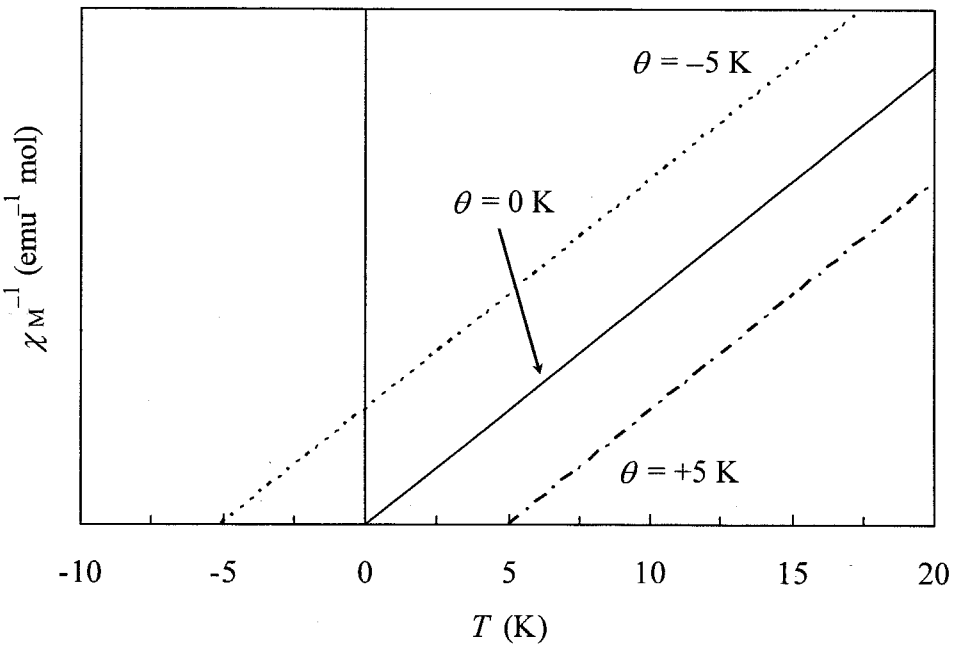

Figure 2. χ_M^{-1} versus T plot for an assembly of 1 mol of species obeying the Curie–Weiss law.

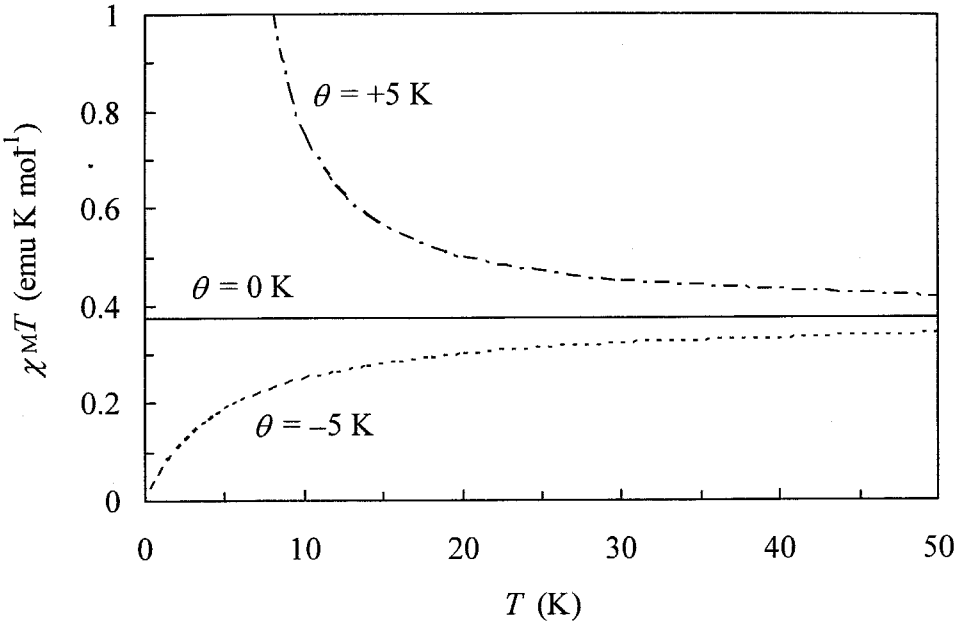

Figure 3. $\chi_M T$ versus T plot for an assembly of 1 mol of species with C = 0.375 emu K mol^{-1} obeying the Curie–Weiss law.

Although the Weiss constant θ implies the short-range magnetic interaction between the spins, there can be a case where a long-range order takes place among all the spins under a specific temperature. If the spins are ordered in parallel for long range at a temperature known as the Curie or the critical temperature T_C, the material shows bulk ferromagnetism, resulting in a ferromagnet (Figure 4(b)). The transition metals (e.g., Fe, T_C = 1043 K; Co, 1338 K; Ni, 631 K) show ferromagnetism at room temperature. On the contrary, the antiparallel ordering for long-range leads to antiferromagnetism (Figure 4(c)), in which the magnetic susceptibility exhibits the anisotropy below the Néel temperature T_N (e.g., MnO, T_N = 122K; Cr_2O_3, 331 K; FeS, 613 K; $FeCl_2$, 24 K). Ferrimagnetism arises from the antiferromagnetic interaction between the spins having different magnetic moments, resulting in the incomplete cancellation of the up (↑) and the down (↓) spins (Figure 4(d)). Of course, since the saturation magnetization M_s of ferrimagnets is smaller than the magnetization expected

from the completely parallel alignment of all the spins, the ferrimagnet can be discriminated from the ferromagnet. As the example of ferrimagnet, magnetite (Fe_3O_4) is well known, and its spontaneous magnetization is ascribed to the incomplete cancellation among the spins of $S = 5/2$ in Fe^{III} sites and $S = 2$ in Fe^{II} sites.

By applying a magnetic field to a ferromagnet or a ferrimagnet below T_C, magnetic domains in the material can be parallel-aligned, and the field dependence of magnetization exhibits a hysteresis loop with a coercive field H_{cr} and a remanent magnetization M_r, where the coercive field is defined at which the magnetization is reduced to zero and the remanent magnetization is the remaining magnetization at the zero field. With regard to the commercial utility of magnets, the above described properties, T_C, M_s, M_r, and H_{cr}, are most important to determine the utilization of those for, e.g., magnetic storage of data, ac motors, magnetic shielding, and so on.

Several magnetic phenomena are known except for the aforementioned magnetisms. The Dzyaloshinsky–Moriya interaction in addition to antiferromagnetic interaction makes the spins cant, leading to a net magnetization. This is called as canted antiferromagnetism or weak ferromagnetism (Figure 4(e)). A spin glass is observed in the system such as amorphous magnetic polymer, in which the short-range ordering of the spins occurs without the long-range ordering below a certain temperature T_g. Under such a situation, the spins point to all the directions like a paramagnet, but the spin orientations are fixed or change very slowly due to the local correlations in spin glass. Therefore, a spin glass is discriminated from a paramagnet, in which the spins change the directions instantaneously, that is, there is no barrier for the inversion of magnetization. The assembly of small ferromagnetic or ferrimagnetic particles exhibits superparamagnetism. Superparamagnetic materials do not show the magnetic ordering since the magnetic moment of each particle (a tiny magnet) is easily random-oriented by the thermal excitation. Metamagnetism is the field-dependent transition from the antiferromagnetic state to the ferromagnetic one.

All of the magnetic behaviors described in this section have also been discovered in the molecule-based magnets as well as in the traditional metal atom/ion-based magnets so far.

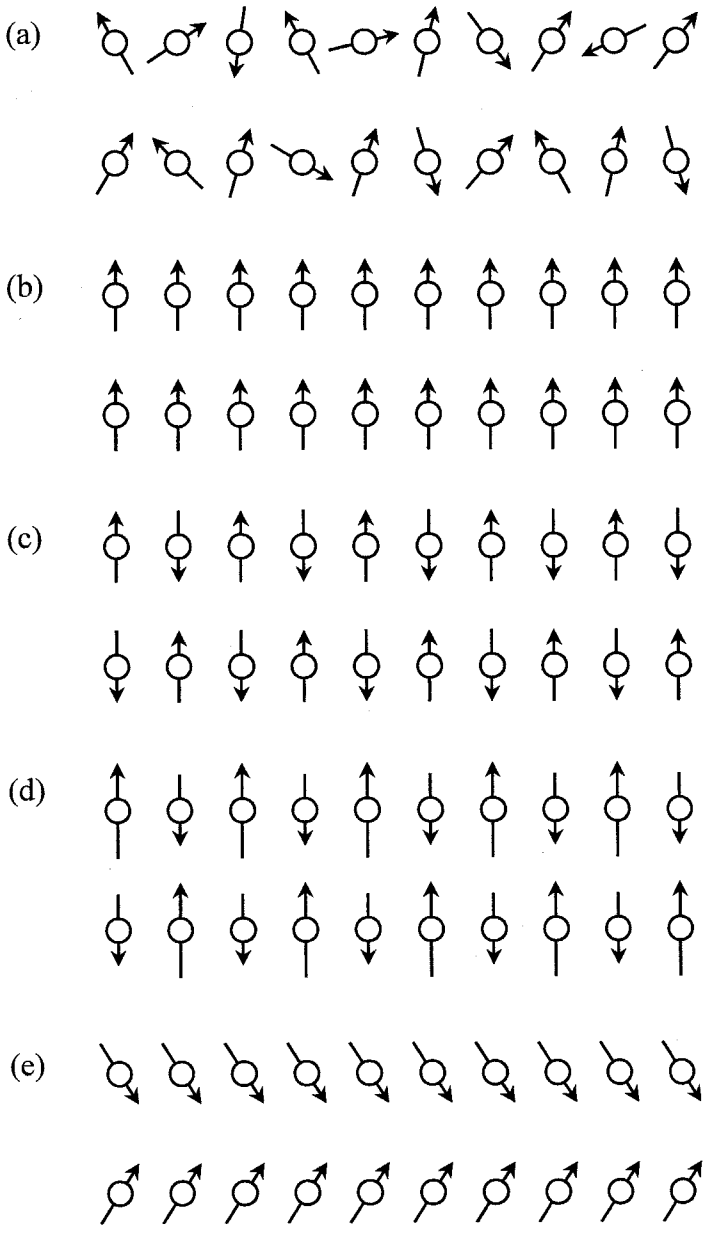

Figure 4. 2D illustration of various magnetic-ordering phenomena: (a) paramagnetism, (b) ferromagnetism, (c) antiferromagnetism, (d) ferrimagnetism, (e) canted antiferromagnetism.

3. Molecular Magnetic Materials

3.1 Organic radical crystal

Neutral organic radicals comprised of odd numbers of electrons, i.e., possessing an unpaired electron, are often highly chemically reactive. However, they can be isolated as more stable species by adding aromatic rings to delocalize the unpaired electron toward thermodynamic stabilization, or by introducing bulky substituents toward kinetic stabilization. Crystalline organic radicals, stabilized by the chemical modifications, usually exhibit paramagnetism at the high temperature region unless the dimerization of radicals can be lead to lose unpaired electrons. They usually show a very small negative Weiss constant θ, indicating weak antiferromagnetic interaction. This is because the intermolecular overlaps of the singly occupied molecular orbitals (SOMOs), in which the up spin (↑) exists in one SOMO and the down spin (↓) in the other, lead to make a bonding orbital. This is natural, considering that two hydrogen atoms form a covalent bond to become a diamagnetic hydrogen molecule. Although McConnell proposed the theoretical approach toward an organic ferromagnet in 1963 [1], the ferromagnetic interaction between organic radicals was not discovered in the radical crystals.

In spite of such a natural tendency, in 1969, Mukai *et al.* reported the intermolecular ferromagnetic interaction which follows the Curie–Weiss law with a positive Weiss constant (θ = 19 K) above 85 K in the crystal of 4-[[3,5-bis(1,1-dimethylethyl)-4-oxo-2,5-cyclohexadien-1-ylidene]methyl]-2,6-bis(1,1-dimethylethyl) phenoxy (known as galvinoxyl) [2]. However, below this temperature, the galvinoxyl exhibits a phase transition from paramagnetic state to diamagnetic or some remaining paramagnetic one, depending on a sample preparation. In later years, Awaga *et al.* prepared the mixed crystal between galvinoxyl and its closed-shell precursor, hydrogalvinoxyl, and investigated the origin of the intramolecular ferromagnetic

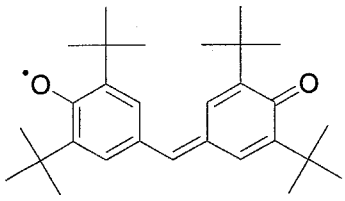

galvinoxyl

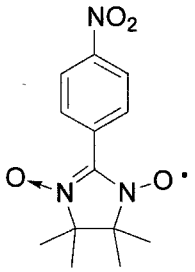

p-NPNN

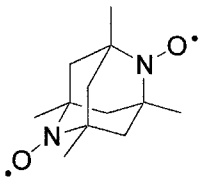

TMAO

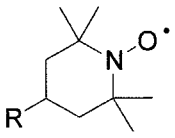

TEMPO

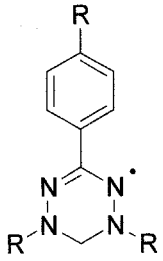

verdazyl

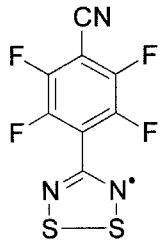

p-NCC_6F_4CNSSN

interaction [3]. In this course of study, the crucial conditions for achieving the intermolecular ferromagnetic interaction in the radical crystal are pointed out as follows: (1) large spin polarization in a radical molecule to stabilize the excited triplet states by the intermolecular charge transfer rather than the excited singlet states; (2) small SOMO–SOMO and large SOMO–NHOMO (or NLUMO) overlaps between the adjacent radicals, where NHOMO signifies the next-highest occupied molecular orbital and NLUMO the next-lowest unoccupied molecular orbital.

In 1991 Kinoshita *et al.* reported that the β-phase of *p*-nitrophenyl nitronyl nitroxide (*p*-NPNN) is the first purely organic ferromagnet with a T_C of 0.60 K [4]. After this discovery, many organic ferromagnets have been found not only in the nitronyl nitroxide family but also in the other neutral radical families such as TEMPO, verdazyl radicals, and so on. However, the T_C of radical crystals is usually very low, typically below 1 K, which is ascribed to the weak intermolecular magnetic interaction.

By Rassat *et al.*, even 1,3,5,7-tetramethyl-2,6-diazaadamantane-*N*,*N*'- dioxyl (TMAO) showed the T_C of no more than 1.48 K [5]. Recently, (4-cyanotetrafluorophenyl) dithiadiazolyl radical (*p*-NCC_6F_4CNSSN) was found to be a weak ferromagnet below 35 K, and the T_C could be elevated to 65 K by applying the hydrostatic pressure of 16 kbar [6]. These sulfur-containing radicals may exhibit even higher transition temperature.

3.2 High spin molecule and polymer

In 1950, Longuet-Higgins theoretically predicted that the alternant hydrocarbon has at least (*N*–2*T*) non-bonding molecular orbitals (NBMOs), where *N* is the number of the carbon atoms and *T* the maximum number of double bonds in possible resonance structures [7]. The alternant hydrocarbons with (*N*–2*T*) = 0 are called as Kekulé molecules, while the others non-Kekulé molecules with non-zero value of (*N*–2*T*). For example, *o*- and *p*-benzoquinodimethanes (*o*-QDM, *p*-QDM) are the Kekulé

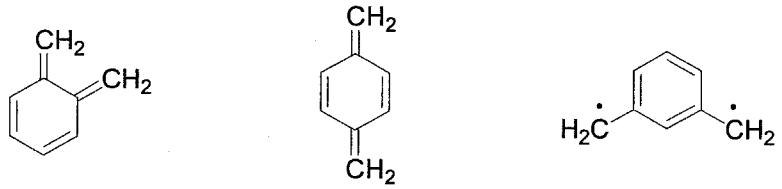

o-QDM $S = 0$ | *p*-QDM $S = 0$ | *m*-QDM $S = 1$

Figure 5. The prediction of ground states by the MO approach [7].

molecules, whereas *m*-benzoquinodimethane (*m*-QDM) is the non-Kekulé molecule with (*N*–2*T*) = 2. On the basis of the Hund's rule [8], it is predictable that each of *o*- and *p*-isomer with no degenerate NBMO has the spin quantum number of $S = 0$, i.e., the

ground singlet state, and *m*-isomer has $S = 1$, i.e., the ground triplet state, in which each of the two degenerate NBMOs are occupied with one electron (Figure 5). This theory based on the simple Hückel molecular orbital (MO) theory and the Hund's rule teaches us that the topological symmetry dominates the spin multiplicity of the alternant hydrocarbon.

Furthermore, taking the configuration interaction into account, Borden and Davidson introduced the concept of *disjoint* and *non-disjoint* to the non-Kekulé molecule in 1977 [9]. When one NBMO does not share the same atomic orbital with another NBMO, this electronic system is termed as *disjoint*, resulting in weak exchange interaction between the unpaired electrons. On the contrary, the electronic system with the atomic orbitals shared between the NBMOs is *non-disjoint*. In this situation, the parallel alignment of the two spins is stabilized due to the one-center Coulombic repulsion between the two unpaired electrons, leading to the ground triplet state. Tetramethyleneethane (TME) [10] and trimethylenemethane (TMM) [11] have been investigated from the viewpoint of *disjoint* and *non-disjoint*, respectively (Figure 6).

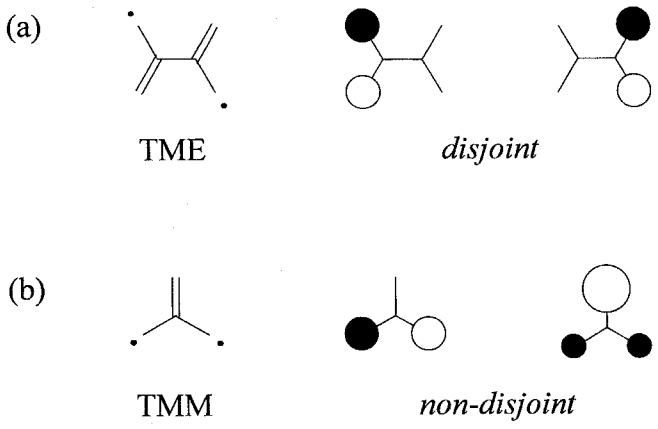

Figure 6. The NBMOs of (a) TME (*disjoint*) and (b) TMM (*non-disjoint*).

On the basis of the valence bond (VB) theory, Ovchinnikov proposed the following formula for the spin quantum number S of alternant hydrocarbons:

$$S = (n^* - n)/2 \tag{6}$$

where n^* and n are the numbers of starred and unstarred carbon atoms, respectively, when the carbon atoms in the alternant hydrocarbon are starred according to the following rule: (1) starred atoms are created as many as possible; (2) one starred carbon atom is never located adjacent to another starred one (Figure 7) [12].

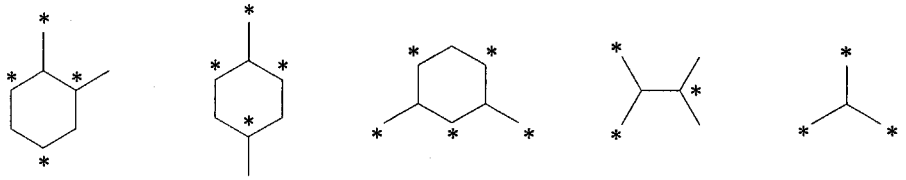

o-QDM	*p*-QDM	*m*-QDM	TME	TMM
$S = 0$	$S = 0$	$S = 1$	$S = 0$	$S = 1$

Figure 7. Prediction of the ground states by the VB approach [12].

Starting from the experimental confirmation of the quintet dicarbene by Ito [13] and the proposed model of high-spin polymers by Mataga [14], many organic high spin molecules and polymers have been designed and prepared on the basis of the above theory so far. In 2001, Rajca *et al.* prepared the polyarylmethyl radical exhibiting a huge magnetic moment of $S \approx 5000$ at low temperature, for which magnetic property can be categorized to be between insulating spin glasses and blocked superparamagnets [15]. Recently, Nishide *et al.* showed that a very weak magnetic signal of

nanometer-sized high-spin polyphenoxyl radical dispersed on a highly oriented pyrolytic graphite (HOPG) surface could effectively be detected by magnetic force microscopy (MFM) [16]. The atomic force microscopy (AFM) as well as MFM has been successfully used in that work to produce images of the obtained single-molecule-based magnetic quantum dots, which may be important for information storage and quantum computing applications.

3.3 Charge transfer complex

The ferromagnetic spin alignment on the charge transfer (CT) complex was described by McConnell in 1967 [17]. This McConnell's model has been developed by Breslow [18], Torrance [19], and Wudl [20] thereafter.

After the discovery of the molecular metamagnet, $[Fe^{III}Cp^*_2]^+[TCNQ]^-$ (Cp^* = pentamethylcyclopentadienide; TCNQ = 7,7,8,8-tetracyano-*p*-quinodimethane) [21], Miller and Epstein reported that the CT complex, $[Fe^{III}Cp^*_2]^+[TCNE]^-$ (TCNE = tetracyanoethylene), is the first ferromagnet (T_C = 4.8 K) with the spins accommodated in p-orbitals [22]. The magnetic properties for this class of CT complexes have been systematically investigated [23]. Furthermore, these authors discovered that the reaction of either $V(C_6H_6)_2$ or $V(CO)_6$ with TCNE forms $V(TCNE)_x{\cdot}y(CH_2Cl_2)$ ($x \sim 2$; $y \sim 1/2$), which is a bulk ferrimagnet below its thermal decomposition temperature of 350 K with a T_C of *ca.* 400 K [24]. This is the first example of a molecule-based ferrimagnet with a critical temperature exceeding the room temperature.

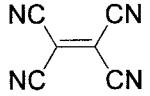

TCNE

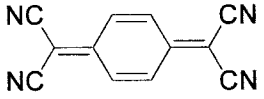

TCNQ

Ferromagnetism was also discovered for the purely organic CT complex, tetrakis(dimethylamino)ethylene–C_{60} (TDAE–C_{60}), with a relatively high T_C of 16 K [25]. However, the interpretation of ferromagnetism was controversial: itinerant ferromagnetism [25], spin glass [26], superparamagnetic [27], 3D Heisenberg ferromagnetism [28], and non-magnetic [29]. It was confirmed that this problem is related with the orientation of the C_{60} molecules in TDAE–C_{60} [30].

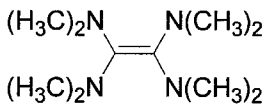

TDAE

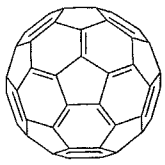

C_{60}

3.4 Photo- and redox-tunable magnetic properties

The creation of optically controllable magnetic materials is one of the most important subjects because of the future applications for optical memory. In the transition metal complexes [31], the light-induced excited spin state trapping (LIESST) for spin-crossover complexes [32] and the photo-induced magnetization in Prussian blue analogues [33] have been demonstrated to date.

Recently, several photo-magnetic properties have also been reported in organic spin systems. Matsuda *et al.* have reported that the photo-switching of intramolecular magnetic interaction has been achieved by inserting a photochromic 1,2-bis(3-thienyl) ethene or 1,2-bis(2-thienyl)ethene between two radical moieties (Figure 8) [34]. It

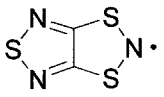

TTTA

was discovered by Awaga *et al.* that the crystal of 1,3,5-trithia-2,4,6-triazapentalenyl (TTTA) exhibits the paramagnetic regular stack at the high temperature region while the diamagnetic dimerized stack at the low temperature region. The temperature-dependent magnetic susceptibility of TTTA shows the hysteresis, i.e., $T_C\downarrow$ = 230 K and $T_C\uparrow$= 305 K, resulting in magnetic bistability at room temperature [35]. Furthermore, the photo-switching of TTTA has also been reported [36].

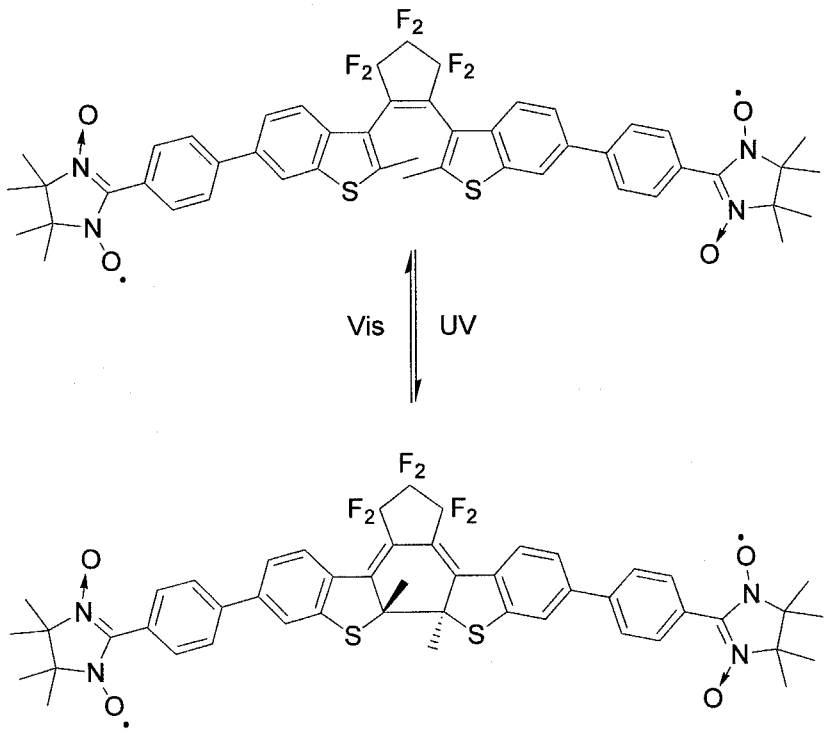

Figure 8. Photo-switching of the intramolecular magnetic interaction [34f].

The hybrid systems between paramagnetic metal ions and carbenes generated by photolysis [37] have also been investigated by Koga *et al.* In these systems, the reaction of bis(hexafluoroacetylacetonato)copper with diazodi(4-pyridyl)methane affords the one-dimensional chain complex, which can make ferromagnetic chain after

the photolysis of diazo groups [37b]. This type of magnetic material is expected to work as a photo-magnetic device in which only the illuminated part can be a magnet.

On the other hand, the redox-control of spin state based on the π-topological symmetry of NBMOs has been investigated [38]. Ito *et al.* demonstrated by pulsed ESR spectroscopy that the mono-, di-, and tricationic species of *N*,*N*,*N*',*N*',*N*'',*N*''-hexakis[4-(dimethylamino)phenyl]-1,3,5-benzentriamine have the doublet, triplet, and quartet spin multiplicities, respectively [38d]. The redox-switching of the spin distribution, termed as redox-based spin diversity [39], was also reported by Morita *et al.* In Chapters 1-3, the author will discuss about the redox-switching of intramolecular magnetic interaction on the basis of structural change of tetraphenylethylene.

3.5 Magnetic conductor

The itinerant magnetism originated from the magnetic interaction between conduction electrons and localized spins is widely known among the inorganic magnetic materials, in which s- and d-electrons behave as conduction electrons and localized spins, respectively. These magnetic interactions in which the localized spins indirectly interact with each other through conduction electrons are called as the Ruderman-Kittel-Kasuya-Yoshida (RKKY) interaction [40] (e.g., the origin of ferromagnetism in iron) and the double-exchange interaction [41] (e.g., in $La_{1-x}Sr_xMnO_3$). In the molecular systems, d-π systems have been constructed by the combination of paramagnetic metal ions bearing localized d-electrons with organic conductors in which π-electrons play a role of conduction electrons. Bis(ethylenedithio)tetrathiafulvalene (BEDT-TTF) and bis(ethylenedithio)tetraselena fulvalene (BETS) have been well known as donors in the field of molecular conductors, and the CT complexes of these donors exhibit metallic and superconducting properties. The interesting examples of d-π systems including BEDT-TTF and BETS are shown as follows.

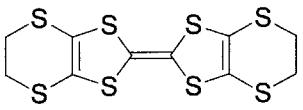

BEDT-TTF

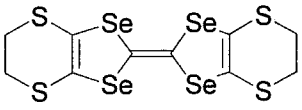

BETS

Day *et al.* reported that $(BEDT\text{-}TTF)_3CuCl_4{\cdot}H_2O$ shows the metallic behavior without transition to the superconducting state and the short-range ferromagnetic interaction at low temperatures. Since the distance between the Cu ions are greater than 8.5 Å, this behavior seems to be described as the indirect magnetic interaction through conduction electrons [42].

Even the long-range magnetic order was discovered by Coronado *et al.*, in which the molecule-based layered compound β-$(BEDT\text{-}TTF)_3[Mn^{II}Cr^{III}(ox)_3]$, where ox is the oxalate dianion $(C_2O_4)^{2-}$, was prepared by the electrocrystallization to exhibit coexistence of ferromagnetism and metallic conductivity for the first time [43]. The organic layers of BEDT-TTF cations alternate with the 2D honeycomb layers of $[Mn^{II}Cr^{III}(ox)_3]^-$ to behave as a ferromagnet with T_C of 5.5 K and exhibit metallic conductivity down to 0.3 K, without becoming superconductor. Although the negative magnetoresistance was observed by applying a magnetic field perpendicular to the layers below about 10 K, ferromagnetic and conducting lattices seem to be quasi-independent.

The isostructural salts, λ-$(BETS)_2GaCl_4$ with diamagnetic anion and λ-$(BETS)_2FeCl_4$ with paramagnetic anion (Fe^{III}, S = 5/2), were found to exhibit the quite different properties by Kobayashi *et al.* [44]. Although λ-$(BETS)_2GaCl_4$ shows metallic behavior with a superconducting transition at *ca.* 6 K, λ-$(BETS)_2FeCl_4$ exhibits a metal to insulator (MI) transition ascribed to the antiferromagnetic ordering of the spins in Fe^{III} ions. However, by applying a magnetic field, the antiferromagnetic insulating phase is destroyed and, hence, the superconductivity appears as field-induced

superconductivity [42e, f].

As the example of purely organic magnetic conductor, there have been attempts by Sugawara *et al.*, in which the electron donors substituted by organic radical, called as spin-polarized donors, have been exploited to built molecular magnetic conductors [45], but every attempt for the bulk spin alignment has met with failure so far. On the other hand, they have proposed that the spin-polarized donor would serve as the spin-polarized molecular wire [46] and reported that localized spins of the radical moieties can interact with conduction electrons in the gold nano-particles chemisorbed by the diphenyl disulfide compound bearing nitronyl nitroxide radicals (DSPN-hex) [47]. However, these results are still unestablished at the present, and further reports have to be waited for. In Chapters 5 and 6, the author will discuss about the organic spin system in which localized and delocalized spins coexist.

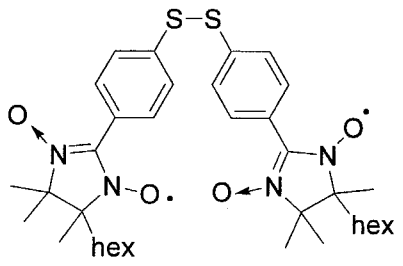

DSPN-hex, hex = hexyl group

3.6 Single-molecule magnet

At the beginning of the 1990s, it was found by Gatteschi *et al.* that the compound $[Mn_{12}O_{12}(CH_3COO)_{16}(H_2O)_4]\cdot 4H_2O\cdot 2CH_3COOH$ (Mn12ac) with a $S = 10$ ground state exhibits the slow relaxation time of the magnetization [48], being of the order of a few months at 2 K and 50 years at 1.5 K [48d, e]. That is to say, a single Mn12ac

molecule becomes a small magnet, in the sense that if magnetized by an applied field, it retains the magnetization for days at low temperature. Indeed, the field-dependent magnetization shows the hysteresis, which is one of the requirements for storing a piece of information in a single molecule. Therefore, Mn12ac behaves like a classical magnet. More interestingly, Mn12ac also shows large quantum effects. In fact, the quantum tunneling of magnetization was observed as characteristic step-like structures in the magnetic hysteresis loop [48d]. The origin of the steps is ascribed to two relaxation mechanisms, i.e., the thermally activated and quantum tunnelings. Nowadays, such molecules are often called "single-molecule magnets" (SMMs), and Mn12ac is the first SMM. Moreover, Caneschi *et al.* has reported the first experimental evidence of single-chain magnet (SCM) corresponding to the Glauber's theoretical prediction [49] in the complex of bis(hexafluoroacetylacetonato)cobalt ($Co(hfac)_2$) with 4'-methoxyphenyl-4,4,5,5-tetramethylimidazoline-1-oxyl-3-oxide (NITPhOMe), [$Co(hfac)_2$(NITPhOMe)], which has a spiral one-dimensional chain structure [50]. After this discovery, a different research group also reported the SCM [51]. On the other hand, further attempts have also been made to organize the SMMs into layers in which it would be possible to address individual molecules for the information storage [52]. As a new attempt, the SMMs are about to be applied to quantum computation by implementing Grover's algorithm [53].

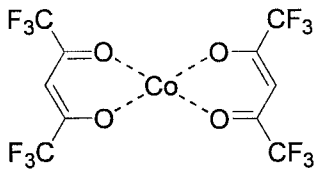

$Co(hfac)_2$

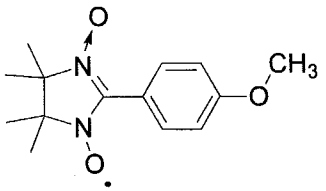

NITPhOMe

4. Survey of This Thesis

In this thesis, the syntheses, the electronic properties, and the theoretical analyses of several spin systems based on the π-conjugated organic molecules are presented to explore the idea of novel organic spin systems.

In Chapter 1, tetraarylethylene having two *tert*-butylnitroxide, 1,2-bis[4-(*N*-*tert*-butylaminoxyl)phenyl]-1,2-bis[4-{*N*,*N*-bis(4-methoxyphenyl)amino} phenyl]ethylene, has been synthesized through the McMurry coupling reaction with a low-valent titanium reagent. The electrochemical property of this compound has been investigated by cyclic voltammetry. Moreover, it has been confirmed that the intramolecular magnetic interaction can drastically change through the chemical oxidation and reduction by the ESR spectroscopy, and the redox-switching is reversible by the electrochemical UV–Vis–NIR spectroscopy.

In Chapter 2, 1,2-bis[3-(*N*-*tert*-butylaminoxyl)phenyl]-1,2-bis[4-{*N*,*N*-bis(4-methoxyphenyl)amino}phenyl]ethylene as a structural isomer of the compound in Chapter 1 has been investigated by means of the electrochemistry and ESR spectroscopy. It has been suggested that the electrochemical behavior is characterized by two closely spaced consecutive one-electron transfers in contrast to the compound in Chapter 1. The ESR spectroscopy makes it clear that the target molecule can also change the intramolecular magnetic interaction by the chemical oxidation as shown in Chapter 1.

In Chapter 3, the model compound of 1,2-bis[*x*-(*N*-*tert*-butylaminoxyl)phenyl]-1,2-bis[4-{*N*,*N*-bis(4-methoxyphenyl)amino}phenyl]ethylene (x = 3 or 4) has theoretically been studied on the basis of the hybrid Hartree–Fock (HF)/density functional theory (DFT). It has been shown not only that the molecular structure and the intramolecular magnetic interaction of dicationic tetraarylethylene with two nitroxide groups can completely be changed in comparison with the neutral state for the *para*-nitroxyl substituted isomer but also that the electronic structures are influenced by

the substituted position of the nitroxyl groups.

In Chapter 4, the syntheses and the electrochemical and the magnetic properties of triradical, tris[4-(1-oxyl-3-oxide-4,4,5,5-tetramethylimidazolin-2-yl)phenyl]amine, and diradical, *N,N*-bis[4-(1-oxyl-3-oxide-4,4,5,5-tetramethylimidazolin-2-yl)phenyl]-4-methoxyphenylamine have been investigated. It has been found that the neutral radicals in the solid states show weak antiferromagnetic interactions by the magnetic susceptibility measurements. However, the electrochemical and ESR measurements have shown the nitronyl nitroxide moieties have the lower oxidation potentials than the core triphenylamine moieties even in the case of electron-donating methoxy-group-substitution.

In Chapter 5, the synthesis and the electronic properties of *N,N'*-bis[3-*tert*-butyl-5-(*N*-*tert*-butyl-*N*-oxylamino)phenyl]-*N,N'*-dimethyl-*p*-phenylene diamine have been investigated. The analysis of inter valence CT (IVCT) band in the cationic state by UV-Vis-NIR spectroscopy and the determination of spin-multiplicity by cw- and pulsed ESR demonstrates the first example of ferromagnetic spin alignment mediated by the mixed-valence state for multi-spin organic molecule. The present triradical cation is also considered to be novel from the point of view that the localized spin and the delocalized spin coexist.

In Chapter 6, the models of *p*-phenylenediamine with *tert*-butylnitroxide radicals, *N,N'*-bis[3-*tert*-butyl-5-(*N*-*tert*-butyl-*N*-oxylamino)phenyl]-*N,N'*-dimethyl-*p*-phenylene diamine, and *p*-phenylenediamine with nitronyl nitroxide radicals, *N,N'*-bis[4-(1-oxyl-3-oxide-4,4,5,5-tetramethylimidazolin-2-yl)phenyl]-*N,N'*-dimethyl-*p*-phenylenediamine, have theoretically been studied on the basis of quantum chemical calculations. It has been predicted that the cationic *p*-phenylenediamine derivatives with radical substituents have the ground quartet states while the singlet and triplet states are nearly degenerated for those in the neutral state. Moreover, it has been shown that the SOMO on the *p*-phenylenediamine moiety tend to intrude into the outside aryl groups in

the case of nitronyl nitroxide substitution as compared with nitroxide substitution.

References

[1] H.M. McConnell, J. Chem. Phys. 39 (1963) 1910.

[2] (a) K. Mukai, H. Nishiguchi, Y. Deguchi, J. Phys. Soc. Jpn. 23 (1967) 125; (b) K. Mukai, Bull. Chem. Soc. Jpn. 42 (1969) 40.

[3] (a) K. Awaga, T. Sugano, M. Kinoshita, Solid State Commun. 57 (1986) 453; (b) K. Awaga, T. Sugano, M. Kinoshita, J. Chem. Phys. 85 (1986) 2211; (c) K. Awaga, T. Sugano, M. Kinoshita, Chem. Phys. Lett. 128 (1986) 587; (d) K. Awaga, T. Sugano, M. Kinoshita, J. Chem. Phys. 87 (1987) 3062; (e) K. Awaga, T. Sugano, M. Kinoshita, Chem. Phys. Lett. 141 (1987) 540; (f) K. Awaga, T. Sugano, M. Kinoshita, Synth. Met. 27 (1988) B631; (g) T. Sugano, Polyhedron 20 (2001) 1285.

[4] (a) M. Tamura, Y. Nakazawa, D. Shiomi, K. Nozawa, Y. Hosokoshi, M. Ishikawa, M. Takahashi, M. Kinoshita, Chem. Phys. Lett. 186 (1991) 401; (b) Y. Nakazawa, M. Tamura, N. Shirakawa, D. Shiomi, M. Takahashi, M. Kinoshita, M. Ishikawa, Phys. Rev. B 46 (1992) 8906; (c) M. Kinoshita, Synth. Met. 56 (1993) 3279; (d) M. Kinoshita, Physica B 213/214 (1995) 257; (e) K. Awaga, Y. Maruyama, Chem. Phys. Lett. 158 (1989) 556; (f) Y.J. Uemura, G. M. Luke, Synth. Met. 56 (1993) 2845; (g) L.P. Le, A. Keren, G. M. Luke, W.D. Wu, Y.J. Uemura, M. Tamura, M. Ishikawa, M. Kinoshita, Chem. Phys. Lett. 206 (1993) 405; (h) K. Oshima, H. Kawanoue, Y. Haibara, H. Yamazaki, K. Awaga, M. Tamura, M. Ishikawa, M. Kinoshita, Synth. Met. 71 (1995) 1821; (i) K. Oshima, Y. Haibara, H. Yamazaki, K. Awaga, M. Tamura, M. Kinoshita, Mol. Cryst. Liq. Cryst. 271 (1995) 29; (j) A. Zheludev, E. Ressouche, J. Schweizer, P. Turek, M. Wan, H. Wang, Solid State Commun. 90 (1994) 233; (k) K. Takeda, K. Konishi, M. Tamura, M. Kinoshita, J. Mag. Mag. Mater. 140-144 (1995) 1451; (l) K. Takeda, K. Konishi, M. Tamura,

M. Kinoshita, Mol. Cryst. Liq. Cryst. 273 (1995) 57; (m) K. Takeda, K. Konishi, M. Tamura, M. Kinoshita, Phys. Rev. B 53 (1996) 3374.

[5] R. Chiarell, M.A. Novak, A. Rassat, J.L. Tholence, Nature 363 (1993) 147.

[6] (a) A.J. Banister, N. Bricklebank, I. Lavender, J.M. Rawson, C.I. Gregory, B.K. Tanner, W. Clegg, M.R.J. Elsegood, F. Palacio, Angew. Chem. Int. Ed. Engl. 35 (1996) 2533; (b) F. Palacio, G. Antorrena, M. Gastro, R. Burriel, J.M. Rawson, J.N.B. Smith, N. Bricklebank, J. Novoa, C. Ritter, Phys. Rev. Lett. 79 (1997) 2336; (c) M. Mito, T. Kawae, K. Takeda, S. Takagi, Y. Matsushita, H. Deguchi, J.M. Rawson, F. Palacio, Polyhedron 20 (2000) 1509; (d) F.L. Pratt, A.E. Goeta, F. Palacio, J.M. Rawson, J.N.B. Smith, Physica B 289 (2000) 119; (e) J. Luzon, J. Campo, F. Palacio, G.J. McIntyre, A.E. Goeta, E. Ressouche, C.M. Pask, J.M. Rawson, Physica B 335 (2003) 1; (f) G. Antorrena, J.E. Davies, M. Hartley, F. Palacio, J.M. Rawson, J.N.B. Smith, A. Steiner, Chem. Commun. (1999) 1393; (g) N. Feeder, R.J. Less, J.M. Rawson, P. Oliete, F. Palacio, Chem. Commun. (2000) 2449.

[7] H.C. Longuet-Higgins, J. Chem. Phys. 19 (1950) 265.

[8] F. Hund, Z. Phys. 51 (1928) 759.

[9] (a) W.T. Borden, E.R. Davidson, J. Am. Chem. Soc. 99 (1977) 4587; (b) W.T. Borden, E.R. Davidson, Acc. Chem. Res. 14 (1981) 69; (c) D.A. Dougherty, Acc. Chem. Res. 24 (1991) 88; (d) W.T. Borden, H. Iwamura, J.A. Berson, Acc. Chem. Res. 27 (1994) 109.

[10] (a) P. Du, W.T. Borden, J. Am. Chem. Soc. 109 (1987) 930; (b) P. Nachtigall, K.D. Jordan, J. Am. Chem. Soc. 114 (1992) 4743; (c) P. Nachtigall, K.D. Jordan, J. Am. Chem. Soc. 115 (1993) 270; (d) J.J. Nash, P. Dowd, K.D. Jordan, J. Am. Chem. Soc. 114 (1992) 10071.

[11] (a) W.T. Borden, J. Am. Chem. Soc. 98 (1976) 2695; (b) E.R. Davidson, W.T. Borden, J. Chem. Phys. 64 (1976) 633; (c) E.R. Davidson, W.T. Borden, J. Am. Chem. Soc. 99 (1977) 2053.

[12] A.A. Ovchinnikov, Theor. Chim. Acta 47 (1978) 297.

[13] K. Ito, Chem. Phys. Lett. 1 (1967) 235.

[14] N. Mataga, Theor. Chim. Acta 10 (1968) 372.

[15] (a) J. Wongsriratanakul, S. Rajca, Science 294 (2001) 1503; (b) A. Rajca, Chem. Eur. J. 8 (2002) 4834.

[16] H. Nishide, T. Ozawa, M. Miyasaka, E. Tsuchida, J. Am. Chem. Soc. 123 (2001) 5942.

[17] H.M. McConnell, Proc. Robert A. Welch Found. Conf. Chem. Res. 11 (1967) 144.

[18] (a) R. Breslow, B. Juan, R.Q. Kluttz, C.Z. Xia, Tetrahedron 38 (1982) 863; (b) R. Breslow, Pure Appl. Chem. 54 (1982) 927; (c) J. Thomaides, P. Maslak, R. Breslow, J. Am. Chem. Soc. 110 (1988) 3970.

[19] J.B. Torrance, I. Bagus, A.I. Nazzal, S. Parkin, J. Appl. Phys. 63 (1988) 2962.

[20] E. Dorman, M.J. Nowak, K. Williams, R.G. Angus, F. Wudl, J. Am. Chem. Soc. 109 (1987) 2594.

[21] G.A. Candela, L. Swartzendruber, J.S. Miller, M.J. Rice, J. Am. Chem. Soc. 101 (1979) 2755.

[22] (a) J.S. Miller, J.C. Calabrese, H. Rommelmann, S. Chittapeddi, J.H. Zhang, W.M. Reiff, J. Am. Chem. Soc. 109 (1987) 769; (b) S. Chittapeddi, K.R. Cromack, J.S. Miller, A.J. Epstein, Phys. Rev. Lett. 58 (1987) 2695.

[23] (a) F. Zuo, A.J. Epstein, C. Vazquez, R.S. McLean, J.S. Miller, J. Mater. Chem.3 (1993) 215; (b) G.T. Yee, J.M. Manriquez, D.A. Dixon, R.S. McLean, D.M. Groski, R.B. Flippen, K.S. Narayan, A.J. Epstein, J.S. Miller, Adv. Mater. 3

(1991) 309; (c) W.E. Broderick, D.M. Eichhorn, X. Liu, P.J. Toscano, S.M. Owens, B.M. Hoffman, J. Am. Chem. Soc. 117 (1995) 3641; (d) W.E. Broderick, J.A. Thompson, E.P. Day, B.M. Hoffman, Science 249 (1990) 401; (e) W.E. Broderick, B.M. Hoffman, J. Am. Chem. Soc. 113 (1991) 6334; (f) J.S. Miller, A.J. Epstein, W.M. Reiff, Science 240 (1988) 40; (g) J.S. Miller, A.J. Epstein, W.M. Reiff, Acc. Chem. Res. 21 (1988) 144; (h) J.S. Miller, A.J. Epstein, W.M. Reiff, Chem. Rev. 88 (1988) 201

[24] (a) J.M. Manriqez, G.T. Yee, R.S. McLean, A.J. Epstein, J.S. Miller, Science 252 (1991) 1415; (b) P. Zhou, B.G. Morin, J.S. Miller, A.J. Epstein, Phys. Rev. B 48 (1993) 1325; (c) P. Zhou, S.M. Long, J.S. Miller, A.J. Epstein, Phys. Lett. A 181 (1993) 71; (d) G. Du, J. Joo, A.J. Epstein, J.S. Miller, J. Appl. Phys. 73 (1993) 6566; (e) J.S. Miller, A.J. Epstein, Coord. Chem. Rev. 206-207 (2000) 651; (f) J.S. Miller, Inorg. Chem. 39 (2000) 4392.

[25] P.-M. Allemand, K.C. Khemani. A. Koch, F. Wudl, K. Holczer, S. Donovan, G. Gruner, J.D. Thompson, Science 253 (1991) 301.

[26] (a) P. Cevc, R. Blinc, V. Erzen, D. Arcon, B. Zalar, D. Mihailovic, P. Venturini, Solid State Commun. 90 (1994) 543; (b) R. Blinc, P. Cevc, D. Aron, D. Mihailovic, P. Venturini, Phys. Rev. B 50 (1994) 13051.

[27] K. Tanaka, A.A. Zakhidov. K. Yoshizawa, K. Okahara, T. Yamabe, K. Yakushi, K. Kikuchi, S. Suzuki, I. Ikemoto, Y. Achiba, Phys. Rev. B 47 (1993) 7554.

[28] D. Aron, P. Cevc, A. Omerzu, R. Blinc, Phys. Rev. Lett. 80 (1998) 1529.

[29] T. Kambe, Y. Nogami, K. Oshima, Phys. Rev. B 61 (2000) R862.

[30] B. Narymbetov, A. Omerzu, V.V. Kabanov, M. Tokumoto, H. Kobayashi, D. Mihailovic, Nature 407 (2000) 883.

[31] O. Sato, S. Hayami, Y. Einaga, Z.-Z. Gu, Bull. Chem. Soc. Jpn. 76 (2003) 443.

[32] (a) S. Decurtins, P. Gütlich, C.P. Köhler, H. Spiering, A. Hauser, Chem. Phys. Lett. 105 (1984) 1; (b) S. Hayami, Z.-Z. Gu, M. Shiro , Y. Einaga, A. Fujishima, O. Sato, J. Am. Chem. Soc. 122 (2000) 7126; (c) S. Hayami, Z.-Z. Gu, M. Shiro , Y. Einaga, A. Fujishima, O. Sato, J. Am. Chem. Soc. 123 (2001) 11644; (d) G. Juhasz, S. Hayami, O. Sato, Y. Maeda, Chem. Phys. Lett. 364 (2002) 164; (e) S. Hayami, Z.-Z. Gu, Y. Einaga, Y. Kobayashi, Y. Ishikawa, Y. Yamada, A. Fujishima, O. Sato, Inorg. Chem. 40 (2001) 3240; (f) F. Rentz, H. Oshio, V. Ksenofontov, M. Waldeck, H. Spiering, P. Gütlich, Angew. Chem. Int. Ed. Engl. 39 (2000) 3699; (g) E. Breuning, M. Ruben, J.M. Lehn, F. Renz, Y. Garcia, V. Ksenofontov, P. Gütlich, E. Wegelius, K. Rissanen, Angew. Chem. Int. Ed. Engl. 39 (2000) 2504.

[33] (a) O. Sato, T. Iyoda, A. Fujishima, K. Hashimoto, Science 272 (1996) 704; (b) O. Sato, Y. Einaga, T. Iyoda, A. Fujishima, K. Hashimoto, J. Electrochem. Soc. 144 (1997) L11; (c) O. Sato, Y. Einaga, T. Iyoda, A. Fujishima, K. Hashimoto, J. Phys. Chem. B 101 (1997) 3903; (d) Y. Einaga, Z.-Z. Gu, Y. Kobayashi, O. Sato, T. Iyoda, F. Ambe, K. Hashimoto, A. Fujishima, Hyperfine Interactions 116 (1998) 159; (e) T. Yokoyama, T. Ohta, O. Sato, K. Hashimoto, Phys. Rev. B 58 (1998) 8257; (f) O. Sato, Y. Einaga, T. Iyoda, A. Fujishima, K. Hashimoto, Inorg. Chem. 38 (1999) 4405; (g) T. Yokoyama, M. Kiguchi, T. Ohta, O. Sato, Y. Einaga, K. Hashimoto, Phys. Rev. B 60 (1999) 9340; (h) N. Shimamoto, S. Ohkoshi, O. Sato, K. Hoshimoto, Mol. Cryst. Liq. Cryst. 344 (2000) 95; (i) N. Shimamoto, S. Ohkoshi, O. Sato, K. Hoshimoto, Inorg. Chem. 41 (2002) 678; (j) H.-W. Liu, K. Matsuda, Z.-Z. Gu, K. Takahashi, A.-L. Cui, R. Nakajima, A. Fujishima, O. Sato, Phys. Rev. Lett. 90 (2003) 167403-1.

[34] (a) K. Matsuda, M. Irie, Chem. Lett. (2000) 16; (b) K. Matsuda, M. Irie, Tetrahedron. Lett. 41 (2000) 2577; (c) K. Matsuda, M. Irie, J. Am. Chem. Soc.

122 (2000) 7195; (d) K. Matsuda, M. Irie, J. Am. Chem. Soc. 122 (2000) 8309; (e) K. Matsuda, M. Matsuo, M. Irie, Chem. Lett. 436 (2001);(f) K. Matsuda, M. Irie, Chem. Eur. J. 7 (2001) 3466; (g) K. Matsuda, M. Irie, J. Am. Chem. Soc. 123 (2001) 9896; (h) K. Matsuda, M. Matsuo, M. Irie, J. Org. Chem. 66 (2001) 8799; (i) K. Matsuda, M. Matsuo, S. Mizoguti, K. Higashiguchi, M. Irie, J. Phys. Chem. B 106 (2002) 11218.

[35] (a) W. Fujita, K. Awaga, Science 286 (1999) 261; (b) W. Fujita, K. Awaga, Polyhedron 20 (2001) 1517; (c) G.D. McManus, J.M. Rawson, N. Feeder, J. van Duijin, E.J.L. J.J. Novoa, R. Burriel, F. Palacio, P. Oliete, J. Mater. Chem. 11 (2001) 1992 (d) W. Fujita, K. Awaga, H. Matsuzaki, H. Okamoto, Phys. Rev. B 65 (2002) 064434.

[36] H. Matsuzaki, W. Fujita, K. Awaga, H. Okamoto, Phys. Rev. B 91 (2003) 017403.

[37] (a) N. Koga, Y. Ishimaru, H. Iwamura, Angew. Chem. Int. Ed. Engl. 35 (1996) 755; (b) Y. Sano, M. Tanaka, N. Koga, K, Matsuda, H. Iwamura, P. Rabu, M. Drillon, J. Am. Chem. Soc. 119 (1997) 8246; (c) S. Karasawa, M. Tanaka, N. Koga, H. Iwamura, Chem. Commun. (1997) 1359; (d) S. Karasawa, Y. Sano, T. Akita, N. Koga, T. Itoh, H. Iwamura, P. Rabu, M. Drillon, J. Am. Chem. Soc. 120 (1998) 10080; (e) H. Iwamura, N. Koga, Pure Appl. Chem. 71 (1999) 231; (f) H. Morikawa, F. Imamura, Y. Tsurukami, T. Itoh, H. Kumada, S. Karasawa, N. Koga, H. Iwamura, J. Mater. Chem. 11 (2001) 493; (g) S. Karasawa, N. Koga, Polyhedron 20 (2001) 1387; (h) S. Karasawa, H. Kumada, N. Koga, H. Iwamura, J. Am. Chem. Soc. 123 (2001) 9685; (i) S. Karasawa, N. Koga, Polyhedron 22 (2003) 1877.

[38] (a) M. Matsushita, T. Nakamura, T. Momose, T. Shida, Y. Teki, T. Takui, T. Kinoshita, K. Itoh, J. Am. Chem. Soc. 114 (1992) 7470; (b) T. Nakamura, T. Momose, T. Shida, K. Sato, S. Nakazawa, T. Kinoshita, T. Takui, K. Itoh, T.

Okuno, A. Izuoka, T. Sugawara, J. Am. Chem. Soc. 118 (1996) 8684; (c) S. Rajca, A. Rajca, J. Am. Chem. Soc. 117 (1995) 9172; (d) A. Ito, H. Ino, Y. Matsui, Y. Hirao, K. Tanaka, J. Phys. Chem. A 108 (2004) 5715.

[39] (a) Y. Morita, S. Nishida, J. Kawai, K. Fukui, S. Nakazawa, K. Sato, D. Shiomi, T. Takui, K. Nakasuji, Org. Lett. 4 (2002) 1985; (b) Y. Morita, S. Nishida, J. Kawai, K. Fukui, S. Nakazawa, K. Sato, D. Shiomi, T. Takui, K. Nakasuji, Polyhedron 22 (2003) 2209.

[40] (a) M.A. Ruderman, C. Kittel, Phys. Rev. 96 (1954) 99; (b) T. Kasuya, Prog. Theor. Phys. 16 (1956) 45; (c) K. Yoshida, Phys. Rev. 106 (1957) 893.

[41] C. Zener, Phys. Rev. 82 (1951) 403.

[42] P. Day, M. Kurmoo, T. Mallah, I.R. Marsden, R.H. Friend, F.L. Pratt, W. Hayes, D. Chasseau, J. Gaultier, G. Bravic, L. Ducasse, J. Am. Chem. Soc. 114 (1992) 10722.

[43] (a) E. Coronado, J.R. Galán-Mascarós, C.J. Gómez-García, V. Laukhin, Nature 408 (2000) 447; (b) E. Coronado, A. Forment-Aliaga, J.R. Galán-Mascarós, C. Giménez-Sainz, C.J. Gómez-García, E. Martinéz-Ferrero, A. Nuez, F.M. Romero, Solid State Sci. 5 (2003) 917.

[44] (a) A. Kobayashi, T. Udagawa, H. Tomita, T. Naito, H. Kobayashi, Chem. Lett. (1993) 2179; (b) H. Tanaka, A. Kobayashi, A. Sato, H. Akutsu, H. Kobayashi, J. Am. Chem. Soc. 121 (1999) 760; (c) H. Kobayashi, H. Tomita, T. Naito, A. Kobayashi, F. Sakai, T. Watanabe, P. Cassoux, J. Am. Chem. Soc. 118 (1996) 368; (d) O. Cepas, R.H. McKenzie, J. Merino, Phys. Rev. B 65 (2002) 100502; (e) S. Uji, H. Shinagawa, T. Terashima, T. Yakabe, Y. Terai, M. Tokumoto, A. Kobayashi, H. Tanaka, H. Kobayashi, Nature 410 (2001) 908; (f) L.B. Balicas, J.S. Brooks, K. Storr, S. Uji, M. Tokumoto, H. Tanaka, H. Kobayashi, A. Kobayashi, V. Barzykin, L.P. Gor'kov, Phys. Rev. Lett. 87 (2001) 067002.

[45] (a) R. Kumai, M.M. Matsushita, A. Izuoka, T. Sugawara, J. Am. Chem. Soc. 116 (1994) 4523; (b) H. Sakurai, R. Kumai, A. Izuoka, T. Sugawara, Chem. Lett. (1996) 879; (c) J. Nakazaki, M.M. Matsushita, A. Izuoka, T. Sugawara, Tetrahedron Lett. 40 (1999) 5027; (d) H. Sakurai, A. Izuoka, T. Sugawara, J. Am. Chem. Soc. 122 (2000) 9723; (e) J. Nakazaki, Y. Ishikawa, A. Izuoka, T. Sugawara, Y. Kawada, Chem. Phys. Lett. 319 (2000) 385.

[46] (a) J. Nakazaki, I. Chung, R. Watanabe, T. Ishitsuka, Y. Kawada, M.M. Matsushita, T. Sugawara, Internet Electron. J. Mol. Des. 2 (2003) 112; (b) J. Nakazaki, I. Chung, M.M. Matsushita, T. Sugawara, R. Watanabe, A. Izuoka, Y. Kawada, J. Mater. Chem. 13 (2003) 1011.

[47] G. Harada, H. Sakurai, M.M. Matsushita, A. Izuoka, T. Sugawara, Chem. Lett. (2002) 1030.

[48] (a) A. Caneschi, D. Gatteschi, R. Sessoli, A.L. Barra, L.C. Brunel, M. Guillot, J. Am. Chem. Soc. 113 (1991) 5873; (b) R. Sessoli, D. Gatteschi, A. Caneschi, M. A. Novak, Nature 365 (1993) 141; (c) R. Sessoli, H. Tsai, A.R. Schake, S. Wang, J.B. Vincent, K. Folting, D. Gatteschi, G. Christou, D.N. Hendrickson, J. Am. Chem. Soc. 115 (1993) 1804; (d) L. Thomas, F. Lionti, R. Ballou, D. Gatteschi, R. Sessoli, B. Barbara, Nature 383 (1996) 145; (e) L. Thomas, A. Caneschi, B. Barbara, Phys. Rev. Lett. 83 (1999) 2398; (f) D. Gatteschi, R. Sessoli, Angew. Chem. Int. Ed. Engl. 42 (2003) 268; (g) D. Gatteschi, R. Sessoli, J. Mag. Mag. Mater. 272-276 (2004) 1030.

[49] R.J. Glauber, J. Math. Phys. 4 (1963) 294.

[50] (a) A. Caneschi, D. Gateschi, N. Lalioti, C. Sangregorio, R. Sessoli, G. Venturi, A. Vindigni, A. Rettori, M.G. Pini, M.A. Novak, Angew. Chem. Int. Ed. Engl. 40 (2001) 1760; (b) A. Caneschi, D. Gateschi, N. Lalioti, R. Sessoli, L. Sorace, V. Tangoulis, A. Vindigni, Chem. Eur. J. 8 (2002) 286; (c) A. Caneschi, D. Gateschi,

N. Lalioti, C. Sangregorio, R. Sessoli, G. Venturi, A. Vindigni, A. Rettori, M.G. Pini, M.A. Novak, Europhys. Lett. 58 (2002) 771.

[51] R. Clérac, H. Miyasaka, M. Yamashita, C. Coulon, J. Am. Chem. Soc. 124 (2002) 12837.

[52] (a) M. Clemente-León, H. Soyer, E. Coronado, C. Mingotaud, C.J. Gómez-García, P. Delhaès, Angew. Chem. Int. Ed. Engl. 37 (1998) 2842; (b) E. Coronado, M. Clemente-León, C.J. Gómez-Garcia, H. Soyer, C. Mingotaud, P. Delhaès, Synth. Met. 103 (1999) 2263; (c) E. Coronado, M. Feliz, A. Forment-Aliaga, C.J. Gómez-García, R. Llusar, F.M. Romero, Inorg. Chem. 40 (2001) 6048; (d) M. Clemente-León, E. Coronado, P. Delhaes, C.J. Gómez-García, C. Mingotaud, Adv. Mater. 13 (2001) 574; (e) M. Clemente-León, E. Coronado, A. Forment-Aliaga, F.M. Romero, C. R. Chimie 6 (2003) 683.

[53] M.N. Leuenberger, D. Loss, Nature 410 (2001) 789.

Chapter 1

Tetraarylethylene Having Two Nitroxide Groups: Redox-Switching of Through-Bond Magnetic Interaction by Conformation Change

1.1 Introduction

Sterically congested hydrocarbon molecules often exhibit the remarkable structural changes upon a redox input [1]. Upon oxidation of tetraphenylethylene (TPE), the C=C double bond is elongated to a C–C single bond and concomitantly rotational motion about the olefinic bond takes place. The X-ray structural analyses of the isolated mono- and dications of TPE derivatives revealed that the rotational angle increases on going from cation to dication [2]. In conjunction with this intriguing structural change, TPE has attracted much attention from the viewpoint of new electrochromic system [3]. In particular, tetrakis(4-dimethylaminophenyl)ethylene (**1**) can be reversibly converted to the diamagnetic dication in which the two cyanine moieties [4] are generated by rotational motion about the olefinic bond [3]. Hence, **1** is recognized as a novel organic electrochromic system with the long wavelength absorptions and high extinction coefficients.

Scheme 1.

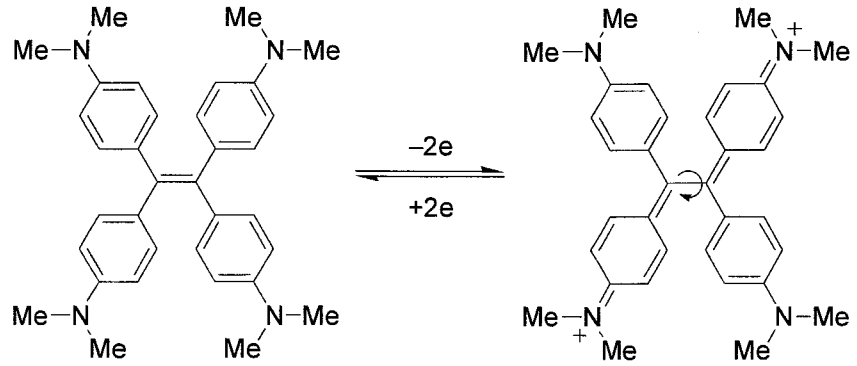

On the other hand, the drastic structural change in TPE including change of π-conjugation connection pathway can be utilized as a redox-switchable magnetic coupling unit. To date, although a large number of studies have been made on the redox-generation of non-Kekulé high-spin organic molecules [5], little is known about the control of through-bond magnetic interactions using interconversion of π-conjugation pathway [6]. To create a new type of organic electrochromic system having a function of redox-switch of through-bond magnetic interaction, we have designed and synthesized the novel TPE derivative carrying two nitroxide radical (**2**). In neutral form of **2**, a strong exchange interaction (J) through π-conjugated network [7a] is expected between two radical centers. On the other hand, the through-bond magnetic interaction in the dication of **2** disappear by interception of π-conjugation between two nitroxide groups originating from rotational motion about the olefinic bond (Scheme 1). In other words, the TPE moiety of $\mathbf{2}^{2+}$ is considered to have a twisted tetramethyleneethane (TME) structure, in which singlet and triplet states are virtually degenerate ($J \approx 0$) [7].

Scheme 1 Bisnitroxide **2** and the redox-switching of through-bond magnetic interaction.

Strong intramolecular magnetic interaction

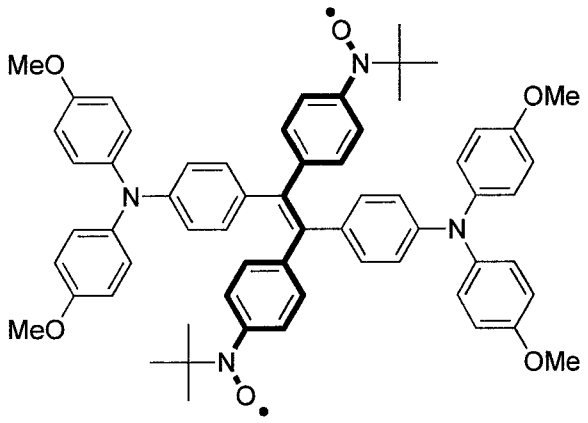

2

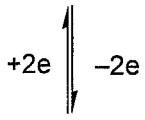

Weak intramolecular magnetic interaction

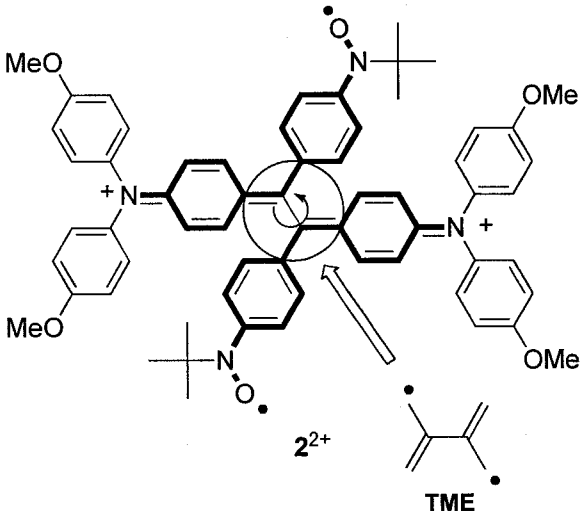

2^{2+} **TME**

1.2 Experimental Section

General Methods

^{1}H and ^{13}C spectra were recorded on a JEOL JNM-AL400, JNM-EX400 or JNM-AL300 spectrometer, and chemical shifts are given in parts per million (ppm) relative to internal tetramethylsilane (δ 0.00 ppm). Elemental analyses were performed by Center for Organic Elemental Microanalysis, Kyoto University.

Materials

Toluene and *n*-butyronitrile were distilled from CaH_2 under an argon atmosphere, tetrahydrofuran (THF) was distilled from potassium–benzophenone under an argon atmosphere, *N*,*N*-dimethylformamide (DMF) was dried over molecular sieves 4A, and benzonitrile was dried through alumina (ICN, Alumina N, Akt. I) column with bubbling of argon, just before use. All the other purchased reagents and solvents were used without further purification. Column chromatography was performed using silica gel (Kanto Chemical Co., Inc., Silica gel 60N, spherical neutral).

***N*-4-Bromophenyl-*N*-*tert*-butylhydroxyamine (3).** To a solution of 1,4-dibromobenzene (22.0 g, 93.0 mmof) in THF (250 mL) was added *n*-butyllithium (1.55 M hexane solution, 66.0 mL, 102.3 mmol) at −78 °C under argon atmosphere. The solution was stirred for 1 h. A solution of 2-methyl-2-nitrosopropane (8.92 g, 102.4 mmol) in THF (80 mL) was dropped for 50 min. The mixture was stirred for 2 h at −78 °C, and then stirred at room temperature for 1 h. To the mixture was added 5 % aqueous ammonium chloride (200 mL). The organic layer was separated and the aqueous layer was extracted with Et_2O. The organic layer was combined and dried over $MgSO_4$. After filtration, the solvent was evaporated. The orange solid was washed with *n*-hexane and ethyl acetate to give **3** as white solid (8.29 g, 36 %). The filtrate was evaporated to remove solvent and chromatographed on silica gel

(AcOEt:*n*-hexane = 1:4 as eluent). A fraction (R_f = 0.51) afforded **3** as pale orange solid (7.23 g, 32 %). Total amount of **3** through this reaction was 15.52 g (68 %): ^{1}H NMR (300MHz, $CDCl_3$) δ 7.34 (d, J = 8.81 Hz, 2H), 7.08 (d, J = 8.81 Hz, 2H), 6.91 (br-s, 1H), 1.08 (s, 9H); ^{13}C NMR (75 MHz, $CDCl_3$) δ 148.3, 130.5, 126.2, 118.3, 60.7, 25.8.

***N*-4-Bromophenyl-*N*-*tert*-butyl-*N*-*tert*-butyldimethylsiloxyamine (4).** To a solution of *tert*-butyldimethylchlorosilane (6.69 g, 44.4 mmol) and imidazole (6.31 g, 90.8 mmol) in DMF (30 mL) was added **3** (7.23 g, 29.6 mmol). The resulting solution was stirred at 40 °C for 17 h under argon atmosphere. To the mixture was added *n*-hexane and water. The organic layer was separated and the aqueous layer was extracted with *n*-hexane. The organic layer was combined and dried over $MgSO_4$. After filtration, the solvent was evaporated. The residue was chromatographed on silica gel (*n*-hexane as eluent). A fraction (R_f = 0.63) afforded **4** as colorless oil (10.62 g, 100 %): ^{1}H NMR (300MHz, $CDCl_3$) δ 7.32 (d, J = 8.81 Hz, 2H), 7.10 (br-d, J = 8.26 Hz, 2H), 1.05 (s, 9H), 0.88 (s, 9H); ^{13}C NMR (75 MHz, $CDCl_3$) δ 150.2, 130.3, 126.8, 117.8, 60.9, 26.1, 26.0, 17.9, –4.7.

Bis(4-methoxyphenyl)aminobenzonitrile (5). 4-Aminobenzonitrile (2.58 g, 20.7 mmol), 4-iodoanisole (12.11 g, 51.7 mmol), copper(I) iodide (1.25 g, 6.23 mmol) and powdered anhydrous potassium carbonate (15.09 g, 108.6 mmol) were placed in a flask equipped with a reflux condenser under argon atmosphere. The mixture was heated to *ca.* 165 °C for 4 days. During the reaction, the sublimates of the top of a flask were returned into the reaction mixture by heating them. After cooling to room temperature, dichloromethane was added into the resulting black mixture to dissolve the products and unreacted materials. The undissolved solid was removed by filtration and the solvent was evaporated. The residue was chromatographed on silica gel (AcOEt:CH_2Cl_2:*n*-hexane = 1:49:50 as eluent). A fraction (R_f = 0.55) afforded **5** as pale yellow solid (4.55 g, 67 %): ^{1}H NMR (400MHz, $CDCl_3$) δ 7.35 (d, J = 8.79 Hz,

2H), 7.10 (d, J = 8.79 Hz, 4H), 6.88 (d, J = 8.79 Hz, 4H), 6.78 (d, J = 8.79 Hz, 2H), 3.81 (s, 6H); ^{13}C NMR (100 MHz, $CDCl_3$) δ 157.2, 152.2, 138.6, 133.0, 127.9, 120.0, 117.0, 115.1, 100.6, 55.5.

4-(*N-tert*-Butyl-*N-tert*-butyldimethylsiloxyamino)-4'-[bis(4-methoxyphenyl)amino]benzophenone (6). To a solution of **4** (15.4 g, 42.9 mmol) in THF (100 mL) was added *n*-butyllithium (1.55 M hexane solution, 27.5 mL, 42.6 mmol) at −78 °C under argon atmosphere. The solution was stirred for 1.5 h. A solution of **5** (13.6 g, 41.2 mmol) in THF (100 mL) was dropped for 45 mim. The mixture was stirred for 2 h at −78 °C, and then stirred at room temperature for 1 h. To the mixture was added water (100 mL) and stirred over night. The organic layer was separated and the aqueous layer was extracted with Et_2O. The organic layer was combined and dried over $MgSO_4$. After filtration, the solvent was evaporated. The residue was chromatographed on silica gel (AcOEt:*n*-hexane = 1:9 as eluent). A fraction (R_f = 0.31) afforded **6** as yellow solid (22.9 g, 91 %): ^{1}H NMR (400MHz, $CDCl_3$) δ 7.67 (d, J = 3.91 Hz, 2H), 7.64 (d, J = 3.91 Hz, 2H), 7.30 (br-d, J = 7.81 Hz, 2H), 7.14 (d, J = 8.79 Hz, 4H), 6.88 (d, J = 8.79 Hz, 4H), 6.85 (d, J = 8.79 Hz, 2H), 3.81 (s, 6H), 1.12 (s, 9H), 0.92 (s, 9H) −0.12 (br-s, 6H); ^{13}C NMR (100 MHz, $CDCl_3$) δ 194.5, 156.8, 154.5, 152.4, 139.2, 134.7, 131.9, 129.1, 128.2, 127.7, 124.3, 116.7, 114.9, 61.4, 55.5, 26.3, 26.2, 18.0, −4.6; Anal. Calcd for $C_{37}H_{46}N_2O_4Si$: C, 72.75; H, 7.59; N, 4.59. Found: C, 72.95; H, 7.56; N, 4.52.

1,2-Bis[4-(*N-tert*-butyl-*N-tert*-butyldimethylsiloxyamino)phenyl]-1,2-bis[4-{*N*, *N*-bis(4-methoxyphenyl)amino}phenyl]ethylene (7). This compound was prepared by low valent titanium induced reductive coupling reaction, using the modified method of literature [8]. $TiCl_4$· 2THF complex (3.44 g, 9.99 mmol) was placed in a flask equipped with a reflux condenser and a dropping funnel under argon atmosphere. Dry THF (40 mL) was added at −10 °C in ice-acetone bath. Zinc powder (1.81 g, 24.9 mmol) was added, and the resulting mixture was warmed to room temperature for

30 mim and refluxed for 2.5 h. After cooling to −10 °C in ice-acetone bath, dry pyridine (1 mL) was added. A solution of **6** (3.05 g, 4.99 mmol) in dry THF (35 mL) was dropped for 30 min. The resulting mixture was refluxed for 20 h. After cooling to 0 °C in ice-water bath and diluted with CH_2Cl_2, the mixture was poured over cold saturated $NaHCO_3$aq. The suspension was filtered through celite. The organic layer was separated, and the aqueous layer was extracted with CH_2Cl_2. The organic layer was dried over $MgSO_4$. After filtration, the solvent was evaporated. The residue was chromatographed on silica gel (AcOEt:CH_2Cl_2:*n*-hexane = 1:39:60 as eluent). A fraction (R_f = 0.61) afforded **7** as yellow solid (1.19 g, 40 %, mixture of *E*- and *Z*- isomer): ^{1}H NMR (400MHz, $CDCl_3$) δ 6.57–7.04 (m, 32H, Ar), 3.77 (s, 12H, OCH_3), 1.07 1.03 (*E*- or *Z*-, s, total-18H, *t*-Bu), 0.87 (s, 18H, *t*-Bu) −0.16 (br-s, 12H, $SiCH_3$);^{13}C NMR (100 MHz, $CDCl_3$) δ 155.5, 155.4, 148.9, 146.4, 146.3, 141.0, 140.9, 140.8, 140.4, 139.1, 136.9, 136.2, 132.1, 132.0, 130.4, 126.5, 126.2, 124.3, 119.6, 119.1, 114.5, 114.4, 60.7, 60.6, 55.4, 26.2, 18.0, −4.5, −4.6 (29 lines because of mixture of *E*- and *Z*- isomer); FAB HRMS m/z calcd for $C_{74}H_{92}N_4O_6Si_2$ 1188.6555 $[M]^+$, found 1188.6567; calcd for $C_{74}H_{93}N_4O_6Si_2$ 1189.6634 $[M+H]^+$, found 1189.6594; Anal. Calcd for $C_{74}H_{92}N_4O_6Si_2$: C, 74.71; H, 7.79; N, 4.71. Found: C, 74.98; H, 7.84; N, 4.99.

1,2-Bis[4-(*N*-*tert*-butyl-*N*-hydroxyamino)phenyl]-1,2-bis[4-{*N*,*N*-bis(4-methoxy phenyl)amino}phenyl]ethylene (8). To a solution of **7** (449.4 mg, 0.38 mmol) in THF (10 mL) was added tetrabuhylammonium fluoride (1.0 M THF solution, 2.5 mL, 2.5 mmol) at 0 °C under argon atmosphere and stirred for 30 min. The reaction mixture was warmed to room temperature and stirred for 2 h. After addition of Et_2O and water, the organic layer was separated, and the aqueous layer was extracted with Et_2O. The organic layer was dried over $MgSO_4$. After filtration, the solvent was evaporated. The yellowish brown solid was washed with *n*-hexane and CH_2Cl_2 to give **8** as white solid (242.6 mg, 67 %). The filtrate was evaporated to remove solvent and chromatographed on silica gel (AcOEt:CH_2Cl_2:*n*-hexane = 2:48:50 to

10:40:50 as eluent) to afford **8** as yellowish brown solid (99.9 mg, 27 %). Total amount of **8** through this reaction was 324.5 mg (94 %): ^{1}H NMR (400MHz, $CDCl_3$) δ 6.53–7.01 (m, 32H, Ar), 3.74 3.72 (*E*- or *Z*-, s, total-12H, OCH_3), 1.09 1.04 (*E*- or *Z*-, s, total-18H, *t*-Bu); ^{13}C NMR (100 MHz, $CDCl_3$) δ 155.4, 146.5, 146.4, 140.8, 140.6, 139.3, 136.6, 135.8, 132.1, 132.0, 130.7, 130.5, 126.4, 126.2, 123.3, 119.5, 118.8, 114.4, 60.6, 60.3, 55.4, 26.0, 25.9 (23 peaks because of mixture of *E*- and *Z*- isomer).

1,2-Bis[4-(*N*-*tert*-butylaminoxyl)phenyl]-1,2-bis[4-{*N*,*N*-bis(4-methoxyphenyl)amino}phenyl]ethylene (2). To a solution of **8** (54.7 mg, 0.0569 mmol) in CH_2Cl_2 (10 mL) was added Ag_2O (134.1 mg, 0.573 mmol) and stirred for 2 h at room temperature. The reaction mixture was filtered througth Celite. The filtrate was evaporated to remove solvent and chromatographed on silica gel (Et_2O:CH_2Cl_2:*n*-hexane = 10:40:50 as eluent) to afford **2** as reddish brown solid (46.9 mg, 86 %): FAB HRMS m/z calcd for $C_{62}H_{63}N_4O_6$ 959.4748 $[M+H]^+$, found 959.4763; calcd for $C_{62}H_{64}N_4O_6$ 960.4826 $[M+2H]^+$, found 960.4818; Anal. Calcd for $C_{62}H_{62}N_4O_6$: C, 77.64; H, 6.52; N, 5.84; O, 10.01. Found: C, 77.46; H, 6.68; N, 5.57; O, 10.00.

4-[Bis(4-methoxyphenyl)amino]benzophenone (9). To a solution of bromobenzene (2.80 g, 17.7 mmol) in THF (45 mL) was added *n*-butyllithium (1.55 M hexane solution, 11.5 mL, 17.8 mmol) at −78 °C under argon atmosphere. The solution was stirred for 70 min. A solution of **5** (5.53 g, 16.7 mmol) in THF (30 mL) was dropped for 20 mim. The mixture was stirred for 30 mim at −78 °C, and then stirred at room temperature for 1.5 h. To the mixture was added water (100 mL) and stirred over night. The organic layer was separated and the aqueous layer was extracted with Et_2O. The organic layer was combined and dried over MgSO4. After filtration, the solvent was evaporated. The residue was chromatographed on silica gel (AcOEt:CH_2Cl_2:*n*-hexane = 1:49:50 as eluent). A fraction (R_f = 0.41) afforded **9** as yellow solid (5.28 g, 73 %): ^{1}H NMR (400MHz, $CDCl_3$) δ 7.74 (d, *J* =

6.84 Hz, 2H, Ar), 7.67 (d, J = 8.79 Hz, 2H, Ar), 7.52 (t, J = Hz, 1H, Ar), 7.44 (t, J = Hz, 2H, Ar), 7.14 (d, J = 8.79, 4H, Ar),6.88 (d, J = 8.79, 4H, Ar), 3.81 (s, 6H, OCH_3); ^{13}C NMR (100 MHz, $CDCl_3$) δ 194.9, 156.9, 152.6, 139.2, 138.7, 132.0, 131.3, 129.5, 128.0, 127.8, 116.7, 114.9, 55.5.

1,2-Bis[4-{di(4-methoxyphenyl)amino}phenyl]-1,2-diphenylethylene (10). This compound was prepared by low valent titanium induced reductive coupling reaction, using the modified method of literature [9]. $TiCl_4$·2THF complex (4.76 g, 13.8 mmol) was placed in a flask equipped with a reflux condenser and a dropping funnel under argon atmosphere. Dry THF (30 mL) was added at −10 °C in ice-acetone bath. A solution of **9** (3.77 g, 9.21 mmol) in dry THF (35 mL) was dropped into the yellow suspension for 40 min, and the reaction mixture turned to black. Zinc powder (2.05 g, 28.2 mmol) was added for 10 mim. The resulting mixture was stirred at room temperature for 1 h and refluxed for 18 h. After cooling to 0 °C in ice–water bath and diluted with CH_2Cl_2, the mixture was poured over cold saturated $NaHCO_3$aq. The organic layer was separated, and the aqueous layer was extracted with CH_2Cl_2. The organic layer was combined and dried over $MgSO_4$. After filtration, the solvent was evaporated. The residue was washed with hot $CHCl_3$-*n*-hexane to afforded **10** as yellow powder (2.84 g, 78 %). The filtrate and washing was evaporated and chromatographed on silica gel (AcOEt:CH_2Cl_2:*n*-hexane = 2:38:60 as eluent). A fraction (R_f = 0.55) afforded **10** as yellow powder (0.24 g, 7 %). Total amount of **10** through this reaction was 3.08 g (85 %, mixture of *E*- and *Z*-isomer): ^1H NMR (400MHz, $CDCl_3$) δ 6.61–7.16 (m, 34H, Ar), 3.77 (s, 12H, OCH_3); ^{13}C NMR (100 MHz, $CDCl_3$) δ 155.5, 155.4, 146.6, 146.5, 144.2, 143.9, 140.9, 140.8, 139.8, 139.7, 136.4, 136.1, 131.9, 131.4, 127.4, 126.3, 126.2, 126.0, 119.6, 114.5, 114.4, 55.5 (22 peaks because of mixture of *E*- and *Z*- isomer); FAB HRMS m/z calcd for $C_{54}H_{46}N_2O_4$ 786.3458 $[M]^+$, found 786.3484; Anal. Calcd for $C_{54}H_{46}N_2O_4$: C, 82.42; H, 5.89; N, 3.56; O, 8.13. Found: C, 82.14; H, 6.14; N, 3.37; O, 8.04.

Electrochemical Measurement

The cyclic voltammetry (CV) measurements were carried out in benzonitrile solution containing 0.1 M tetrabutylammonium tetrafluoroborate as a supporting electrolyte (25 °C, scan rate 100 mV/sec) using an ALS/chi Electrochemical Analyzer Model 612A. A three-electrode assembly was used, which was equipped with a platinum disk (2 mm^2), a platinum wire, and Ag/0.01 M $AgNO_3$ (acetonitrile) as the working, the counter, and the reference electrode, respectively. The redox potentials were referenced against ferrocene/ferrocenium (Fc/Fc^+) couple.

UV/Vis/NIR Spectrum Measurement

UV/Vis/NIR spectra were obtained with a Perkin Elmer Lambda 19 spectrometer. Spectroelectrochemical measurements were carried out with self-constructed optically transparent thin-layer electrochemical (OTTLE) cell (light pass length = 1mm) equipped with a platinum mesh, a platinum coil, and a silver wire as the working, the counter, and the pseudo-reference electrode, respectively. The potential was applied with an ALS/chi Electrochemical Analyzer Model 612A.

ESR Measurement

ESR spectra were recorded on a JEOL JES-SRE2X or a JEOL JES-TE200 X-band spectrometer, in which temperature was controlled by a JEOL DVT2 variable-temperature unit or an Oxford ITC503 temperature controller combined with an ESR 910 continuous flow cryostat, respectively. A Mn^{2+}/MnO solid solution was used as a reference for the determination of *g* values and hyperfine coupling constants. Pulsed ESR measurements were carried out on a Bruker ELEXES E580 X-band FT ESR spectrometer.

Magnetic Susceptibility Measurement

Magnetic susceptibilities of the powder samples were measured by a Quantum Design MPMS-5S system. The raw data were corrected for both the magnetization of sample holder alone and the diamagnetic contribution of the sample itself. The estimation of the diamagnetic contribution was done by using Pascal's constants.

1.3 Results and Discussion

1.3.1 Synthesis

The synthesis of bisnitroxide **2** is outlined in Scheme 3. Monolithiated 1,4-dibromobenzene was coupled with 2-methyl-2-nitrosopropane to give hydroxylamine (**3**). The hydroxylamine **3** was protected with *tert*-butyldimethylsilyl group to afford **4**. On the other hand, cyano-substituted triphenylamine (**5**) was prepared using Ullmann coupling reaction from corresponding 4-aminobenzonitrile and 4-idoanisole. The yield is comparable to that of the Pd(0)-catalyzed amination reaction. Asymmetrically substituted diarylketone (**6**) was prepared by addition of the nitrile (**5**) to the lithiated **4** and subsequent hydrolysis. The reductive coupling of the ketone **6** with a low-valent titanium reagent [8] gave a mixture of *cis*- and *trans*-isomers of **7**. After desilylation of **7** with tetrabutylammonium fluoride to afford bishydroxylamine (**8**), the desired bisnitroxide **2** was obtained by oxidation with Ag_2O. The ratio of the two isomers for the precursor **8** was estimated to be 41:59 from the ^{1}H- and ^{13}C-NMR spectra.

Scheme 3. Synthetic route for **2**[a]

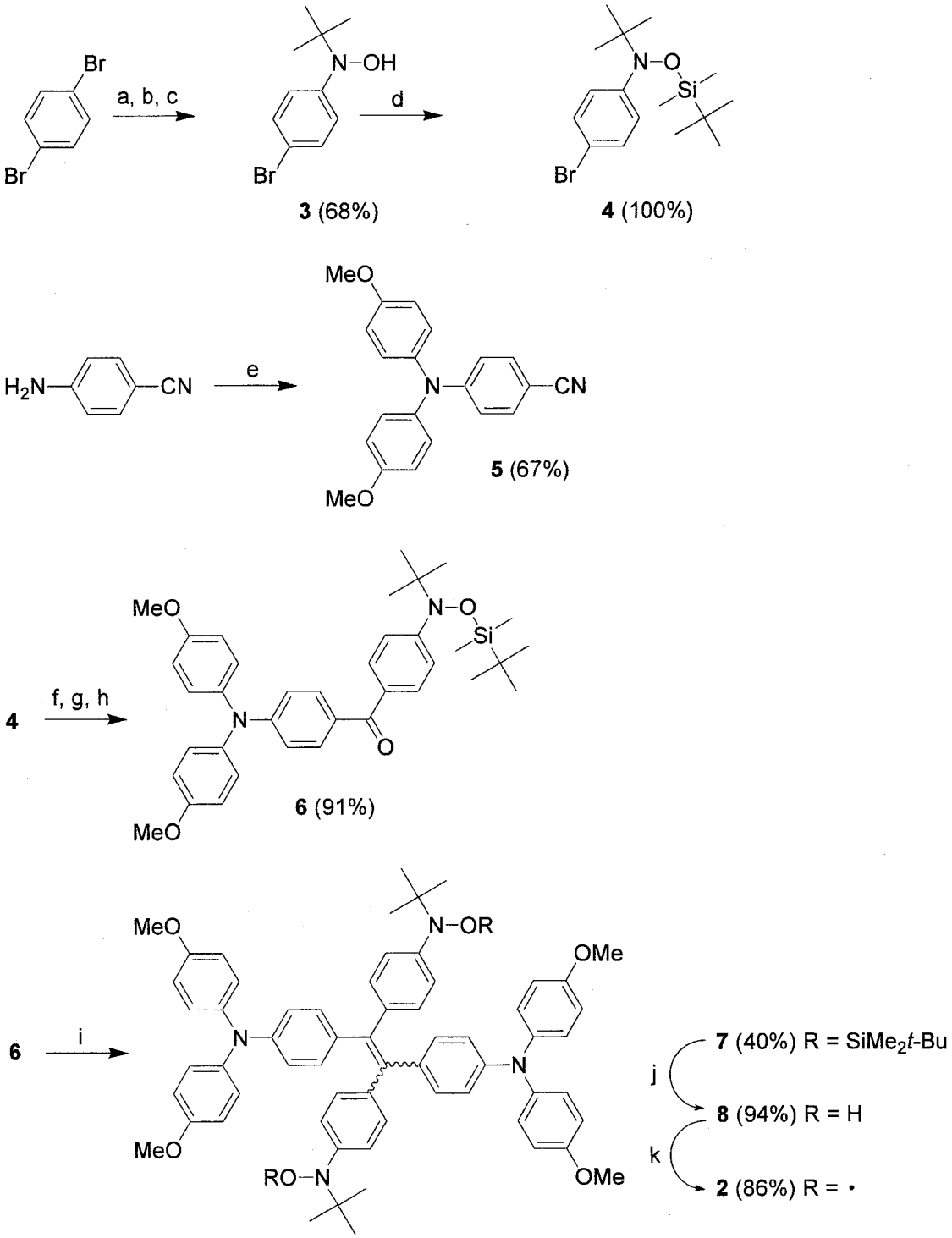

[a]Reagents: (a) *n*-BuLi, THF; (b) *t*-BuNO, THF; (c) aq. NH_4Cl; (d) *t*-$BuMe_2Cl$, imidazole, DMF; (e) 4-iodoanisole, CuI, K_2CO_3; (f) *n*-BuLi, THF; (g) **4**, THF; (h) H_2O; (i) $TiCl_4$, Zn, pyridine, THF; (j) *n*-Bu_4F, THF; (k) Ag_2O, CH_2Cl_2.

1.3.2 Electrochemistry

Effective conversion of through-bond magnetic interaction after and before oxidation of **2** postulates a lower oxidation potential of the TPE moiety than the two nitroxide groups. The cyclic voltammogram of **2** in 1 mM benzonitrile solution containing 0.1 M tetrabutylammonium tetrafluoroborate is shown in Figure 1, and the redox potentials of **2** and related compounds are summarized in Table 1. In comparison with the first oxidation potential of the non-nitroxide-substituted TPE (**10**) [9] and the *N-tert*-butyl-*N*-phenylnitroxide (**11**) [10], it was confirmed that the first two consecutive reversible one-electron transfer steps correspond to the oxidation of the TPE moiety, while the third two-electron transfer process to the oxidation of the two nitroxide groups. The observed peak separations of 74, 70, and 69 mV for the first to third redox processes were larger than the theoretical value of 56.5 mV at 298 K [11]. All these peak separations are probably caused by *cis-trans* mixture of the present sample.

Table 1. Redox potentials (V) of **2** and its related compounds[a]

	E_1	E_2	E_3
2	0	0.25	0.49[b]
10	0.15[b]		
11	0.41[c]		

[a]0.1 M *n*-Bu_4NBF_4 in PhCN, potential vs. Fc/Fc^+, Pt electrode, 25°C, scan rate 100 mV s^{-1}. [b]Quasi two-electron transfer process. [c]Irreversible oxidation process represented by anodic peak potential.

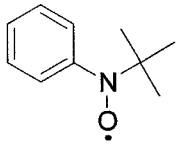

11

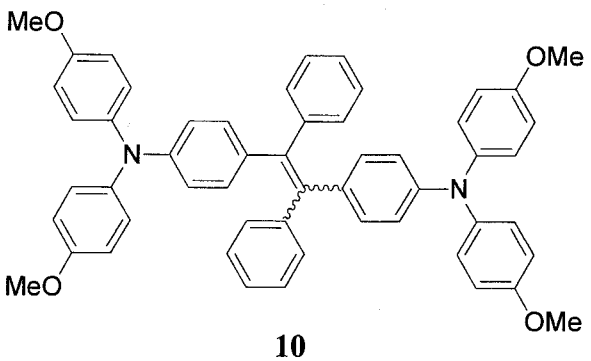

10

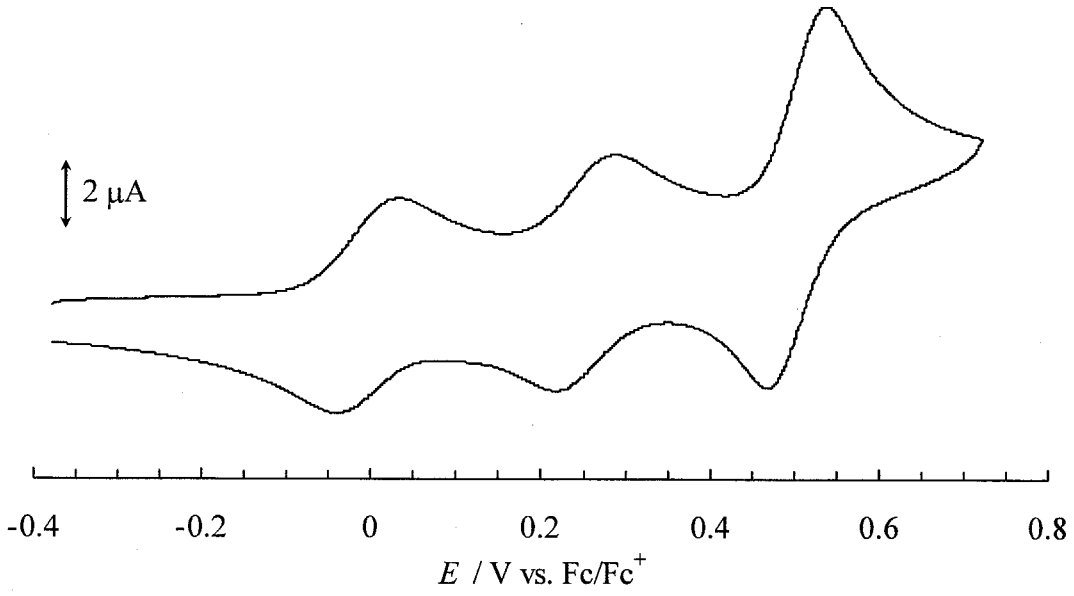

Figure 1. Cyclic voltammogram of **2** in PhCN at 298 K (scan rate 100 mV s^{-1}).

1.3.3 Magnetic Property

Moreover, it was clarified that the two nitroxide groups of **2** are antiferromagnetically coupled from the temperature dependence of the molar magnetic susceptibility (χ_M) of the powder sample measured by the SQUID magnetometer (Figure 2). The $\chi_M T$ value decreases with decreasing temperature from 0.75 emu K

mol^{-1} corresponding to independent two spins of S = 1/2 to 0 emu K mol^{-1} corresponding to antiferromagnetically coupled two spins of S = 1/2. The measured data were analyzed on the basis of equation (1),

$$\chi_M T = f_1 \frac{2N_A g^2 \mu_B^2}{k_B} \frac{1}{3+\exp(-2J_1/k_B T)} + f_2 \frac{2N_A g^2 \mu_B^2}{k_B} \frac{1}{3+\exp(-2J_2/k_B T)} + (1-f_1-f_2)\frac{N_A g^2 \mu_B^2}{2k_B} \quad (1)$$

where f_1 and f_2 are the mole fractions of the two isomers, J_1 and J_2 the magnetic exchange coupling constants (the positive and negative values indicate ferromagnetic and antiferromagnetic interactions, respectively) for the two isomers, N_A the Avogadro number, g the isotropic g-factor, k_B the Boltzmann constant, and μ_B the Bohr magneton. The first two terms represent the Bleany–Bowers singlet–triplet model [13] corresponding to the two isomers, and the third is the Curie term originating from very small quantity of spin doublet impurity like mononitroxide radicals. The best fitted values for f_1, f_2, J_1, and J_2 were estimated to be f_1 = 0.27, f_2 = 0.71, J_1/k_B = –66 K (–0.13 kcal/mol), and J_2/k_B = –93 K (–0.18 kcal/mol), indicating intramolecular antiferromagnetic interaction for both isomers. Moreover, the ratio of the two isomers in **2** can be estimated at 28:72 from f_1 and f_2 values. This ratio is in fairly good accordance with that estimated from the NMR data of the precursor **9**. From the DFT calculations at the UB3LYP/6-31G* level [14], the ground states for *cis*- and *trans*-isomers of **2** were predicted to be both singlet state, and the singlet *trans*-isomer lies 0.24 kcal/mol lower than the singlet *cis*-isomer. This suggests that the *trans*-isomer is a thermodynamically favorable isomer. In addition, the energy

differences between the singlet and triplet states ΔE_{S-T} (= $2J$) for *cis*- and *trans*-isomers were predicted to be –0.47 and –0.49 kcal/mol, respectively. This indicates that the *trans*-isomer has a large J value as compared with the *cis*-isomer. Therefore, f_1 and f_2 are likely to be assignable to the *cis*- and *trans*-isomers, respectively.

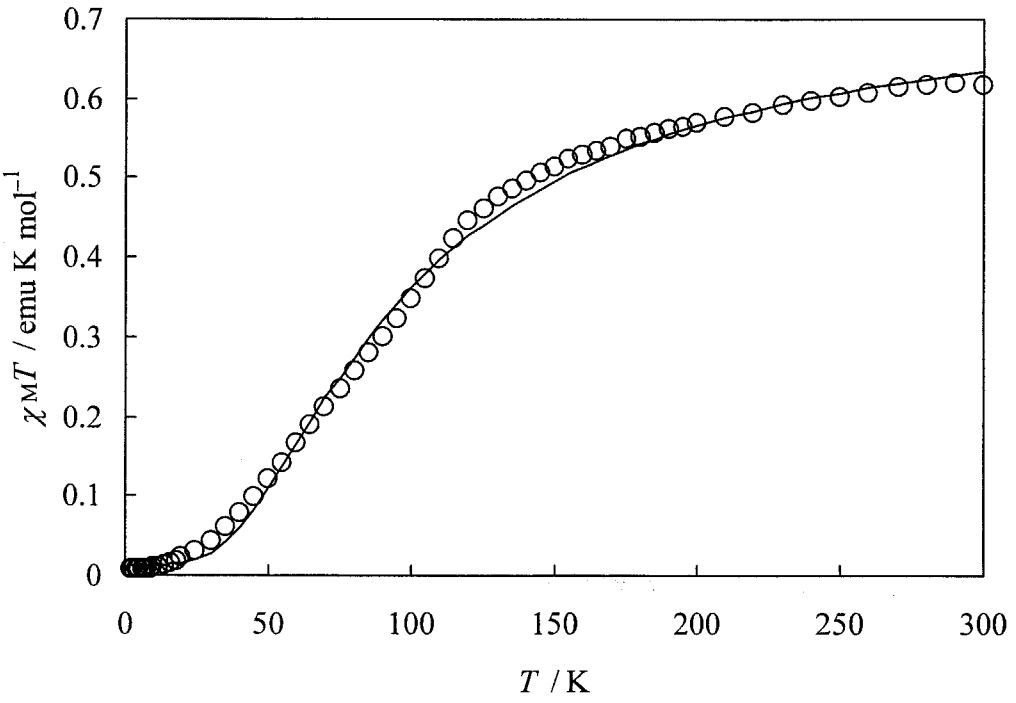

Figure 2. Temperature dependence of magnetic susceptibility (χ_M) of **2** (open circle). Solid curve represent the best theoretical fit to the data (see text).

1.3.4 ESR Spectroscopy

The EPR spectrum of **2** in a frozen toluene matrix at 123 K showed a fine-structured spectrum characteristic for the spin triplet species (Figure 3). The forbidden $\Delta M_S = \pm 2$ resonance was also detected in a half-field region of the allowed $\Delta M_S = \pm 1$ resonance, indicating the existence of spin triplet species [12].

On the other hand, when 2 equiv. of tris(4-bromophenyl)aminium hexachloro

antimonate are added to **2** in toluene/*n*-butyronitrile 1:1 solution at 195 K, the EPR spectrum of $\mathbf{2}^{2+}$ was completely changed from the one observed for neutral **2** to the one with the typical anisotropic hyperfine structure for the randomly oriented mononitroxide radical (Figure 4). This strongly indicates that the two nitroxide groups in $\mathbf{2}^{2+}$ are no longer coupled magnetically owing to rotational motion about the olefinic bond [13]. Note that the principal value (A_{ZZ}) [15] for the perpendicular direction to the nitroxide plane of the hyperfine coupling tensor of $\mathbf{2}^{2+}$ takes a small value (19.28 G) as compared with the corresponding value (27.99 G) of **11**. This suggests that spin density on the nitrogen atoms of the nitroxide groups decreases on going from **2** to $\mathbf{2}^{2+}$, reflecting the spin delocalization over the whole molecule.

To check the reversibility between **2** and $\mathbf{2}^{2+}$, $\mathbf{2}^{2+}$ was treated with an excess of hydrazine monohydrate. Consequently, the same EPR spectrum as as-prepared **2** (Figure 3) was retrieved from the hyperfine-structured spectrum due to the independent nitroxide radical of $\mathbf{2}^{2+}$ (Figure 4). From the viewpoint of redox-switching of through-bond magnetic interaction, on- and off-states correspond to the *cis-trans* mixture of **2** and the dication $\mathbf{2}^{2+}$, respectively.

1.3.5 Spectroelectrochemistry

The reversibility was also confirmed spectroelectorochemically. Absorption spectra for $\mathbf{2}^{2+}$ at a forward bias of +0.4 V vs. Fc/Fc^+ and **2** at a reverse bias at –0.1 V vs. Fc/Fc^+ in dichloromethane solution containing 0.1 M tetrabutylammonium tetrafluoroborate are shown in Figure 5. In applying a forward bias of +0.4 V, the increase of the band at 536 and 760 nm, and the decrease of the band at 309 nm were observed. The several electrochemical cycling experiments reversibly reproduced the spectra corresponding to **2** and $\mathbf{2}^{2+}$ (Figure 5).

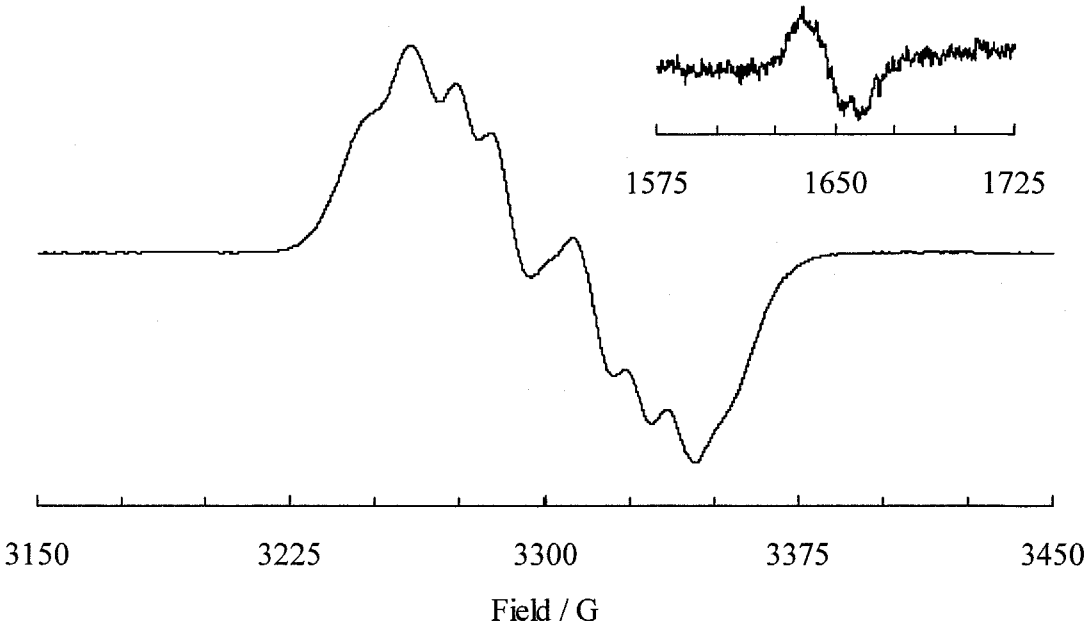

Figure 3. EPR spectra of **2** in frozen toluene solution at 123 K and the forbidden $\Delta M_S = \pm 2$ resonance at 123 K (inset).

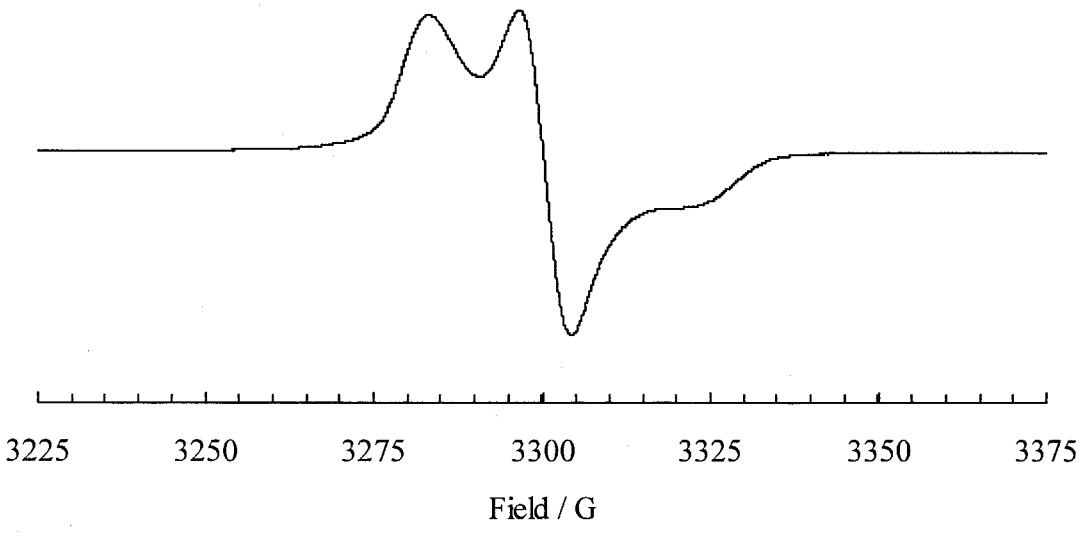

Figure 4. EPR spectrum of **2** after treatment with 2 equiv. of tris(4-bromophenyl)aminium hexachloroantimonate in toluene/*n*-butyronitrile = 1:1 at 123 K.

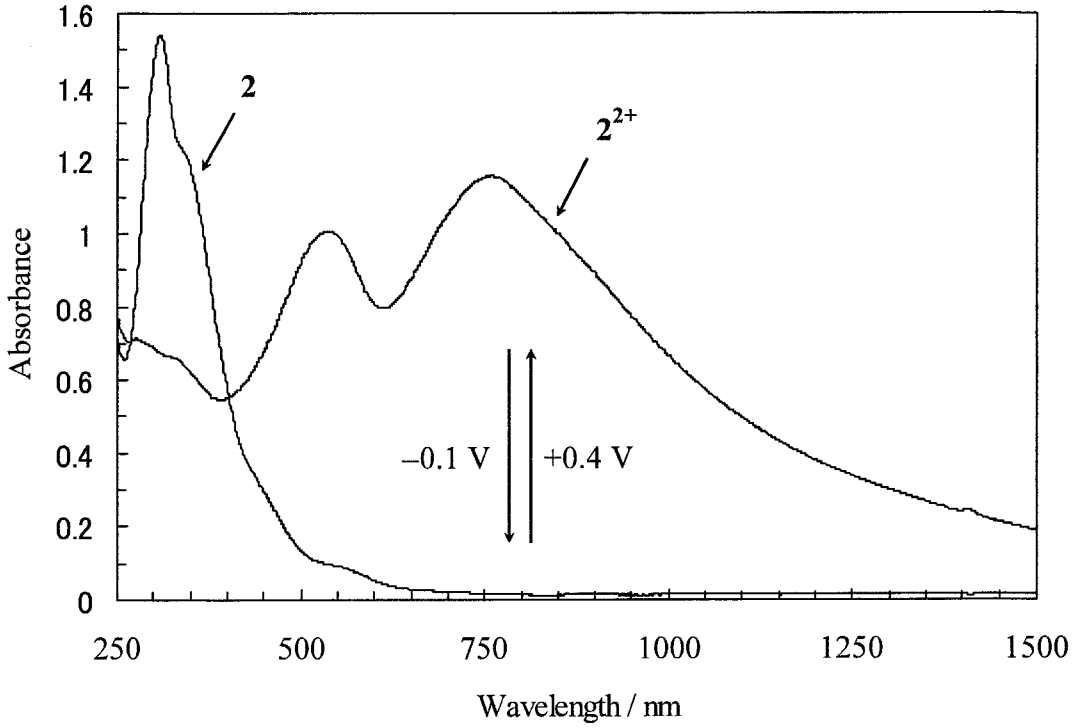

Figure 5. Absorption spectral change of **2** in CH_2Cl_2 at room temperature upon several electrochemical cycling between +0.4 and –0.1 V vs. Fc/Fc^+.

1.4 Conclusion

The synthesis of diradical **2** having the tetraphenylethylene skeleton was succeeded by using a low-valent titanium reagent, although the separation of *cis*- and *trans*-isomers is met with failure so far, and it is found that the neutral diradical **2** in the solid state showed antiferromagnetic interaction between radical spins. The electrochemical measurement showed the core tetraphenylethylene skelton have the lower oxidation potential than the substituted nitroxide moiety. It was found by ESR measurement in frozen solution that the neutral diradical **2** shows the fine-structured spectrum characteristic for the spin triplet species, while **2** after treatment with 2 equiv. of tris(4-bromophenyl)aminium hexachloroantimonate shows the typical anisotropic

hyperfine-structured one for the randomly oriented mononitroxide radical, indicating the dramatical change of intramolecular magnetic interaction. The reversibility was confirmed from the fact that the ESR spectrum for neutral diradical **2** is recovered with a chemical reduction, and the absorption spectrum is spectroelectrochemically reversible for several cycles.

The above described results strongly suggest that the present diradical **2** can operate as a redox-switch of through-bond magnetic interaction. It is anticipated that current investigations will lead to more versatile switching systems when the radical centers are incorporated into TPE so as to create required through-bond magnetic interactions.

References

[1] H. Bock, K. Ruppert, C. Näther, Z. Havlas, H.-F. Herrmann, C. Arad, I. Göbel, A. John, J. Meuret, S. Nick, A. Rauschenbach, W. Seitz, T. Vaupel, B. Solouki, Angew. Chem. Int. Ed. Engl. 31 (1992) 550.

[2] R. Rathore, S.V. Lindeman, A.S. Kumar, J.K. Kochi, J. Am. Chem. Soc., 120 (1998) 6931.

[3] (a) S. Hünig, M. Kemmer, H. Wenner, I. F. Perepichka, P. Bäuerle, A. Emge, G. Gescheid, Chem. Eur. J. 5 (1999) 1969; (b) S. Hünig, M. Kemmer, H. Wenner, F. Barbosa, G. Gescheid, I.F. Perepichka, P. Bäuerle, A. Emge, K. Peters, Chem. Eur. J. 6 (2000) 2618.

[4] J. Fabian, H. Hartmann, Light Absorption of Organic Colorants, Springer, New York, 1980, pp. 162–197.

[5] Representative examples are: (a) S. Rajca, A. Rajca, J. Am. Chem. Soc. 117 (1995) 9172; (b) J. Sedó, D. Ruiz, J. Vidal-Gancedo, C. Rovira, J. Bonvoisin, J.-P. Launay, J. Veciana, Adv. Mater. 8 (1996) 748.

[6] Recently, the control of through-bond magnetic interaction has been achieved by using 1, 2-bis(3-thienyl)ethene as a photo-switchable spin coupling unit, see: K. Matsuda, M. Irie, Chem. Eur. J. 7 (2001) 3466.

[7] (a) J.A. Crayston, J.N. Devine, J.C. Walton, Tetrahedron 56 (2000) 7829; (b) W.T. Borden, E.R. Davidson, J. Am. Chem. Soc. 99 (1977) 4587; (c) P. Dowd, W. Chang, Y.H. Paik, J. Am. Chem. Soc. 108 (1986) 7416; (d) P. Nachtigall, K.D. Jordan, J. Am. Chem. Soc. 115 (1993) 270; (e) K. Matsuda, H. Iwamura, J. Am. Chem. Soc. 119 (1997) 7412.

[8] I. Agranat, S. Cohen, R. Isaksson, J. Sandström, M. R. Suissa, J. Org. Chem., 55 (1990) 4943.

[9] Compound **10** was prepared from 4-bis(4-methoxyphenyl)aminophenyl phenyl

ketone by using the Mukaiyama method, see: T. Mukaiyama, T. Sato, J. Hanna, Chem. Lett. (1973) 1041.

[10] H. Lemaire, Y. Marechel, R. Ramasseul, A. Rassat, Bull. Soc. Chim. France, (1965) 372.

[11] J. Heinze, Angew. Chem. Int. Ed. Engl. 23 (1984) 831.

[12] Preliminarily, we have also determined the spin multiplicity for 4 (triplet) and 4^{2+} (doublet) on the basis of the pulsed EPR spectroscopy. For determination of spin-multiplicity for high-spin molecules by using the pulsed EPR technique, see: (a) J. Isoya, H. Kanda, J.R. Norris, J. Tang, M.K. Brown, Phys. Rev. B 41 (1990) 3905; (b) A.V. Astashkin, A. Schweiger, Chem. Phys. Lett. 174 (1990) 595; (c) A. Ito, H. Ino, K. Tanaka, K. Kanemoto, T. Kato, J. Org. Chem. 67 (2002) 491.

[13] B. Bleaney, K.D. Bowers, Proc. R. Soc. London Ser. A 214 (1952) 451.

[14] GAUSSIAN 98 (Revision A.9) program was used for the present DFT calculations.

[15] The separation between the lowest and the highest field resonance peaks corresponds to the value of $2A_{ZZ}$, see: (a) O.H. Griffith, P.W. Cornell, H.M. McConnell, J. Chem. Phys. 43 (1965) 2909; (b) L.J. Libertini, O. H. Griffith, J. Chem. Phys. 53 (1970) 1359; (c) O. Takizawa, J. Yamauchi, H. Ohya-Nishiguchi, Y. Deguchi, Bull. Chem. Soc. Jpn. 46 (1973) 1991.

Chapter 2

Redox-Switching of Intramolecular Magnetic Interaction: Tetraarylethylene Bearing Two *meta*-Nitroxyl Groups

2.1 Introduction

It is well known that tetraphenylethylene (TPE) involves the drastic change of molecular structure with responding to the redox reaction; that is to say, the C=C double bond is elongated like a C–C single bond and concomitantly rotational motion about the olefinic bond takes place. Such free rotation was experimentally confirmed by reversal coulometric experiments. For example, when the *cis*-form of 1,2-bis(4-dimethylaminophenyl)-1,2-diphenylethylene was subjected to complete oxidation and subsequent complete reduction, the NMR spectrum of the fully reduced product gave an evidence for a mixture of *cis*- and *trans*-isomers [1]. More unequivocal evidence was afforded by the X-ray structural analyses of the isolated mono- and dications of 1,1,2,2-tetrakis(4-methoxyphenyl)ethylene, in which the rotational angle around ethylenic C–C bond increases on going from mono- to di-cationic state as compared with neutral state [2].

Such drastic structural change including conversion of π-conjugation can be utilized as a redox-switchable spin coupling unit. The interconversion of intramolecular magnetic interactions between two radical moieties has been achieved by using 1,2-bis(3-thienyl)ethene and 1,2-bis(2-thienyl)ethene as a photo-switchable spin coupling unit [3]. To create a new type of redox-switchable intramolecular magnetic interaction converting organic molecules, it has been designed and synthesized, the novel TPE carrying two nitroxide radical, 1,2-Bis[4-(*N*-*tert*-butylaminoxyl)phenyl]-1,2-bis[4-{*N*,*N*-bis(4-methoxyphenyl)amino}phenyl]ethylene (**1**) in Chapter 1 of this thesis. The neutral **1** showed a strong antiferromagnetic interaction through π-conjugated network between radical centers. On the other hand, the spin-spin correlation in the oxidized **1** disappears in conjunction with interception of π-conjugation between two nitroxide groups (Scheme 1). In this chapter, 1,2-Bis[3-(*N*-*tert*-butylaminoxyl)phenyl]-1,2-bis[4-{*N*,*N*-bis(4-methoxyphenyl)amino}phenyl]ethylene (**2**) as a structural isomer of **1** was investigated by means of the electrochemistry and the ESR spectroscopy.

Scheme 1. Redox-switching of through-bond magnetic interaction

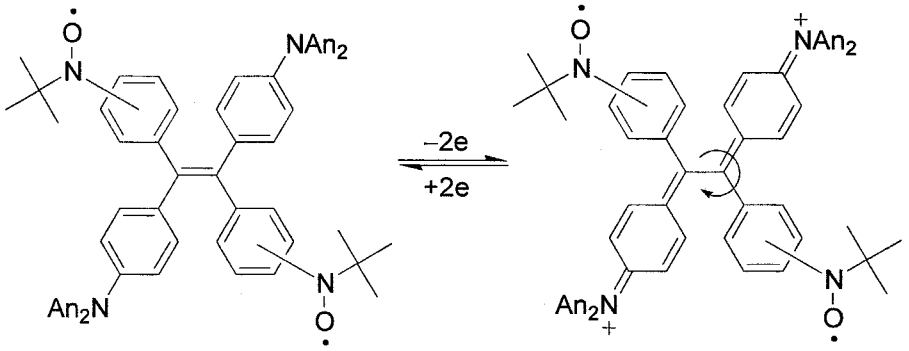

1: *p*,*p*'- **1**$^{2+}$: *p*,*p*'-

2: *m*,*m*'- **2**$^{2+}$: *m*,*m*'-

2.2 Experimental Section

General Methods

^{1}H and ^{13}C spectra were recorded on a JEOL JNM-AL400, JNM-EX400 or JNM-AL300 spectrometer, and chemical shifts are given in parts per million (ppm) relative to internal tetramethylsilane (δ 0.00 ppm). Elemental analyses were performed by Center for Organic Elemental Microanalysis, Kyoto University.

Materials

Toluene and *n*-butyronitrile were distilled from CaH_2 under an argon atmosphere, tetrahydrofuran (THF) was distilled from potassium–benzophenone under an argon atmosphere, *N*,*N*-dimethylformamide (DMF) was dried over molecular sieves 4A, and benzonitrile was dried through alumina (ICN, Alumina N, Akt. I) column with bubbling of argon, just before use. All the other purchased reagents and solvents were used without further purification. Column chromatography was performed using silica gel (Kanto Chemical Co., Inc., Silica gel 60N, spherical neutral).

***N*-3-Bromophenyl-*N*-*tert*-butylhydroxyamine (3).** To a solution of 1,3-dibromobenzene (7.08 g, 30.0 mmof) in THF (100 mL) was added *n*-butyllithium (1.55 M hexane solution, 22.0 mL, 34.1 mmol) at −78 °C under an argon atmosphere. The solution was stirred for 45 min. A solution of 2-methyl-2-nitrosopropane (3.14 g, 36.0 mmol) in THF (50 mL) was dropped for 30 min. The mixture was stirred at −78 °C for 1 h, and then stirred at room temperature for 4 h. To the mixture was added 5 % aqueous ammonium chloride (100 mL). The organic layer was separated and the aqueous layer was extracted with Et_2O. The organic layer was combined and dried over $MgSO_4$. After filtration, the solvent was evaporated. The residue was washed with *n*-hexane and ethyl acetate to give **3** as white solid (4.07 g, 56 %). The filtrate was evaporated to remove solvent and chromatographed on silica gel

(AcOEt:*n*-hexane = 1:9 as eluent). A fraction (R_f = 0.49) afforded **3** as gray solid (1.51 g, 20 %). Total amount of **3** through this reaction was 5.58 g (76 %): ^{1}H NMR (300MHz, $CDCl_3$) δ 7.43–7.42 (m, 1H), 7.24–7.21 (m, 1H), 7.12–7.08 (m, 2H), 6.14 (s, 1H), 1.12 (s, 9H); ^{13}C NMR (75 MHz, $CDCl_3$) δ 150.9, 128.7, 128.0, 127.4, 123.2, 121.3, 60.9, 25.9.

***N*-3-Bromophenyl-*N*-*tert*-butyl-*N*-*tert*-butyldimethylsiloxyamine (4).** To a solution of *tert*-butyldimethylchlorosilane (1.36 g, 9.00 mmol) and imidazole (1.28 g, 18.6 mmol) in DMF (5 mL) was added **3** (1.83 g, 7.50 mmol). The resulting solution was stirred at 40 °C for 16 h under an argon atmosphere. To the mixture was added CH_2Cl_2 and water. The organic layer was separated and the aqueous layer was extracted with CH_2Cl_2. The organic layer was combined and dried over $MgSO_4$. After filtration, the solvent was evaporated. The residue was chromatographed on silica gel (*n*-hexane as eluent) to afford **4** as colorless oil (2.58 g, 96 %): ^{1}H NMR (300MHz, $CDCl_3$) δ 7.41 (br-s, 1H), 7.22–7.03 (m, 3H), 7.24–7.21 (m, 1H), 1.07 (s, 9H), 0.89 (s, 9H), –0.14 (br-s, 6H); ^{13}C NMR (75 MHz, $CDCl_3$) δ 152.7, 128.5, 128.1, 127.7, 123.8, 121.0, 61.2, 26.1, 17.9, –4.7.

3-(*N*-*tert*-Butyl-*N*-*tert*-butyldimethylsiloxyamino)-4'-[bis(4-methoxyphenyl)amino]benzophenone (5). To a solution of **4** (6.18 g, 17.2 mmol) in THF (50 mL) was added *n*-butyllithium (1.55 M hexane solution, 13 mL, 20.2 mmol) at –78 °C under an argon atmosphere. The solution was stirred for 1 h. A solution of bis(4-methoxy phenyl)aminobenzonitrile (6.84 g, 20.7 mmol) in THF (60 mL) was dropped for 30 mim. The mixture was stirred for 1 h at –78 °C, and then stirred at room temperature for 1 h. To the mixture was added water (100 mL) and stirred over night. The organic layer was separated and the aqueous layer was extracted with Et_2O. The organic layer was combined and dried over $MgSO_4$. After filtration, the solvent was evaporated. The residue was chromatographed on silica gel (ethyl acetate:*n*-hexane = 1:4 as eluent) to afford **5** as yellow solid (7.93 g, 75 %): ^{1}H NMR (400MHz, $CDCl_3$) δ 7.64 (d, J = 8.9

Hz, 2H), 7.57 (br-s, 1H), 7.48 (dt, J = 7.3, 1.3 Hz, 1H), 7.42 (br-s, 1H), 7.31 (t, J = 7.7 Hz, 1H), 7.13 (d, J = 8.9 Hz, 4H), 6.88 (d, J = 8.9 Hz, 4H), 6.82 (d, J = 8.9 Hz, 2H), 3.81 (s, 6H), 1.09 (s, 9H), 0.89 (s, 9H), –0.11 (br-s, 6H); ^{13}C NMR (100 MHz, $CDCl_3$) δ 195.0, 156.9, 152.5, 150.7, 139.2, 138.0, 131.9, 128.2, 127.9, 127.8, 127.1, 126.1, 125.9, 116.6, 114.9, 61.1, 55.5, 26.2, 26.1, 18.0, –4.5; ^{1}H NMR (400MHz, C_6D_6) δ 7.97 (br-s, 1H), 7.93 (d, J = 8.8 Hz, 2H), 7.65 (d, J = 7.6, 1H), 7.38 (br-s, 1H), 7.06 (dd, J = 7.8, 7.6 Hz, 1H), 7.00 (d, J = 9.0 Hz, 4H), 6.95 (d, J = 8.8 Hz, 2H), 6.69 (d, J = 9.0 Hz, 4H), 3.28 (s, 6H), 1.05 (s, 9H), 0.97 (s, 9H), 0.00 (br-s, 6H); Anal. Calcd for $C_{37}H_{46}N_2O_4Si$: C, 72.75; H, 7.59; N, 4.59. Found: C, 72.59; H, 7.47; N, 4.51.

1,2-Bis[3-(*N*-*tert*-butyl-*N*-*tert*-butyldimethylsiloxyamino)phenyl]-1,2-bis[4-{*N*, *N*-bis(4-methoxyphenyl)amino}phenyl]ethylene (6). **6** was prepared by low valent titanium induced reductive coupling reaction, using the modified method of literature [4]. $TiCl_4$·2THF complex (4.31 g, 12.5 mmol) was placed in a flask equipped with a reflux condenser and a dropping funnel under argon atmosphere. Dry THF (40 mL) was added at –10 °C in ice-acetone bath. Zinc powder (2.27 g, 31.2 mmol) was added and the resulting mixture was stirred at room temperature for 1 h and refluxed for 3 h. After cooling to –10 °C in ice-acetone bath, dry pyridine (1 mL) was added. **7** (3.06 g, 5.01 mmol) in dry THF (50 mL) was dropped for 20 min. The resulting mixture was refluxed for 16 h. After cooling to room temperature and diluted with CH_2Cl_2, the mixture was poured over cold saturated $NaHCO_3$aq. The suspension was filtered through celite. The organic layer was separated, and the aqueous layer was extracted with CH_2Cl_2. The organic layer was combined and dried over $MgSO_4$. After filtration, the solvent was evaporated. The residue was chromatographed on silica gel (ethyl acetate:CH_2Cl_2:*n*-hexane = 1:29:70 as eluent) to afford **6** as yellow solid (fraction A (**6a**) 1.33g, fraction B (**6b**) 0.37g; total 1.70 g, 57 %, (*E*)/(*Z*) = 78/22): **Fraction A** (**6a**) (*E*)-isomer R_f = 0.33 (silica gel, ethyl acetate:*n*-hexane =1:9); ^{1}H NMR (400MHz, $CDCl_3$) δ 6.80–7.04 (m, 8H), 6.94 (d, J = 9.1, 8H), 6.75 (d, J = 9.1 Hz, 8H), 6.72 (d, J =

8.3 Hz, 4H), 6.55 (d, J = 8.3 Hz, 4H), 3.76 (s, 12H), 0.95 (s, 18H), 0.86 (s, 18H), –0.15 (br-s, 12H); ^{13}C NMR (100 MHz, $CDCl_3$) δ 155.4, 150.5, 146.2, 143.9, 140.8, 139.6, 136.1, 131.9, 128.3, 127.8, 126.5, 126.3, 122.9, 119.3, 114.4, 60.6, 55.5, 26.2, 26.1, 18.0, –4.5; FAB HRMS (*m*-nitrobenzyl alcohol) m/z calcd for $C_{74}H_{93}N_4O_6Si_2$ $[M+H]^+$ 1189.6634, found 1189.6677; Anal. Calcd for $C_{74}H_{92}N_4O_6Si_2$: C, 74.71; H, 7.79; N, 4.71. Found: C, 74.41; H, 7.69; N, 4.61; **Fraction B (6b)** (*Z*)-isomer R_f = 0.20 (silica gel, ethyl acetate:*n*-hexane =1:9); ^{1}H NMR (400MHz, $CDCl_3$) δ 7.01 (d, J = 9.0, 8H), 6.90–6.96 (m, 8H), 6.79 (d, J = 9.0 Hz, 8H), 6.77 (d, J = 8.5 Hz, 4H), 6.67 (d, J = 8.5 Hz, 4H), 3.77 (s, 12H), 0.90 (s, 18H), 0.85 (s, 18H), –0.18 (br-s, 12H); ^{13}C NMR (100 MHz, $CDCl_3$) δ 155.4, 150.4, 146.4, 143.3, 141.0, 139.7, 136.8, 131.9, 128.4, 127.9, 126.5, 126.2, 122.8, 119.8, 114.5, 60.7, 55.5, 26.2 [two kinds of carbon concerning methyl group, –C(CH_3)$_3$, have same chemical sift.], 18.0, –4.5; FAB HRMS (*m*-nitrobenzyl alcohol) m/z calcd for $C_{74}H_{93}N_4O_6Si_2$ $[M+H]^+$ 1189.6634, found 1189.6584; Anal. Calcd for $C_{74}H_{92}N_4O_6Si_2$: C, 74.71; H, 7.79; N, 4.71. Found: C, 74.41; H, 7.79; N, 4.61.

1,2-Bis[3-(*N*-*tert*-butyl-*N*-hydroxyamino)phenyl]-1,2-bis[4-{*N*,*N*-bis(4-methoxy phenyl)amino}phenyl]ethylene (7a). To a solution of **6a** (953 mg, 0.801 mmol) in THF (12 mL) was added tetrabuhylammonium fluoride (1.0 M THF solution, 10 mL, 10 mmol) at 0 °C under argon atmosphere and stirred for 15 min. The reaction mixture was warmed to room temperature and stirred for 2 h. After addition of Et_2O and water, the organic layer was separated, and the aqueous layer was extracted with Et_2O. The organic layer was dried over $MgSO_4$. After filtration, the solvent was evaporated. The orange solid was washed with *n*-hexane and CH_2Cl_2 to give **7a** as yellow solid (181 mg, 23 %). The filtrate was evaporated to remove solvent and chromatographed on silica gel (ethyl acetate:CH_2Cl_2:*n*-hexane = 10:40:50 to 20:30:50 as eluent) to afford **7a** as yellow solid (222 mg, 29 %). Total amount of **7a** through this reaction was 403 mg (52 %): ^{1}H NMR (400MHz, $CDCl_3$) δ 7.05–7.08 (m, 4H), 6.99 (br-s, 2H), 6.95 (d, J

= 9.0 Hz, 8H), 6.85–6.88 (m, 2H), 6.76 (d, J = 9.0 Hz, 8H), 6.72 (d, J = 8.8 Hz, 4H), 6.56 (d, J = 8.8 Hz, 4H), 5.96 (br-s, 2H), 3.76 (s, 12H), 0.96 (s, 18H); ^{13}C NMR (100 MHz, $CDCl_3$) δ 155.4, 148.7, 146.2, 144.0, 140.7, 139.5, 135.8, 131.8, 128.1, 127.5, 126.7, 126.3, 122.1, 119.1, 114.4, 60.3, 55.4, 25.9; Anal. Calcd for $C_{62}H_{64}N_4O_6$: C, 77.47; H, 6.71; N, 5.83; O, 9.99. Found: C, 77.38; H, 6.70; N, 5.75; O, 9.99.

1,2-Bis[3-(*N*-*tert*-butyl-aminoxyl)phenyl]-1,2-bis[4-{*N*,*N*-bis(4-methoxyphenyl) amino}phenyl]ethylene (2a). To a solution of **7a** (222 mg, 0.231 mmol) in CH_2Cl_2 (20 mL) was added Ag_2O (326 mg, 1.39 mmol) and stirred for 2 h at room temperature. The reaction mixture was filtered through celite. The filtrate was evaporated to remove solvent and chromatographed on silica gel (ethyl acetate:CH_2Cl_2:*n*-hexane = 20:30:50 as eluent) to afford **2a** as reddish brown solid (52.8 mg, 24 %): ESR (toluene) 5 lines, g = 2.006, $|a_N|/2$ = 6.9 G.

Electrochemical Measurement

The cyclic voltammetry measurements were carried out in benzonitrile solution containing 0.1 M tetrabutylammonium tetrafluoroborate as a supporting electrolyte (25 °C, scan rate 100 mV/sec) using an ALS/chi Electrochemical Analyzer Model 612A. A three-electrode assembly was used, which was equipped with a platinum disk (2 mm^2), a platinum wire, and Ag/0.01 M $AgNO_3$ (acetonitrile) as the working, the counter, and the reference electrode, respectively. The redox potentials were referenced against ferrocene/ferrocenium (Fc/Fc^+) couple.

ESR Measurement

ESR spectra were recorded on a JEOL JES-SRE2X spectrometer, in which temperature was controlled by a JEOL DVT2 variable-temperature unit, and a Mn^{2+}/MnO solid solution was used as a reference for the determination of g values and hyperfine coupling constants.

2.3 Results and Discussion

2.3.1 Synthesis

The synthesis of bisnitroxide **2** was carried out by the similar route with that of **1**, which is outlined in Scheme 2. Monolithiated 1,3-dibromobenzene was coupled with 2-methyl-2-nitrosopropane to give hydroxylamine **3**. The hydroxylamine **3** was protected with *tert*-butyldimethylsilyl group. Asymmetrically substituted diarylketone **5** was prepared by addition of bis(4-methoxyphenyl)aminobenzonitrile to the lithiated **4** and the subsequent hydrolysis. The reductive coupling of the ketone **5** with a low-valent titanium reagent gave **6a** (*trans*-isomer) and **6b** (*cis*-isomer) at the ratio of **6a**/**6b** = 78/22. Here, we regarded **6a** as the *trans*-isomer because the ESR spectrum for **2a** derived from **6a** indicates that **2a** takes the *trans* configuration (see ESR Section). After desilylation of **6a** with tetrabutylammonium fluoride, the desired bisnitroxide **2a** was obtained of **7a** by oxidation with Ag_2O. Bisnitroxide **2a** was unstable as compared with *para*-nitroxyl substituted **1**. The instability of this kind of nitroxide is ascribed to the isomerization to aminoquinone imine *N*-oxide [5].

2.3.2 Electrochemistry

Effective conversion of intramolecular magnetic interaction after and before oxidation of **2a** postulates a lower oxidation potential of the TPE moiety than the two nitroxide groups. The cyclic voltammogram of **2a** measured in 1 mM benzonitrile solution is shown in Figure 1. In comparison with the first oxidation potentials of the non-nitroxide-substituted TPE (**8**) [6] and the *N*-*tert*-butyl-*N*-phenylnitroxide (**9**) [7], it is concluded that the first quasi two-electron transfer process corresponds to the oxidation of the TPE moiety, while the second irreversible two-electron transfer process to the oxidation of the two nitroxide groups (Table 1). The observed separation of the anodic and cathodic current peaks for the first redox process (68 mV) is larger than the

Scheme 2. Synthetic route for diradical **2**[a].

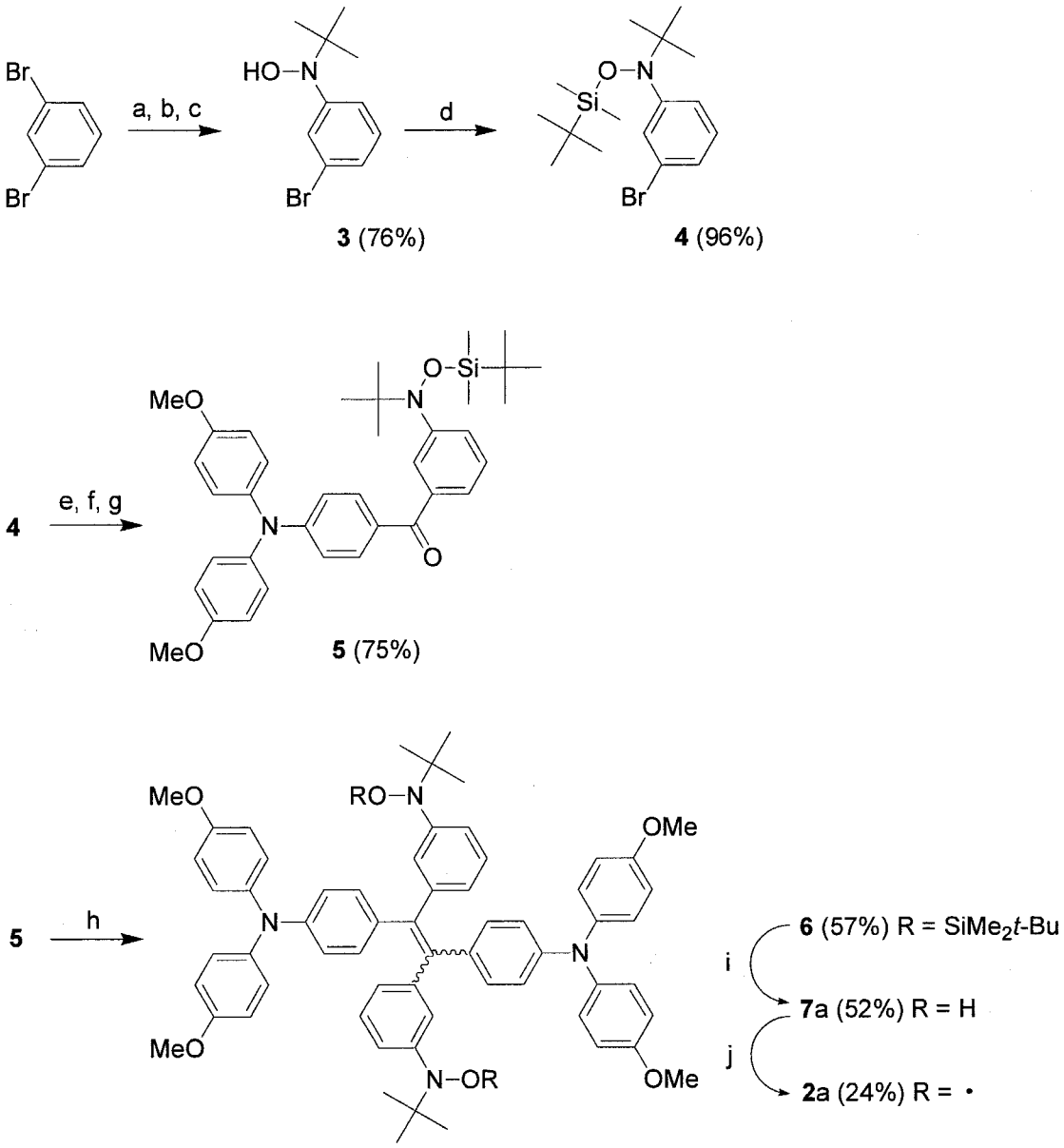

[a]Reagents: (a) *n*-BuLi, THF; (b) *t*-BuNO, THF; (c) aq. NH_4Cl; (d) *t*-$BuMe_2Cl$, imidazole, DMF; (e) *n*-BuLi, THF; (f) bis(4-methoxyphenyl)aminobenzonitrile, THF; (g) H_2O; (h) $TiCl_4$, Zn, pyridine, THF; (i) *n*-Bu_4F, THF; (j) Ag_2O, CH_2Cl_2.

theoretical value of 28 mV for the reversible two-electron transfer process [8]. This indicates that the first oxidation wave for **2a** is an overlap of two closely spaced

consecutive one-electron oxidation processes. The similar redox behavior was also observed for 1,1,2,2-tetrakis(4-methoxyphenyl)ethylene in a polar solvent like acetonitrile [1]. In **2a**, the redox process of the TPE moiety approaches a two-electron transfer, whereas two resolved one-electron transfer redox waves were observed in *para*-nitroxyl substituted **1** (see Chapter 1). This contrast is closely related to the fact that the *para*-substituting nitroxyl groups affect the oxidation process of the TPE moiety through π-conjugation as compared to the *meta*-substituting nitroxyl groups.

Table 1. Redox Potentials of **1** and Related Compounds[a]

	E_1	E_2
1	0.19[b]	0.50[b, c]
8	0.15[b]	
9	0.41[c]	

[a]0.1 M n-Bu_4NBF_4 in PhCN, potential versus Fc/Fc^+, Pt electrode, 298 K, scan rate 100 mV s^{-1}. [b]Quasi two-electron transfer. [c]Anodic peak potential.

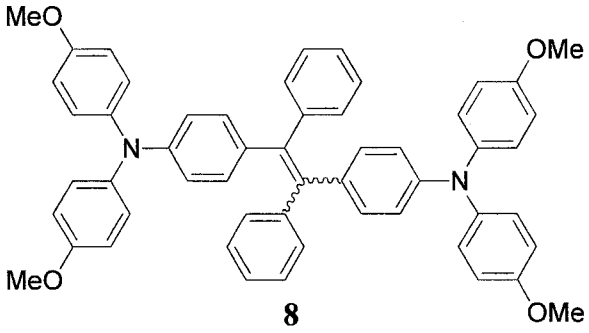

8

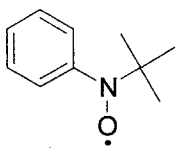

9

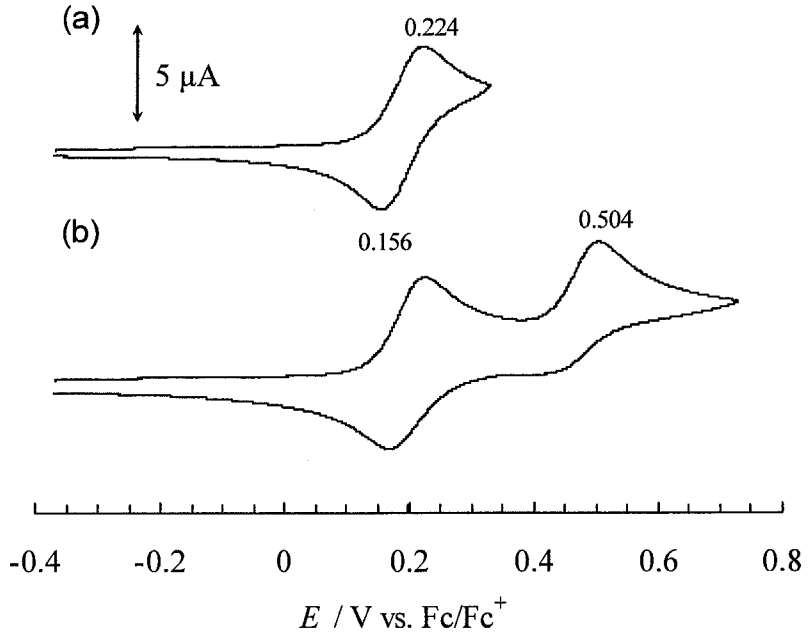

Figure 1. Cyclic voltammograms of **1** in the cases of (a) lower turn-around potential and (b) higher turn-around potential in benzonitrile containing 0.1 M *n*-Bu_4NBF_4 at 298 K, scan rate 100 mV/s.

2.3.3 ESR spectroscopy

The ESR spectrum of **2a** in toluene solution at room temperature showed five lines with 1:2:3:2:1 intensity due to two equivalent nitroxyl nitrogen atoms at $g = 2.006$ with a hyperfine coupling constant $|a_N|/2$ of 6.9 G. The hyperfine coupling constant of **2a** was observed to be slightly larger than that of **9** ($|a_N| = 12.3$ G).

In a frozen toluene solution at 123 K, a unresolved fine-structured spectrum was observed as shown in Figure 2, and the forbidden $\Delta M_S = \pm 2$ resonance was also detected in a half-field region of the allowed $\Delta M_S = \pm 1$ resonance, indicating the spin triplet state. The spectral simulation has been failed so far, which suggest that several conformers with the different parameters have to be considered. However, given that the zero-field splitting parameter (D) is 30.4 G from the separation of the highest and the

lowest field resonances in $g = 2$ region, the average distance between the spin centers was estimated to be 9.7 Å on the basis of the point dipole approximation (eq. 1) [9];

$$D = (3/2)(g\mu_B/r^3) \quad (1)$$

,where g is the isotropic g-factor, μ_B the Bohr magneton and r the average spin-spin distance. On the other hand, the quantum chemical calculations for the model compounds of **2** were carried out at UB3LYP/6-31G* level of theory (see Chapter 3) [10], and the separations of two nitroxyl nitrogen atoms were calculated to be 9.153 and 9.136 Å respectively for the broken-symmetry singlet state and the triplet state of *cis*-isomer; 10.565 and 10.562 Å respectively for the broken-symmetry singlet state and the triplet state of *trans*-isomer. Hence the average interspin distance estimated from the ESR spectrum is somewhat longer than the calculated one between two nitroxyl nitrogen atoms for *cis*-isomer, and is shorter than that for *trans*-isomer. However, it should be noted that the value estimated from the ESR spectrum is shorter than the distance between the two nitrogen atoms because spin density on the nitroxyl moieties is delocalized to some extent over the benzene rings. Therefore, it follows from what has been described that **2a** is *trans*-isomer.

On the other hand, when 2 equiv. of tris(4-bromophenyl)aminium hexachloro antimonate are added to **2a** in *n*-butyronitrile solution at 195 K, the ESR spectrum of $\mathbf{2a}^{2+}$ completely changed from the one observed for neutral **2a** to the one with the typical anisotropic hyperfine structure for the randomly oriented *N*-phenyl-*N*-*tert*-butylnitroxide radical (Figure 3). The principal value (A_{ZZ}) for the perpendicular direction to the nitroxide plane of the hyperfine coupling tensor of $\mathbf{2a}^{2+}$ is estimated to be 27.3 G [11]. This strongly indicates that the two nitroxyl groups in $\mathbf{2a}^{2+}$ are no longer coupled magnetically. Indeed, as confirmed by DFT calculations for the model compound of *transoid* $\mathbf{2a}^{2+}$ at the UB3LYP/6-31G* level, the optimized

geometry, irrespective of the spin state, showed a highly distorted conformation around the olefinic bond: the bond length and the torsion angle about the olefinic bond were 1.471 Å and 40.8° for the broken-symmetry singlet state, and 1.474 Å and 41.7° for the triplet state.

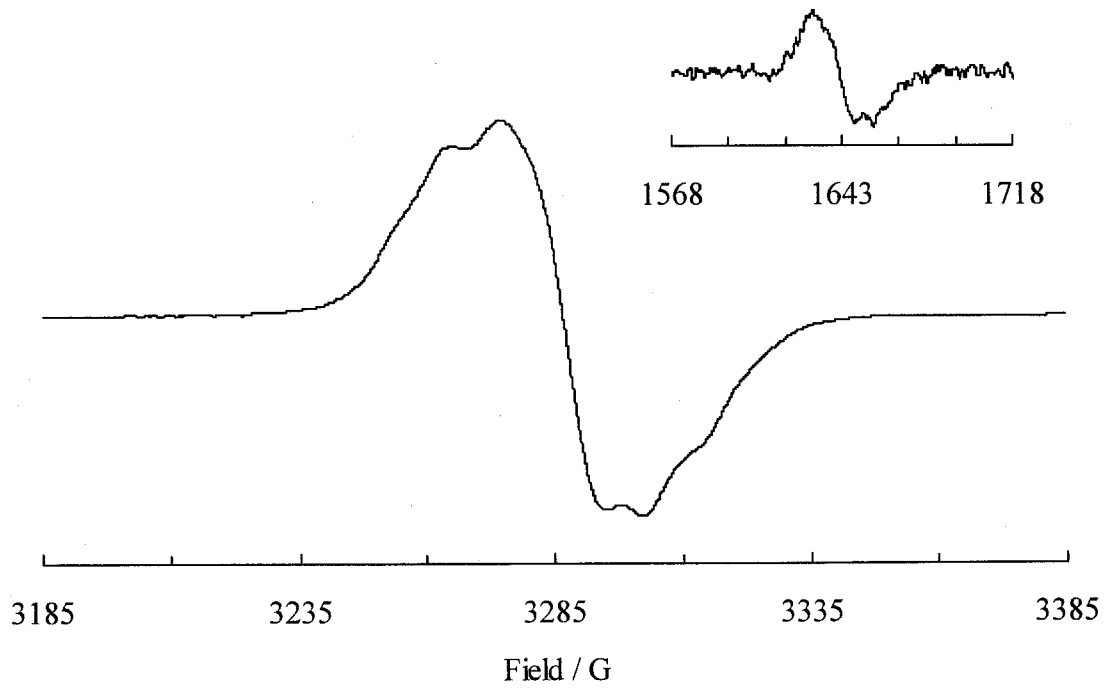

Figure 2. EPR spectra of **2a** in frozen toluene solution at 123 K and the forbidden $\Delta M_S = \pm 2$ resonance at 123 K (inset).

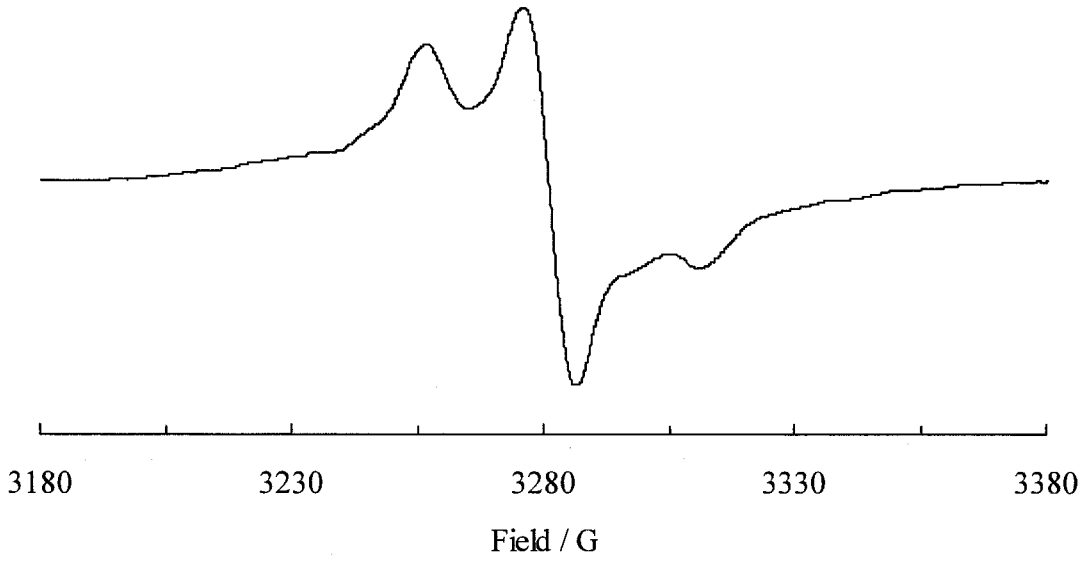

Figure 3. EPR spectrum of **2a** after treatment with 2 equiv. of tris(4-bromophenyl)aminium hexachloroantimonate in *n*-butyronitrile at 123 K.

2.4 Conclusion

Diradical **2a** having nitroxyl groups at the *meta*-position was prepared by applying the synthetic method of **1**, and was found to be *trans*-isomer on the basis of the average spin–spin distance estimated from the ESR spectrum. The cyclic voltammetry showed the core tetraphenylethylene moiety has the lower oxidation potential than the substituted nitroxide moiety. However, the first redox wave corresponding to TPE moiety of **2a** was unresolved in contrast with **1** showing two distinct one-electron transfer processes. It was also found by ESR measurement in frozen solution that the neutral diradical **2a** showed the fine-structured spectrum characteristic for the spin triplet species, while **2a** after treatment with 2 equiv. of tris(4-bromophenyl)aminium hexachloroantimonate showed the anisotropic hyperfine-structured spectrum typical of the randomly oriented mononitroxide radical, indicating the drastic change of intramolecular magnetic interaction, as is the case of *para*-nitroxyl substituted **1**.

These results strongly suggest that the present diradical **2a** can operate as a redox-switchable intramolecular magnetic interaction converting system like the *para*-nitroxyl substituted **1**. However, it was found that the diradical **2a** shows the different electrochemical behavior from the diradical **1** owing to the difference of substitution patterns of the nitroxyl groups.

References

[1] J. Phelps, A.J. Bard, J. Electroanal. Chem. 68 (1976) 313.

[2] R. Rathore, S.V. Lindeman, A.S. Kumar, J.K. Kochi, J. Am. Chem. Soc. 120 (1998) 6931.

[3] (a) K. Matsuda, M. Irie, Chem. Lett. (2000) 16; (b) K. Matsuda, M. Irie, Tetrahedron Lett. 41 (2000) 2577; (c) K. Matsuda, M. Irie, J. Am. Chem. Soc. 122 (2000) 7195; (d) K. Matsuda, M. Irie, Mol. Cryst. Liq. Cryst. 345 (2000) 479; (e) K. Matsuda, M. Irie, J. Am. Chem. Soc. 122 (2000) 8309; (f) K. Matsuda, M. Irie, Polyhedron 20 (2000) 1391; (g) K. Matsuda, M. Matsuo, M. Irie, Chem. Lett. (2001) 436; (h) K. Matsuda, M. Irie, Chem. Eur. J. 7 (2001) 3466; (i) K. Matsuda, M. Irie, J. Am. Chem. Soc. 123 (2001) 9896; (j) K. Matsuda, M. Matsuo, M. Irie, J. Org. Chem. 66 (2001) 8799; (k) K. Matsuda, M. Matsuo, S. Mizoguti, K. Higashiguchi, M. Irie, J. Phys. Chem. B 106 (2002) 11218.

[4] I. Agranat, S. Cohen, R. Isaksson, J. Sandström, M.R. Suissa, J. Org. Chem. 55 (1990) 4943.

[5] A. Calder, A.R. Forrester, P.G. James, G.R. Luckhurst, J. Am. Chem. Soc. 91 (1969) 3724.

[6] Compound **8** was prepared from 4-bis(4-methoxyphenyl)aminophenyl phenyl ketone by using the Mukaiyama method. T. Mukaiyama, T. Sato, J. Hanna, Chem. Lett. (1973) 1041.

[7] H. Lemaire, Y. Marechel, R. Ramasseul, A. Rassat, Bull. Soc. Chim. France (1965) 372.

[8] D. K. Gosser, Jr., *Cyclic Voltammetry Simulation and Analysis of Reaction Mechanisms*; VCH: New York, 1993.

[9] N. Hirota, J. Am. Chem. Soc. 89 (1967) 32.

[10] GAUSSIAN 98 (Revision A.9) program was used for the present DFT calculations.

[11] (a) O.H. Griffith, P.W. Cornell, H.M. McConnell, J. Chem. Phys. 43 (1965) 2909; (b) O. Takizawa, J. Yamauchi, H. Ohya-Nishiguchi, Y. Deguchi, Bull. Chem. Soc. Jpn. 46 (1973) 1991.

Chapter 3

Intramolecular Magnetic Interaction Controlled by Redox Reaction of Tetraphenylethylene-Based Spin System

3.1 Introduction

A molecular-level switch can be expected to play a fundamental role in the future molecular electronic/photonic devices. For instance, when spin-bearing moieties are incorporated into a molecular system showing a reversible structural change in response to some external stimuli, the intramolecular magnetic interaction can be switched on and off. Recently, Matsuda *et al.* have reported the photoswitching of intramolecular magnetic interaction between two nitronyl nitroxide radicals [1].

To achieve effective redox switching of intramolecular magnetic interaction, we focused on a remarkable structural change of tetraphenylethylene upon the redox input. When tetraphenylethylene is oxidized to the cation or the dication, the ethylenic C–C double bond is lengthened to have a single bond character, and concomitantly the torsional angle around the ethylenic bond takes place. Such a structural change was confirmed by Kochi *et al.* [2]. The tetraphenylethylene derivatives with two

tert-butylnitroxide radicals have been designed, 1,2-bis[x-(*N*-*tert*-butylaminoxyl) phenyl]-1,2-bis [4-{*N*,*N*-bis(4-methoxyphenyl)amino}phenyl]ethylene (x = 4, *p*,*p*'-**1**; x = 3, *m*,*m*'-**1**), as a redox-switchable system. In the neutral form (Scheme 1, left) a strong intramolecular magnetic interaction exists between two nitroxide radicals through π-conjugation, whereas the spin-spin correlation in the dication form disappears due to the torsional motion (Scheme 1, right). In this chapter, the author examined the electronic structure of the neutral and dicationic forms for the model compounds of *p*,*p*'-**1** and *m*,*m*'-**1** on the basis of quantum chemical calculations.

Scheme1. Redox switching of intramolecular magnetic interaction.

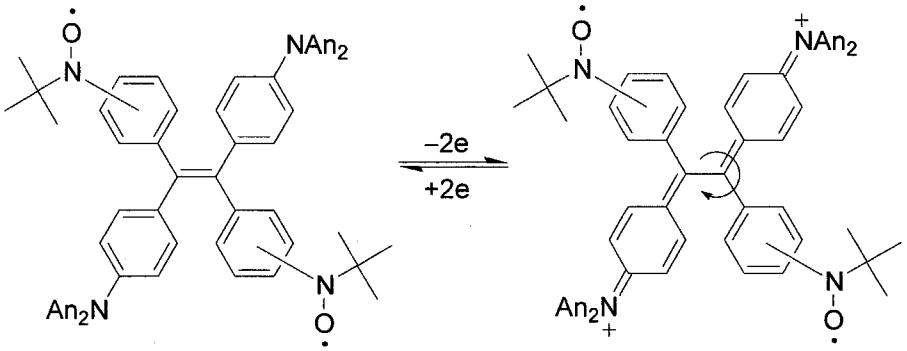

p,*p*'-**1**
m,*m*'-**1**

p,*p*'-$\mathbf{1}^{2+}$
m,*m*'-$\mathbf{1}^{2+}$

An = *p*-$CH_3OC_6H_4$

3.2 Computational Details

For the simplified model compounds, *p*,*p*'-**2** and *m*,*m*'-**2**, where all the *tert*-butyl and anisyl groups of *p*,*p*'-**1** and *m*,*m*'-**1** were replaced with hydrogen atoms, the hybrid HF/DF (UB3LYP) calculations were performed with the 6-31G* basis set. Full

geometry optimizations were carried out in C_2 symmetry. For the calculation of the open-shell singlet state, the broken-symmetry state corresponding to a 50:50 singlet-triplet wave function was calculated, and hereafter such a spin state is referred to as "bs-singlet state". All of the computations were carried out with Gaussian 98 program package.

3.3 Results and Discussion

First of all, the geometry optimization on the *cis*- and *trans*-isomers of *p,p'*-**2** and *m,m'*-**2**, and on the *cisoid* and *transoid* conformers of *p,p'*-$\mathbf{2}^{2+}$ and *m,m'*-$\mathbf{2}^{2+}$ for the triplet and bs-singlet states were performed at the UB3LYP/6-31G* level. The *trans* (or *transoid*) form was found to be stable as compared with the corresponding *cis* (or *cisoid*) form (Figure 1). The atomic numbering and the structural parameters of *p,p'*-**2** and *m,m'*-**2** are defined as shown in Figure 2. The optimized bond lengths, the quinoidal distortion (q), the ethylenic torsional angle (θ), the aryl groups' dihedral angle from the ethylenic plane (φ_1, φ_2) are shown in Table 1.

In the neutral states of *p,p'*-**2** and *m,m'*-**2**, the *cis*- and *trans*-isomers were found to be energetically competing. More noteworthy is that the geometrical accordance between the both isomers except the ethylenic torsional angle (θ) was seen within a discrepancy of 0.001 Å and 2.0° [θ = 194.7° (triplet) and 195.7° (bs-singlet) for *cis-p,p'*-**2**; 193.5° (triplet) and 193.5° (bs-singlet) for *cis-m,m'*-**2**]. Consequently, the similar electronic structures were obtained for the both isomers. Hence, from now on, only the results of the *trans*-isomer are described to avoid repetition. On the other hand, in the oxidized states (*p,p'*-$\mathbf{2}^{2+}$ and *m,m'*-$\mathbf{2}^{2+}$), the spin preference was contrary between the both isomers. In *p,p'*-$\mathbf{2}^{2+}$, it was found that the bs-singlet *transoid* form competes with the excited triplet *cisoid* one. Therefore, we mention the both isomers

of *p,p'*-$\mathbf{2}^{2+}$ in the following discussion. As for *m,m'*-$\mathbf{2}^{2+}$, only the *transoid* form is taken into consideration, because the *cisoid* form lies about 0.5 kcal/mol above the *transoid* one.

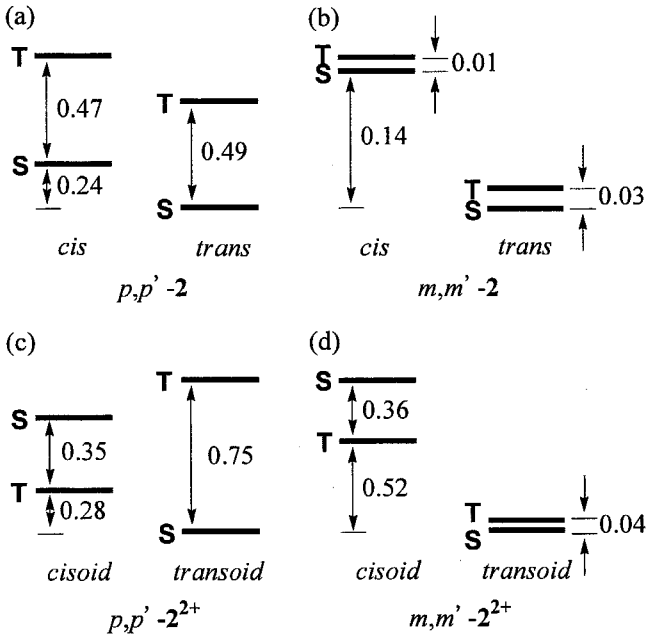

Figure 1. Schematic diagrams of relative energies between two conformers and their spin states for *p,p'*-**2** (a), *m,m'*-**2** (b), *p,p'*-$\mathbf{2}^{2+}$ (c), and *m,m'*-$\mathbf{2}^{2+}$ (d). **T** and **S** represent the triplet and bs-singlet states, respectively. The relative energies are in kcal mol^{-1}.

Here, the quinoidal parameter (q) was evaluated using eq. (1) (ref. [2]);

$$q\ (\%) = 100\ (d_1 - d_2)/(d_1' - d_2') \qquad (1)$$

,where d_1 is the average of the optimized bond lengths, C_9–C_{10} and C_9–C_{12} (ring A) or C_3–C_4 and C_3–C_6 (ring B), d_2 is the average of optimized bond lengths, C_{10}–C_{11} and C_{12}–C_{13} (ring A) or C_4–C_5 and C_6–C_7 (ring B), d_1' and d_2' are taken from the bond lengths of *p*-benzoquinone optimized at the B3LYP/6-31G* level (d_1' = 1.486 Å and d_2' = 1.343 Å).

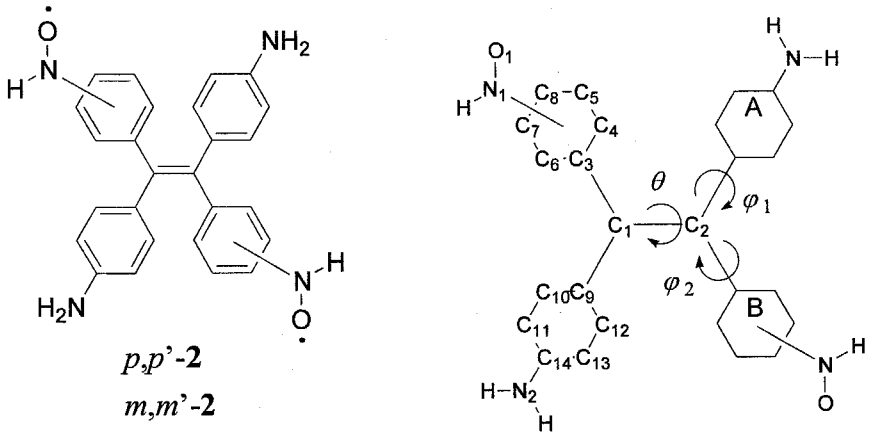

Figure 2. Definition of the atomic numbering and the structural parameters of *p*,*p*'-**2** and *m*,*m*'-**2**. The benzene rings substituted with amino and aminoxyl group are referred to as ring A and B, respectively.

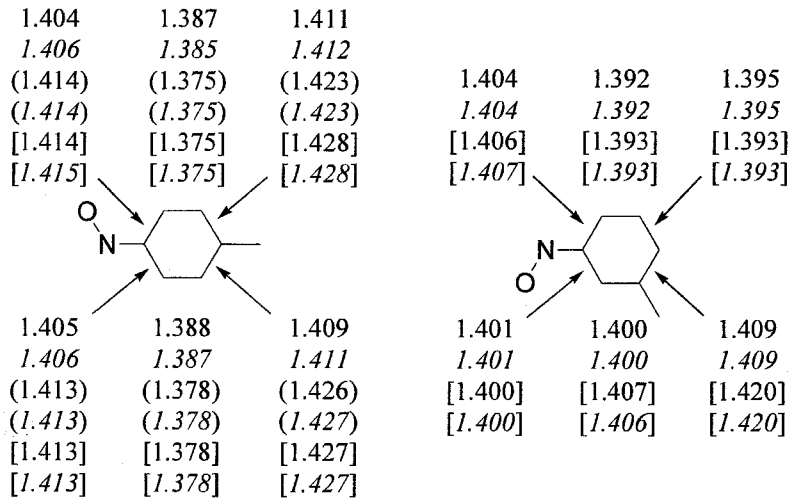

Figure 3. The optimized bond lengths (Å) in aminoxyl-substituted benzene ring for the triplet and bs-singlet (italics) states of *p,p'*-**2** (*trans*), *p,p'*-$\mathbf{2}^{2+}$ (*cisoid* in ( ) and *transoid* in [ ]), *m,m'*-**2** (*trans*) and *m,m'*-$\mathbf{2}^{2+}$ (*transoid* in [ ]).

In the neutral *p,p'*-**2**, the C_3–C_4 (C_3–C_6) bond length is longer than the C_4–C_5 (C_6–C_7) in contrast to the neutral *m,m'*-**2** (Figure 3). This indicates moderate quinoidal distortion in ring B of *p,p'*-2. Note that a remarkable quinoidal distortion was observed in *p*-phenylenebis(*N-tert*-butylaminoxyl) [3]. Apparently, the ethylenic bond lengths (C_1–C_2) are lengthened and the ethylenic torsinal angles (θ) increase on going from the neutral form to the dicationic one. These structural changes are similar to those seen in the related compound [2]. Moreover, such a structural change is accompanied with the increasing of the quinoidal distortion (q) and the decreasing of the dihedral angles (φ_1, φ_2). This result indicates the *geminal* benzene rings, A and B, in *p,p'*-$\mathbf{2}^{2+}$ and *m,m'*-$\mathbf{2}^{2+}$ take a coplanar conformation to cause the increasing of the steric repulsion between *ortho*-hydrogen atoms of the two diarylmethine groups. This leads to the drastic structural changes of *p,p'*-**2** and *m,m'*-**2** upon oxidation. The remarkable difference between *p,p'*-$\mathbf{2}^{2+}$ and *m,m'*-$\mathbf{2}^{2+}$ lies in the contribution of

π-conjugation of the benzene ring B with the nitroxide group. In *p,p'*-$\mathbf{2}^{2+}$, the quinoidal distortion of the benzene ring B is conspicuous (Table 1). On the other hand, such a distortion is not anticipated in *m,m'*-$\mathbf{2}^{2+}$ due to *meta*-substitution of the nitroxide group.

Table 1. Optimized Bond Lengths (Å) and Structural Parameters, q (%), θ (°), φ_1 (°) and φ_2 (°) for *p,p'*-**2**, *p,p'*-$\mathbf{2}^{2+}$, *m,m'*-**2** and *m,m'*-$\mathbf{2}^{2+}$

	p,p'-**2** (*trans*)		*p,p'*-$\mathbf{2}^{2+}$ (*cisoid*)		*p,p'*-$\mathbf{2}^{2+}$ (*transoid*)	
	triplet	bs-singlet	triplet	bs-singlet	triplet	bs-singlet
C_1–C_2	1.373	1.376	1.479	1.483	1.489	1.476
C_1–C_3	1.491	1.487	1.449	1.448	1.447	1.450
$C_8(C_7)$–N_1[a]	1.394	1.391	1.378	1.378	1.378	1.378
N_1–O_1	1.277	1.277	1.257	1.256	1.258	1.255
C_1–C_9	1.491	1.491	1.430	1.429	1.426	1.431
C_{14}–N_2	1.396	1.396	1.340	1.340	1.339	1.341
q_A (%)	11.9	12.0	46.0	45.8	46.9	45.3
q_B (%)	15.7	17.7	35.4	35.3	35.8	35.8
θ (°)	15.0	15.9	226.7	227.2	49.4	45.0
φ_1 (°)	46.5	46.8	25.7	25.8	25.5	27.3
φ_2 (°)	44.8	43.0	31.4	30.8	29.3	30.1

[a] C_8–N_1 for *p,p'*-**2** and *p,p'*-$\mathbf{2}^{2+}$ and C_7–N_1 for *m,m'*-**2** and *m,m'*-$\mathbf{2}^{2+}$.

Table 1. Continued.

	m,m'-**2** (*trans*)		*m,m'*-$\mathbf{2}^{2+}$ (*transoid*)	
	triplet	bs-singlet	triplet	bs-singlet
C_1–C_2	1.369	1.369	1.474	1.471
C_1–C_3	1.497	1.496	1.471	1.472
$C_8(C_7)$–N_1[a]	1.398	1.398	1.394	1.394
N_1–O_1	1.277	1.277	1.267	1.266
C_1–C_9	1.490	1.490	1.418	1.420
C_{14}–N_2	1.397	1.397	1.335	1.335
q_A (%)	11.8	11.8	53.0	52.4
q_B (%)				
θ (°)	13.7	13.8	41.7	40.8
φ_1 (°)	45.9	45.9	23.8	24.2
φ_2 (°)	48.1	48.0	34.8	34.7

To realize the redox switching of intramolecular magnetic interaction in *p,p'*-**2** and *m,m'*-**2**, the electron should be removed from the ethylene moiety. In other words, the energy level of the HOMO distributed over the ethylene moiety must locate above the energy levels of the singly occupied MOs (SOMOs) localized over the nitroxide groups. The relative energy levels of the frontier orbitals and their MO patterns for the triplet *p,p'*-**2** and *m,m'*-**2** are shown in Fig. 4. It was found that the HOMO levels are higher by 0.68 eV for *p,p'*-**2** and 0.22 eV for *m,m'*-**2** than the two SOMOs (SOMO1, SOMO2). These results strongly suggest that the first oxidation process occurs from the ethylene moiety. The energy difference between α-HOMO and β-HOMO of *p,p'*-**2** was larger than that of *m,m'*-**2**. This indicates that the spin polarization effect in *p,p'*-**2** is stronger than that in *m,m'*-**2**. In other words, the π-conjugated system of tetraphenylethylene can be more perturbed by *para*-substitution of the nitroxide group than by *meta*-substitution. In fact, the energy level of the HOMO in *p,p'*-**2** is raised by *para*-substitution of the nitroxide group, owing to the out-of-phase orbital interaction. On the other hand, the HOMO in *m,m'*-**2** has almost no orbital coefficients at the *meta*-substituted carbon atom, indicating negligible orbital interaction.

In order to estimate the magnetic interaction, the effective exchange integral (*J*) was calculated using Yamaguchi's formula (eq. (2)) [4];

$$J = (E_{LS} - E_{HS})/(\langle S^2 \rangle_{HS} - \langle S^2 \rangle_{LS}) \quad (2)$$

where E_{LS} and E_{HS} are the total energies calculated for the low and high spin states, and $\langle S^2 \rangle_{HS}$ and $\langle S^2 \rangle_{LS}$ are the expectation values of total spin angular momentum calculated for the high and low spin states. Table 2 summarizes the relative energies (ΔE_{S-T}), $\langle S^2 \rangle$ values and the effective exchange integrals (*J*). As a result, it was found that *p,p'*-**2** has a strong antiferromagnetic interaction in comparison with *m,m'*-**2**. On the other hand, the calculated *J* values for *m,m'*-**2** and *m,m'*-$\mathbf{2}^{2+}$ were found to be

small.

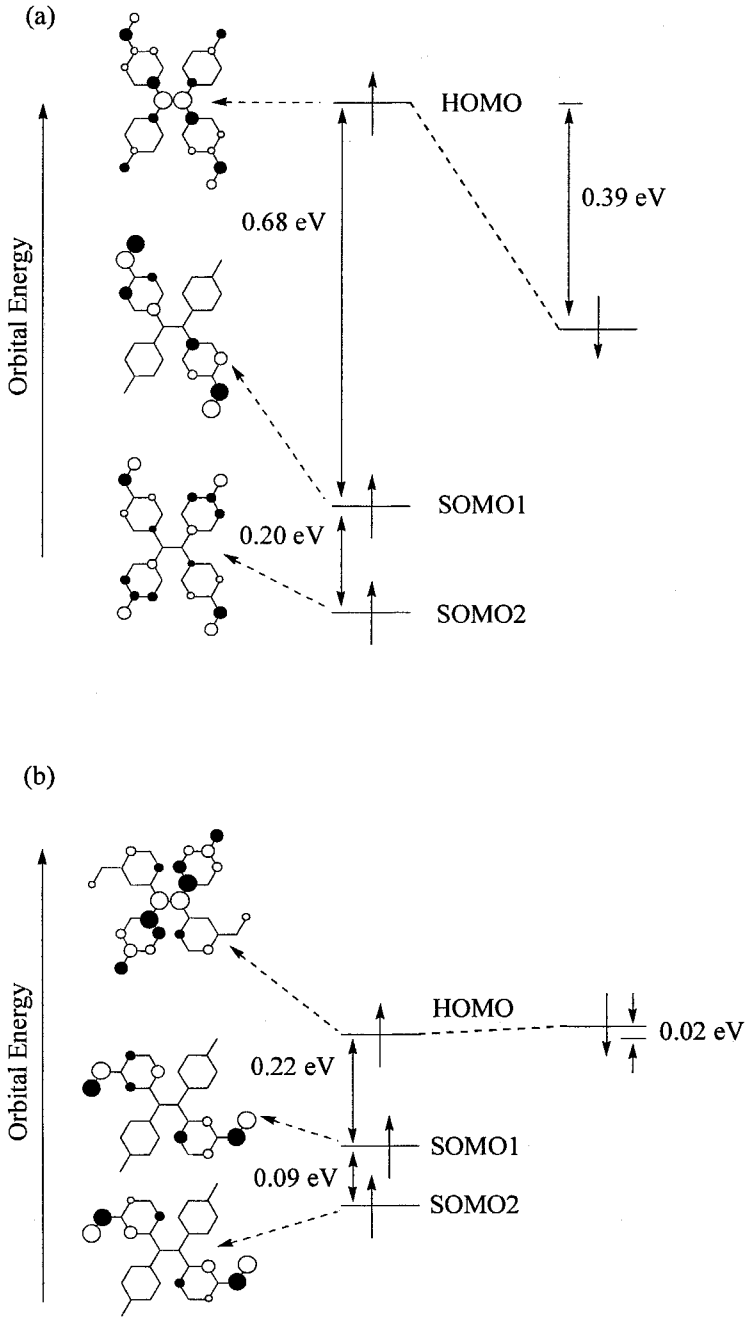

Figure 4. The relative energy levels of the frontier orbitals and the MO patterns for the triplet *p*,*p*'-**2** (a) and *m*,*m*'-**2** (b).

Table 2. Calculated Relative Energies (ΔE_{S-T}), $<S^2>$ Values and Effective Exchange Integrals (J) for *p,p'*-**2**, *p,p'*-$\mathbf{2}^{2+}$, *m,m'*-**2** and *m,m'*-$\mathbf{2}^{2+}$

	ΔE_{S-T} (cal mol^{-1})[a]	$<S^2>_T$	$<S^2>_S$	J (cm^{-1})
p,p'-**2** (*trans*)	−485.1	2.028	1.033	−170.6
p,p'-$\mathbf{2}^{2+}$ (*cisoid*)	+350.0	2.098	1.046	+116.4
p,p'-$\mathbf{2}^{2+}$ (*transoid*)	−749.3	2.078	1.042	−253.0
m,m'-**2** (*trans*)	−29.4	2.027	1.029	−10.3
m,m'-$\mathbf{2}^{2+}$ (*transoid*)	−44.6	2.037	1.030	−15.5

[a]Energy relative to the triplet state, where the negative value means the triplet state is higher in energy than the singlet state.

To explain the magnitude of the calculated effective integrals for the neutral forms, *p,p'*-**2** and *m,m'*-**2**, we focused on their resonance structures. We cannot ignore contribution of the closed-shell quinoid structure (Scheme 2), whereas *m,m'*-**2** has no contribution from such a structure. In other words, *p,p'*-**2** is regarded as a Kekulé molecule, *m,m'*-**2** as a non-Kekulé one. Furthermore, two SOMOs in the bs-singlet state of *m,m'*-**2** do not overlap in their spatial distributions. In this case (*disjoint* in Borden's terminology [5]), *m,m'*-**2** exhibits weak exchange interaction. Therefore, a large antiferromagnetic interaction is expected for *p,p'*-**2** having a Kekulé structure, while a weak magnetic interaction for *m,m'*-**2** having a *disjointed* non-Kekulé structure. For *m,m'*-$\mathbf{2}^{2+}$, the *disjointed* non-Kekulé structure is maintained, and therefore, a weak antiferromagnetic interaction is anticipated like *m,m'*-**2**. On the other hand, the spin preference in $\mathbf{2}^{2+}$ depends sensitively on the torsional angle like tetramethyleneethane, in which the CI calculations showed the triplet ground state for the twisted structure (θ = 59°) and the singlet ground state for the planar (θ = 0°) and perpendicular (θ = 90°) structures [6, 7].

Scheme 2. Resonance structures of *p,p'*-**2**.

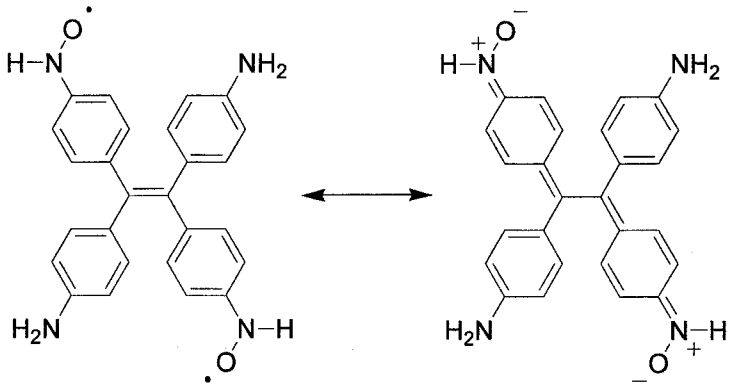

Calculated spin densities are listed in Table 3. The difference in strength of the antiferromagnetic interaction between *p,p'*-**2** and *m,m'*-**2** can be explained by the degree of the spin polarization. In fact, the spin density on C_1 atom for *p,p'*-**2** is larger than that for *m,m'*-**2**, indicating a strong antiferromagnetic interaction in *p,p'*-**2**. In the dicationic form, the spin densities on nitrogen atoms of the nitroxide groups remarkably decrease as compared to those in the neutral form. In addition, the spin densities are delocalized over the aminophenyl groups (ring A). This tendency is stronger in *p,p'*-$\mathbf{2}^{2+}$ than in *m,m'*-$\mathbf{2}^{2+}$.

Table 3. Calculated Spin Densities on *p,p'*-**2**, *p,p'*-$\mathbf{2}^{2+}$, *m,m'*-**2** and *m,m'*-$\mathbf{2}^{2+}$ for the Triplet and Singlet States

	p,p'-**2**		*p,p'*-$\mathbf{2}^{2+a}$		*p,p'*-$\mathbf{2}^{2+b}$		*m,m'*-**2**		*m,m'*-$\mathbf{2}^{2+}$	
	T^{c}	$S^{c,d}$	T^{c}	$S^{c,d}$	T^{c}	$S^{c,d}$	T^{c}	$S^{c,d}$	T^{c}	$S^{c,d}$
O_1	0.52	0.51	0.50	0.50	0.51	0.49	0.53	0.53	0.53	0.52
N_1	0.34	0.33	0.17	0.17	0.18	0.17	0.35	0.35	0.28	0.27
N_2	0.00	0.00	0.09	0.07	0.08	0.08	0.00	0.00	0.02	0.02
C_1	0.01	0.11	0.04	0.05	0.04	0.03	0.00	0.03	0.05	0.00
C_3	0.14	0.16	0.03	0.03	0.05	0.03	0.07	0.07	0.05	0.05
C_4	0.07	0.09	0.03	0.03	0.03	0.04	0.14	0.14	0.06	0.03
C_5	0.13	0.14	0.08	0.07	0.08	0.08	0.07	0.08	0.04	0.02
C_6	0.07	0.09	0.02	0.02	0.02	0.02	0.14	0.14	0.18	0.17
C_7	0.13	0.14	0.06	0.07	0.07	0.06	0.11	0.11	0.09	0.08
C_8	0.11	0.13	0.08	0.07	0.08	0.08	0.13	0.13	0.05	0.02
C_9	0.00	0.02	0.08	0.05	0.06	0.07	0.00	0.00	0.01	0.03
C_{10}	0.00	0.01	0.00	0.01	0.01	0.00	0.00	0.00	0.01	0.00
C_{11}	0.00	0.00	0.03	0.01	0.02	0.03	0.00	0.00	0.01	0.01
C_{12}	0.00	0.01	0.01	0.01	0.00	0.00	0.00	0.00	0.01	0.00
C_{13}	0.00	0.00	0.02	0.02	0.03	0.02	0.00	0.00	0.01	0.00
C_{14}	0.00	0.01	0.04	0.04	0.04	0.04	0.00	0.00	0.02	0.01

[a]*cisoid* form. [b]*transoid* form. [c]T and S represent the triplet and bs-singlet states, respectively. [d]In the bs-singlet state, the spin densities on two atoms related by C_2 symmetry have the same magnitude but the opposite sign. The negative spin densities are underlined.

2.4 Conclusion

The UB3LYP calculations showed that the change from neutral to dicationic state induces the molecular structural change such as that the ethylenic bond lengths are lengthened and the ethylenic torsinal angles increase and that the intramolecular magnetic interaction of *p,p'*-**2** is different from that of *p,p'*-$\mathbf{2}^{2+}$, indicating that *p,p'*-**1** can be a promising candidate for a redox-switching of intramolecular magnetic interaction. It was also found that the electronic structures are different due to the substitution patterns of nitroxyl groups, i.e., the π-conjugated system is more perturbed by *para*-substitution of the nitroxide group than by *meta*-substitution.

References

[1] K. Matsuda, M. Irie, J. Am. Chem. Soc. 122 (2000) 8309.

[2] R. Rathore, S.V. Lindeman, A.S. Kumar, J.K. Kochi, J. Am. Chem. 120 (1998) 6931.

[3] S. Nakazono, S. Karasawa, N. Koga, H. Iwamura, Angew. Chem. Int. Ed. Engl. 37 (1998) 1550.

[4] K. Yamaguchi, H. Fukui, T. Fueno, Chem. Lett. (1986) 625.

[5] W.T. Borden, E.R. Davidson, J. Am. Chem. Soc. 99 (1997) 4587.

[6] P. Nachtigall, K.D. Jordan, J. Am. Chem. Soc. 115 (1993) 270.

[7] E.P. Clifford, P.G. Wenthold, W.C. Lineberger, G.B. Ellison, C.X. Wang, J.J. Grabowski, F. Vila, K.D. Jordan, J. Chem. Soc., Perkin Trans. 2 (1998) 1015.

Chapter 4

Synthesis and Intramolecular Magnetic Interaction of Triphenylamine Derivatives with Nitronyl Nitroxide Radicals

4.1 Introduction

In the field of molecular devices and machines, much attention has been given to the switchable spin system controlled by external stimuli [1]. In addition, redox active molecular systems can be expected to play a fundamental role in the construction of single molecular transistors [2-4]. For example, the switching of spin state [5, 6] or spin distribution [7] has been accomplished by using multi-redox processes. Moreover, the switching of intramolecular magnetic interaction by the photochromic reaction has been realized [8]. Recently, arylamines have been widely employed as hole transport materials [9]. In particular, triphenylamine derivatives are regarded as basic compounds to generate aminium cation radicals easily by chemical and electrochemical oxidations [10]. The triphenylamine derivatives substituted by redox-active groups have been synthesized so far in conjunction with high spin chemistry and chromophore chemistry [11-14]. The triphenylamine derivatives

bearing nitronyl nitroxide radicals, **1** and **2**, were designed. When the aminium radical cation is generated by one electron oxidation of these molecules, the peripherally substituted nitronyl nitroxide radicals can be expected to couple ferromagnetically to the generated aminium cation radical (Scheme 1). In this chapter, the syntheses of triradical **1** and diradical **2** and its electrochemical and magnetic properties are reported in detail.

Scheme 1.

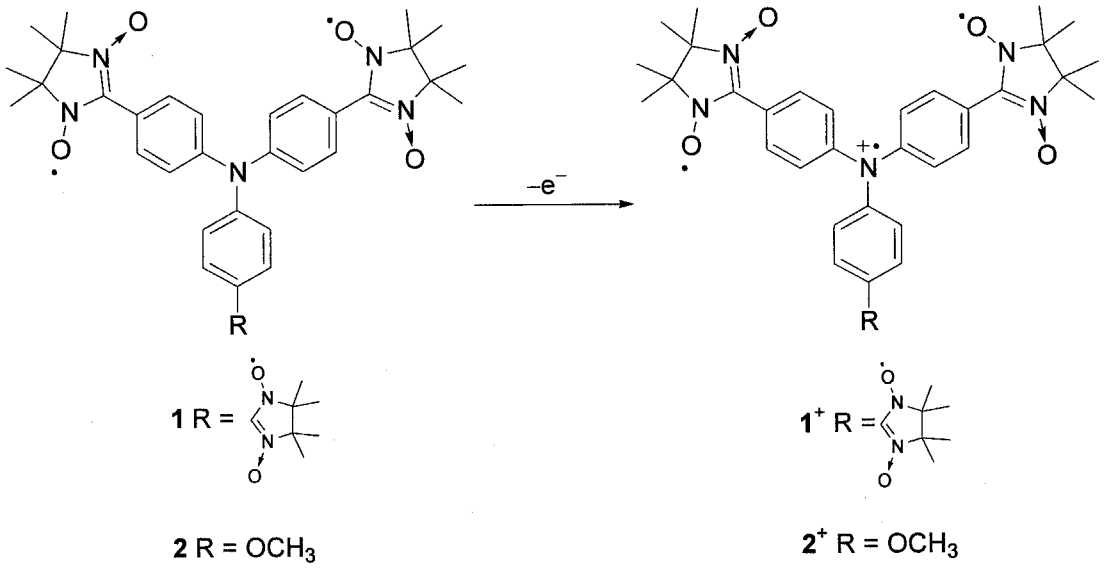

4.2 Experimental Section

General Methods

^{1}H and ^{13}C spectra were recorded on a JEOL JNM-AL400, JNM-EX400 or JNM-AL300 spectrometer, and chemical shifts are given in parts per million (ppm) relative to internal tetramethylsilane (δ 0.00 ppm). IR spectra were recorded using

KBr disks on a JASCO FT/IR-460Plus spectrometer. Elemental analyses were performed by Center for Organic Elemental Microanalysis, Kyoto University.

Materials

Toluene and *n*-butyronitrile were distilled from CaH_2 under an argon atmosphere, tetrahydrofuran (THF) was distilled from potassium–benzophenone under an argon atmosphere, *N*,*N*-dimethylformamide (DMF) was dried over molecular sieves 4A, and benzonitrile was dried through alumina (ICN, Alumina N, Akt. I) column with bubbling of argon, just before use. All the other purchased reagents and solvents were used without further purification. Column chromatography was performed using silica gel (Kanto Chemical Co., Inc., Silica gel 60N, spherical neutral).

Tris(4-formylphenyl)amine (7). This compound was prepared by the modified method of literature procedure [15]. To a solution of imidazole (2.50 g, 36.0 mmol) in acetonitrile (30 mL) was added dropwise trifluoroacetic anhydride (16.00 g, 75.4 mmol) under an argon atmosphere. The mixture was refluxed for 1 h, and then cooled by removal of the oil bath. Triphenylamine (2.50 g, 9.99 mmol) was added to the mixture, and then the reaction mixture was refluxed for 20 h. After cooling to room temperature, the reaction mixture was treated with ice to give a green precipitate, which was filtrated and washed with water. The precipitate was dissolved in CH_2Cl_2, washed with saturated aqueous $NaHCO_3$, and dried over $MgSO_4$, and the solvent was removed under reduced pressure to afford a greenish yellow solid (9.77 g), which was used for the next step without further purification.

To a suspension of this crude product (9.77 g) in acetonitrile (200 mL) was added a dilute hydrochloric acid (20 mL of conc. hydrochloric acid and 100 mL of water) under an argon atmosphere. The mixture was refluxed for 4 h, and extracted with Et_2O after cooling and neutralization with saturated aqueous Na_2CO_3 at 0 °C. The organic layer was dried over $MgSO_4$, and the solvent was removed under reduced pressure. The

residue was chromatographed on silica gel (CH_2Cl_2:*n*-hexane = 3:1 as eluent), and washed with hot ethyl acetate and *n*-hexane to afford **7** (2.12g, 64 %) as a yellow solid: IR(KBr) 2805, 2729, 1697 cm^{-1};^{1}H NMR (400 MHz, $CDCl_3$) δ 9.94 (s, 3H), 7.84 (d, J = 8.7 Hz, 6H), 7.25 (d, J = 8.7 Hz, 6H); ^{13}C NMR (100 MHz, $CDCl_3$) δ 190.3, 151.1, 132.5, 131.4, 124.5. Anal. Calcd for $C_{21}H_{15}NO_3$: C, 76.58; H, 4.59; N, 4.25; O, 14.57. Found: C, 76.30; H, 4.50; N, 4.14; O, 14.54.

Tris[4-(1-oxyl-3-oxide-4,4,5,5-tetramethylimidazolin-2-yl)phenyl]amine (1). A reaction flask equipped with a Soxhlet apparatus filled with molecular sieves 4A was charged with **7** (0.65 g, 1.98 mg), 2,3-bis(hydroxyamino)-2,3-dimethylbutane (1.41 g, 9.51 mmol) and 2,3-bis(hydroxyamino)-2,3-dimethylbutane sulfate (0.47 g, 1.90 mmol) in methanol (150 mL), and refluxed for 18 h under an argon atmosphere. The reaction mixture was concentrated by evaporation, and the resulting precipitate was collected and washed with cold methanol to afford a yellowish white solid (0.64g). The further purification was not performed.

To a solution of the product (0.64 g) in dichloromethane (36 mL) and methanol (3.6 mL) was added a solution of $NaIO_4$ (0.48 g, 2.24 mmol) in water (3.6 mL). The mixture was stirred for 30 min in the open air. The organic layer was separated, dried over $MgSO_4$ and the solvent was removed under reduced pressure. The residue was chromatographed on silica gel (ethyl acetate:n-hexane = 4:1 as eluent), concentrated by evacuation of solvent, and washed with the mixed solvent (CH_2Cl_2:*n*-hexane = 1:9) to afford **1** (30.8 mg, 2 %) as a blue solid: ESR (toluene) 13 lines, g = 2.007, $|a_N|$ = 2.5 G; FAB HRMS (*m*-nitrobenzyl alcohol) m/z (relative intensity %) calcd for $C_{39}H_{50}N_7O_6$ $[M+2H]^+$ 712.3823, found 712.3820 (26.3); $C_{39}H_{51}N_7O_6$ $[M+3H]^+$ 713.3901, found 713.3881 (11.4).

***N,N*-diphenyl-4-methoxyphenylamine (4).** This compound was prepared by the modified method of literature procedure [16]. A mixture of 4-Iodoanisole (7.65 g, 32.7 mmol), diphenylamine (5.53 g, 32.7 mmol), CuI (0.15 g, 0.79 mmol) and KO*t*-Bu (11.0 g,

98.0 mmol) in toluene (120 mL) was refluxed under argon atmosphere for 1 day. After cooling to room temperature, the solvent was evaporated. Water and CH_2Cl_2 was added to the residue, and the organic layer was separated, dried over $MgSO_4$ and evaporated. The residue was chromatographed on silica gel (ethyl acetate:CH_2Cl_2:*n*-hexane = 1:9:30) to afford **4** (4.27 g, 47 %) as a yellow solid: ^{1}H NMR (400 MHz, $CDCl_3$) δ 7.19 (dd, J = 8.5, 7.3 Hz, 4H), 7.06 (d, J = 9.0 Hz, 2H), 7.02 (dd, J = 7.3, 1.2 Hz, 4H), 6.93 (tt, J = 7.3, 1.2 Hz, 2H), 6.83 (d, J = 9.0 Hz, 2H), 3.79 (s, 3H); ^{13}C NMR (100 MHz, $CDCl_3$) δ 156.0, 148.1, 140.7, 129.0, 127.2, 122.8, 121.8, 114.7, 55.5. Anal. Calcd for $C_{19}H_{17}NO$: C, 82.88; H, 6.22; N, 5.09; O, 5.81. Found: C, 82.82; H, 6.08; N, 5.07; O, 5.66.

***N,N*-Bis(4-formylphenyl)-4-methoxyphenylamine (8).** This compound was prepared by the similar method of literature procedure [15]. To a solution of imidazole (2.72 g, 40.0 mmol) in acetonitrile (80 mL) was added dropwise trifluoroacetic anhydride (16.80 g, 80.0 mmol) under an argon atmosphere. The mixture was refluxed for 30 min, and then cooled by removal of the oil bath. **4** (4.27 g, 15.5 mmol) was added to the mixture, and then the reaction mixture was refluxed for 1 d. After cooling to room temperature, the reaction mixture was treated with ice to give a green precipitate, which was filtrated and washed with water.

The precipitate was suspended in acetonitrile (200mL) and a dilute hydrochloric acid (36 mL of conc. hydrochloric acid and 144 mL of water) under an argon atmosphere. The mixture was refluxed for 4 h, and extracted with Et_2O after cooling and neutralization with saturated aqueous K_2CO_3 at 0 °C. The organic layer was dried over $MgSO_4$, and the solvent was removed under reduced pressure. The residue was chromatographed on silica gel (ethyl acetate:n-hexane = 1:4 as eluent) to afford **8** (2.89g, 56 %) as a yellow solid: IR(KBr) 2835, 2739, 1686, 1040 cm^{-1}; ^{1}H NMR (400 MHz, $CDCl_3$) δ 9.87 (s, 2H), 7.75 (d, J = 8.3 Hz, 4H), 7.16 (d, J = 8.3 Hz, 4H), 7.11 (d, J = 8.3 Hz, 2H), 6.94 (d, J = 8.3 Hz, 2H), 3.84 (s, 3H); ^{13}C NMR (100 MHz, $CDCl_3$) δ 190.3, 158.0, 152.0, 138.0,

131.2, 130.8, 128.8, 122.0, 115.4, 55.6. Anal. Calcd for $C_{21}H_{17}NO_3$: C, 76.12; H, 5.17; N, 4.23; O, 14.49. Found: C, 75.98; H, 5.31; N, 4.26; O, 14.60.

***N,N*-Bis[4-(1-oxyl-3-oxide-4,4,5,5-tetramethylimidazolin-2-yl)phenyl]-4-methoxyphenylamine (2).** A reaction flask equipped with a Soxhlet apparatus filled with molecular sieves 4A was charged with 2,3-bis(hydroxyamino)-2,3-dimethylbutane sulfate (1.30 g, 5.28 mmol) and K_2CO_3 (2.42 g, 17.5 mmol) in methanol (150 mL). To the mixture was added **8** (0.58 g, 1.75 mmol) under an argon atmosphere, and refluxed for 1 d. The reaction mixture was filtered, and the organic layer was separated after adding CH_2Cl_2 and water, dried over $MgSO_4$, and the solvent was removed under reduced pressure to afford a yellow solid (0.85g).

To a solution of the product in dichloromethane (58 mL) and methanol (5.8 mL) was added a solution of $NaIO_4$ (0.29 g, 1.35 mmol) in water (5.8 mL). The mixture was stirred for 1 h in the open air. The organic layer was separated, dried over $MgSO_4$ and the solvent was removed under reduced pressure. The residue was chromatographed on silica gel (ethyl acetate:*n*-hexane = 3:1 as eluent) to afford **2** (50 mg, 5 %) as a blue solid: ESR (toluene) 9 lines, $g = 2.007$, $|a_N| = 3.7$ G.

Electrochemical Measurement

The cyclic voltammetry measurements were carried out in benzonitrile solution containing 0.1 M tetrabutylammonium tetrafluoroborate as a supporting electrolyte (25 °C, scan rate 100 mV/sec) using an ALS/chi Electrochemical Analyzer Model 612A. A three-electrode assembly was used, which was equipped with a platinum disk (2 mm^2), a platinum wire, and Ag/0.01 M $AgNO_3$ (acetonitrile) as the working, the counter, and the reference electrode, respectively. The redox potentials were referenced against ferrocene/ferrocenium (Fc/Fc^+) couple.

ESR Measurement

ESR spectra were recorded on a JEOL JES-SRE2X spectrometer, in which temperature was controlled by a JEOL DVT2 variable-temperature unit, and a Mn^{2+}/MnO solid solution was used as a reference for the determination of *g* values and hyperfine coupling constants.

Magnetic Susceptibility Measurement

Magnetic susceptibilities of the powder samples were measured by a Quantum Design MPMS-5S system. The raw data were corrected for both the magnetization of sample holder alone and the diamagnetic contribution of the sample itself. The estimation of the diamagnetic contribution was done by using Pascal's constants.

4.3 Results and Discussion

4.3.1. Synthesis

To synthesize our target molecules **1** and **2** according to the Ullman's method [17], trialdehyde **7** and dialdehyde **8** become key compounds. However, the usual Vilsmeier-Haack formylation of triphenylamine produces **7** in very low yield in spite of using the vigorous reaction conditions [18]. Therefore, we attempted to synthesize **7** and **8** by another method [15]. The synthetic routes of **1** and **2** were summarized in Scheme 2. First of all, imidazole was reacted with trifluoroacetic anhydride to generate the electrophilic *N,N'*-bis(trifluoroacetyl)imidazolium ion. The generated imidazolium ion was treated with the corresponding triphenylamines **3** and **4** to afford tris- and bisadduct **5** and **6**. These adducts were readily hydrolyzed to give **7** and **8** under the acidic condition. The resulting aldehydes were condensed with 2,3-bis (hydroxylamino)-2,3-dimethylbutane to give the corresponding hydroxylamine **9** and **10**.

Finally, **1** and **2** were obtained by the oxidation of hydroxylamine with sodium periodate.

Scheme 2.

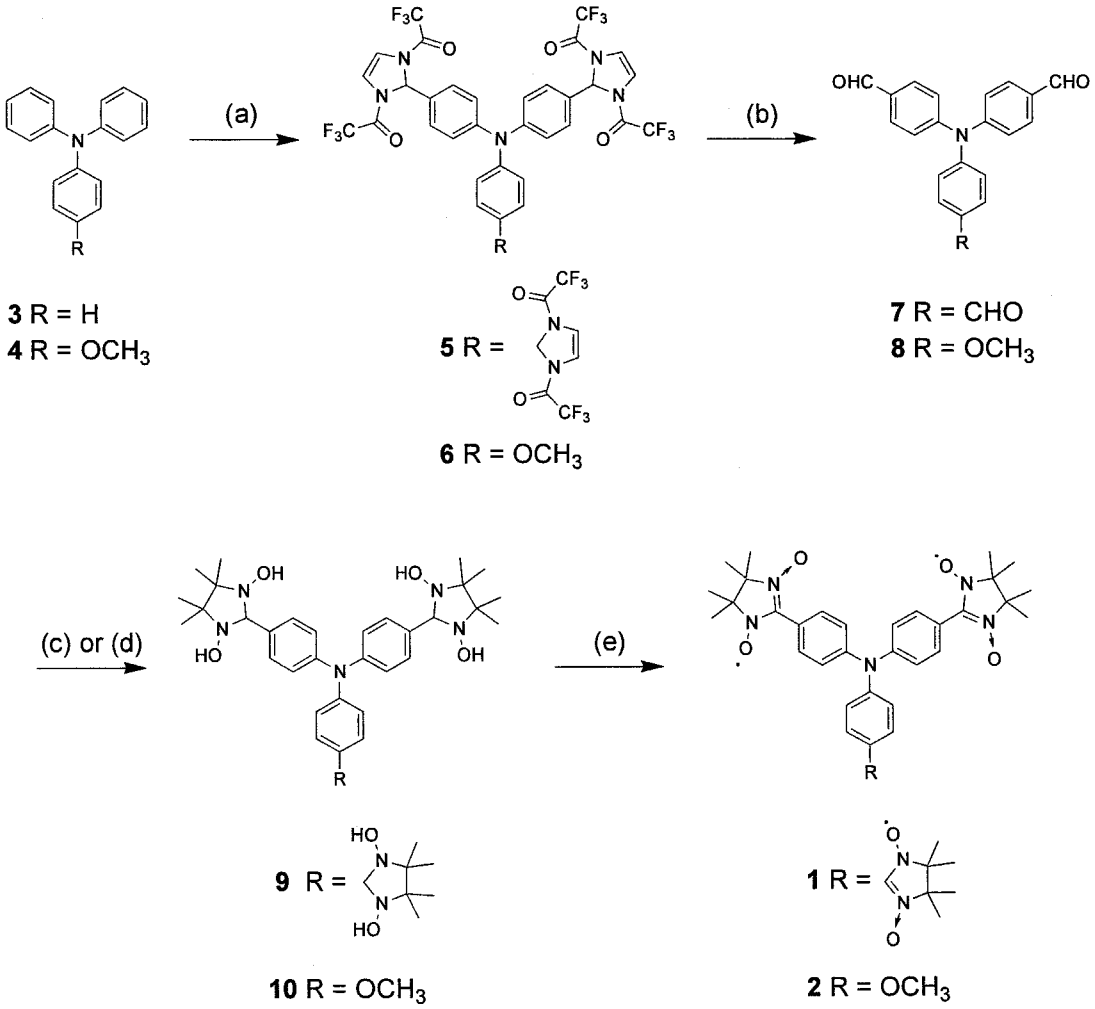

Reagents and conditions: (a) imidazole, trifluoroacetic anhydride, CH_3CN; (b) HCl_{aq}, acetonitrile; (c) 2,3-bis(hydroxyamino)-2,3-dimethylbutane, 2,3-bis(hydroxylamino)-2,3-dimethylbutane sulfate, CH_3OH; (d) 2,3-bis (hydroxylamino)-2,3-dimethylbutane sulfate, K_2CO_3, CH_3OH; (e) $NaIO_4$, H_2O, CH_2Cl_2, CH_3OH.

4.3.2. Electrochemical property

The electrochemical properties for **1** and **2** were investigated by the cyclic voltammetry in benzonitrile at 25 °C. The oxidation potentials versus ferrocene/ferrocenium are summarized together with their related compounds in Table 1, and the cyclic voltammogram of **2** is shown in Figure 1. Judging from the oxidation potentials and the current ratio of the reference compounds, 2-phenyl-4,4,5,5-tetramethylimidazoline-1-oxyl-3-oxide (**11**), triphenylamine (**12**) and 4-methoxytriphenylamine (**13**), the first oxidation process of **1** can be ascribed to the simultaneous three-electron oxidation of the corresponding three nitronyl nitroxide moieties, while the first and second oxidation processes of **2** to stepwise one-electron oxidations of the two nitroxide moieties. On the other hand, the oxidation process for the triphenylamine moiety of **1** was not observed in the range of potential window, whereas the potential value +0.80 V of **2** was due to the oxidation of triphenylamine

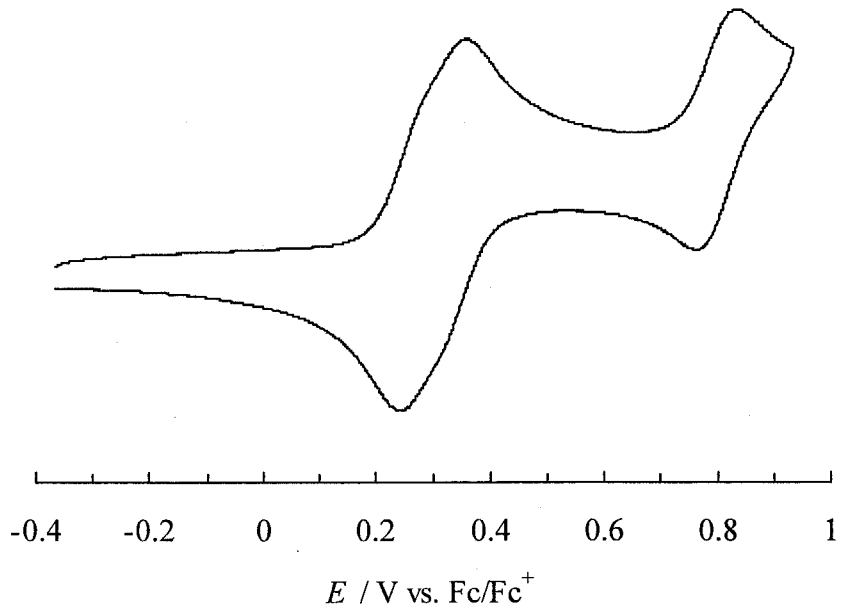

Figure 1. Cyclic voltammogram of **2** in benzonitrile containing 0.1 M *n*-Bu_4BF_4 on a platinum electrode.

moiety. This is probably because **1** has a considerable amount of positive charges after oxidation of the three nitronyl nitroxide moieties and, hence, the triphenylamine moiety becomes no longer oxidizable, as compared with **2**. The oxidation potential for the triphenylamine moiety of **2** increases by 0.42 V compared with **13** owing to such a charging effect of the oxidized nitronyl nitroxide moieties.

Table 1. Redox potentials (V) of **1**, **2** and its related compounds[a]

	E_1	E_2	E_3
1	+0.30[b]		
2	+0.26	+0.34	+0.80
11	+0.32		
12	+0.51[c]		
13	+0.38		

[a]0.1 M *n*-Bu_4BF_4 in PhCN, potential vs. Fc/Fc^+, Pt electrode, 25 °C, scan rate 100 mV s^{-1}. [b]Quasi-three-electron transfer. [c]Irreversible oxidation process represented by anodic peak potential.

4.3.3. Magnetic property

Magnetic measurements of triradical **1** and diradical **2** were carried out on a SQUID susceptometer from 300 to 2 K. The temperature dependences of the molar magnetic susceptibilities (χ_m) of the microcrystalline samples were measured at a constant field of 500 G. The plot of $\chi_m T$ versus T for **1** and **2** are shown in Figure 2.

The $\chi_m T$ value of **1** at 300 K was close to the theoretical one of 1.125 emu K mol^{-1} for isolated three spins of 1/2. On lowering the temperature, the $\chi_m T$ value decreased gradually and reached 0.28 emu K mol^{-1} at 2 K, indicating the antiferromagnetic

interaction between radical spins.

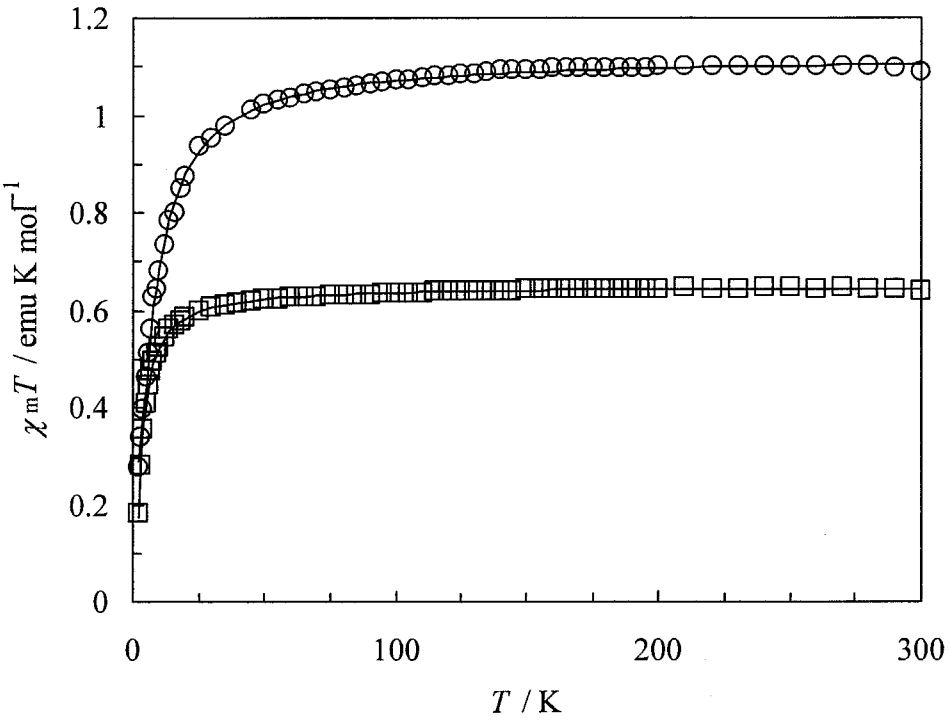

Figure 2. Temperature dependence of $\chi_m T$ of **1** (○) and **2** (□) under a field of 500 G. The solid line represents the best theoretical fit to the data (see text).

The magnetic interaction in a nonsymmetrical triangular three spin system [13,14,19,20] can be described by the spin Hamiltonian (eq. 1), where J_{ij} is the exchange coupling constant between $\boldsymbol{S}_i$ and $\boldsymbol{S}_j$. In this case, the $\chi_m T$ is expressed by eq. 2 as a function of Δ_1 and Δ_2 defined by eqs. 3 and 4, which are the energy differences between the two spin doublet states and the one between the spin doublet state and the spin quartet state, where f is the purity factor for the sample, N_A the Avogadro number, g the g-factor, k_B the Boltzmann constant, μ_B the Bohr magneton, and θ the Weiss constant. Herein,

we assumed the same g value for the three multiplets and, furthermore, the value was fixed $g = 2$ in the fitting procedure for simplicity.

$$H = -2(J_{12}\boldsymbol{S}_1\boldsymbol{S}_2 + J_{23}\boldsymbol{S}_2\boldsymbol{S}_3 + J_{31}\boldsymbol{S}_3\boldsymbol{S}_1) \tag{1}$$

$$\chi_m T = f\frac{N_A g^2 \mu_B^2}{4k_B}\frac{1+\exp(-\Delta_1/k_BT)+10\exp(-\Delta_2/k_BT)}{1+\exp(-\Delta_1/k_BT)+2\exp(-\Delta_2/k_BT)}\frac{T}{T-\theta} \tag{2}$$

$$\Delta_1 = 2(J_{12}^2 + J_{23}^2 + J_{31}^2 - J_{12}J_{23} - J_{23}J_{31} - J_{31}J_{12})^{1/2} \tag{3}$$

$$\Delta_2 = \Delta_1/2 - (J_{12} + J_{23} + J_{31}) \tag{4}$$

Since the crystal structure of **1** is not unknown to date, we carried out the least-squares fitting procedure by assuming the equilateral triangle for three spins, where $J = J_{12} = J_{23} = J_{31}$ and $\Delta_1 = 0$ gives eq 5. The best fit to the data was $f = 0.998\pm0.001$, $J/k_B = -3.93\pm0.06$ K and $\theta = -0.62\pm0.05$ K, roughly indicating the quartet state was above the doubly degenerate doublet states by ca. $3J/k_B = 12$ K. It was revealed that the intramolecular antiferromagnetic interaction of **1** was much smaller than that of tris[4-(*N*-oxy-*N*-*tert*-butylamino)phenyl]amine in the case of assuming the equilateral triangle model ($J/k_B = -135\pm3$ K) [13, 14].

$$\chi_m T = f\frac{N_A g^2 \mu_B^2}{4k_B}\frac{1+5\exp(3J/k_BT)}{1+\exp(3J/k_BT)}\frac{T}{T-\theta} \tag{5}$$

The $\chi_m T$ value of **2** at 300 K was relatively smaller than the theoretical one of 0.75 emu K mol^{-1} for isolated two spins of 1/2. Considering the $\chi_m T$ value of 0.64 emu K mol^{-1} in the wide temperature range, it seems to be not due to the antiferromagnetic interaction but to the experimental errors on weighing a sample or to the purity of a sample. As the temperature was lowered, the $\chi_m T$ value decreased gradually and

reached 0.18 emu K mol^{-1} at 2 K, indicating the antiferromagnetic interaction between radical spins. The observed data was analyzed by the modified Bleaney–Bowers equation for singlet-triplet model [21] (eq. 6) to give the best fit parameters: f = 0.8665±0.0006, J/k_B = −1.85±0.03 K and θ = −1.21±0.04 K.

$$\chi_m T = f \frac{2N_A g^2 \mu_B^2}{k_B} \frac{1}{3 + \exp(-2J/k_B T)} \frac{T}{T - \theta} \tag{6}$$

4.3.4. ESR spectroscopy

The ESR spectrum in toluene at room temperature showed a 13-line pattern centered at g = 2.007 with a hyperfine coupling constant $|a_N|$ = 2.5 G due to six equivalent nitrogen atoms for **1**, and a 9-line pattern (g = 2.007, $|a_N|$ = 3.7 G) due to four equivalent nitrogen atoms for **2**. For instance, the solution ESR spectrum of **1** is shown in Figure 3. The hyperfine coupling constants of **1** and **2** were estimated to one third and a half of the hyperfine coupling constant ($|a_N|$ = 7.4 G) of monoradical **11**, respectively. This indicates that the exchange interactions between radical spins in triradical **1** and diradical **2** are larger than the hyperfine interaction.

After treated with tris(4-bromophenyl)aminium hexachloroantimonate as an oxidizing agent, **1** and **2** in frozen *n*-butyronitrile at 123 K did not show the fine-structured spectra attributed to spin-quintet or quartet species. Instead of the fine-structured spectra, the observed spectra were similar to that of mono nitronyl nitroxide **11**, as shown in Figure 4. This is consistent with the electrochemical result that the nitronyl nitroxide moieties of **1** and **2** are oxidized more easily than the triphenylamine moieties.

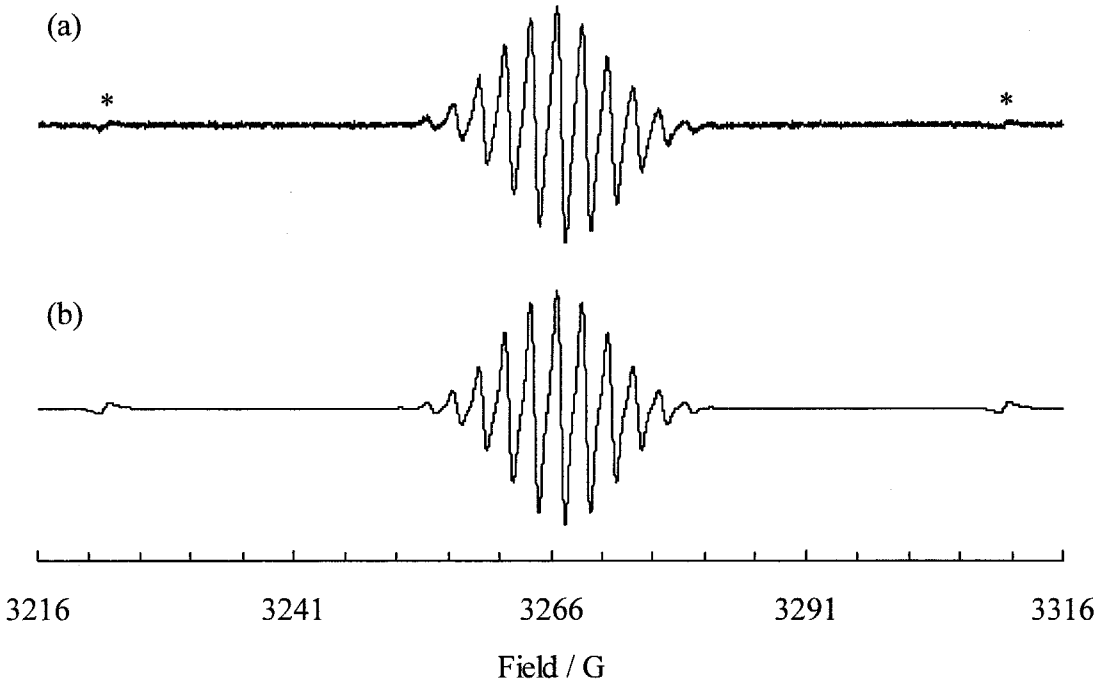

Figure 3. ESR spectrum of **1** in toluene (5×10^{-5} M) at room temperature (a) and its simulation (b) ($|a_N|$ = 2.5 G, ΔH_{pp} = 0.86 G). The asterisks in the spectrum show the signals due to the Mn^{2+} standard.

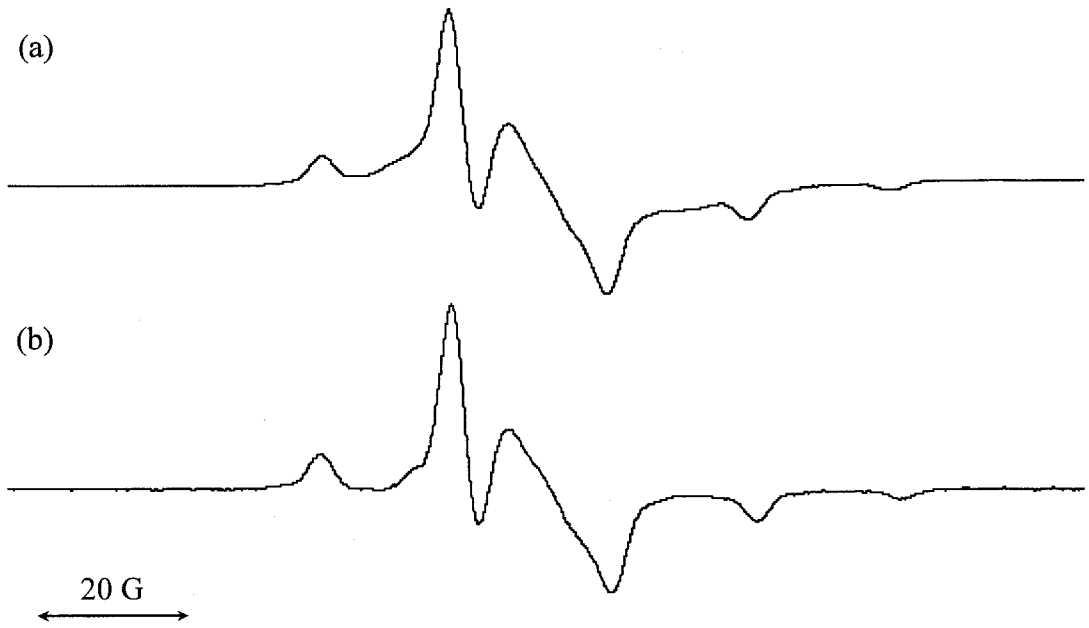

Figure 4. ESR spectra of (a) **2** oxidized with tris(4-bromophenyl)aminium hexachloroantimonate and (b) monoradical **11** in frozen *n*-butyronitrile solution at 123 K

4.4 Conclusion

The syntheses of triradical **1** and diradical **2** having the triphenylamine skeleton were succeeded, and it is found that their neutral radicals in the solid states showed weak antiferromagnetic interactions between radical spins. However, the electrochemical and ESR measurements showed the nitronyl nitroxide moieties had the lower oxidation potentials than the core triphenylamine moieties even in the case of electron-donating methoxy-group-substitution (**2**). Therefore, in order to generate triphenylaminium cation radical and, furthermore, enhance the intramolecular ferromagnetic interaction, it is necessary to introduce more electron-donating substituent, e.g., *N*,*N*-dimethylamino group, to lower the oxidation potential. Actually, 4-*N*,*N*-dimethylaminotriphenylamine exhibits the first oxidation potential of –0.05 V.

References

[1] V. Balzani, M. Venturi, A. Credi, Molecular Devices and Machines, Wiley-VCH, Weinheim, 2003.

[2] J. Park, A.N. Pasupathy, J.I. Goldsmith, C. Chang, Y. Yaish, J.R. Petta, M. Rinkoski, J.P. Sethna, H.D. Abruna, P.L. McEuen, D.C. Ralph, Nature 417 (2002) 722.

[3] W. Liang, M.P. Shores, M. Bockrath, J.R. Long, H. Park, Nature 417 (2002) 725.

[4] S. Kubatkin, A. Danilov, M. Hjort, J. Cornil, J.-L. Brédas, N. Stuhr-Hanson, P. Hedegård, T. Bjørnholm, Nature 425 (2003) 698.

[5] S. Rajca, A. Rajca, J. Am. Chem. Soc. 117 (1995) 9172.

[6] A. Ito, H. Ino, Y. Matsui, Y. Hirao, K. Tanaka, J. Phys. Chem. A 108 (2004) 5715.

[7] Y. Morita, S. Nishida, J. Kawai, K. Fukui, S. Nakazawa, K. Sato, D. Shiomi, T. Takui, K. Nakasuji, Org. Lett. 4 (2002) 1985.

[8] (a) K. Matsuda, M. Irie, J. Am. Chem. Soc. 122 (2000) 7195; (b) K. Matsuda, M. Irie, J. Am. Chem. Soc. 122 (2000) 8309.

[9] Y. Shirota, J. Mater. Chem. 10 (2000) 1.

[10] A.R. Forrester, J.M. Hay, R.H. Thomson, Organic Chemistry of Stable Free Radicals, Academic Press, New York, 1968.

[11] C. Lambert, W. Gaschler, E. Schmälzlin, K. Meerholz, C. Bräuchle, J. Chem. Soc., Perkin Trans. 2 3 (1999) 577.

[12] T. Itoh, K. Matsuda, H. Iwamura, Angew. Chem. Int. Ed. Engl. 38 (1999) 1791.

[13] T. Itoh, K. Matsuda, H. Iwamura, K. Hori, J. Am. Chem. Soc. 122 (2000) 2567.

[14] T. Itoh, K. Matsuda, H. Iwamura, K. Hori, J. Solid State Chem. 159 (2001) 428.

[15] H. Oelschläger, H.J. Peters, Arch. Pharm. (Weinheim) 320 (1987) 379.

[16] A.A. Kelkar, N.M. Patil, R.V. Chaudhari, Tetrahedron Lett. 43 (2002) 7143.

[17] E.F. Ullman, J.H. Osiecki, D.G.B. Boocock, R. Darcy, J. Am. Chem. Soc. 94

(1972) 7049.

[18] G. Lai, X.R. Bu, J. Santos, E.A. Mintz, Synlett. (1997) 1275.

[19] O. Kahn, Molecular Magnetism; VCH: New York, 1993.

[20] A. Bencini, C. Benelli, A. Dei, D. Gatteschi, Inorg. Chem. 24 (1985) 695.

[21] B. Bleaney, K.D. Bowers, Proc. R. Soc. London A 214 (1952) 451.

Chapter 5

Spin Alignment Mediated by Mixed-Valence State: Triradical Cation of *p*-Phenylenediamine Having Two Nitroxide Radicals

5.1 Introduction

The control of spin preference in multi-spin molecular systems is of great importance when applied to molecular electronics devices aiming at novel high-density information storage. For instance, several single molecular magnets have been prepared [1] and are about to be applied to quantum computation [2]. To accomplish the above attempt using organic molecules, it should be established that a lot of stable organic radical centers are assembled to have desirable intramolecular magnetic interaction. In the past few decades, significant progress has been made in rational design and synthesis of high-spin organic molecules containing several stable radical centers [3]. In many cases, the stable radical centers are linked by the so-called ferromagnetic coupling units like 1,3-benzenediyl to generate the (quasi-)degenerate singly-occupied nonbonding molecular orbitals (NBMOs) according to the Hund's rule [4].

On the other hand, the control of charge distribution in the above-mentioned multi-spin organic molecular systems is also regarded as an important issue in conjunction with potential application to spin electronics devices. When a few electrons are added to or removed from the multi-spin organic system, important problems of the relationship between the spin preference and the extra charge distribution emerge from alterations to occupancy number of the NBMOs: whether the high-spin preference among the surviving unpaired electrons remains unchanged or not; whether the extra electrons (or "holes") are localized or delocalized [4c]. With these questions in mind, several polyradical anions [5] and cations [6] have exhibited intriguing aspects of the charge distribution and its influence on the spin preference.

Organic mixed-valence compounds are the simple models for understanding of the intramolecular electron transfer process or for examining to what degree the extra charge is delocalized over a molecule, and nowadays a lot of examples have been reported [7,8,9]. However, the mixed-valence state has never been used to mediate an intramolecular magnetic interaction, in particular, ferromagnetic one. As have

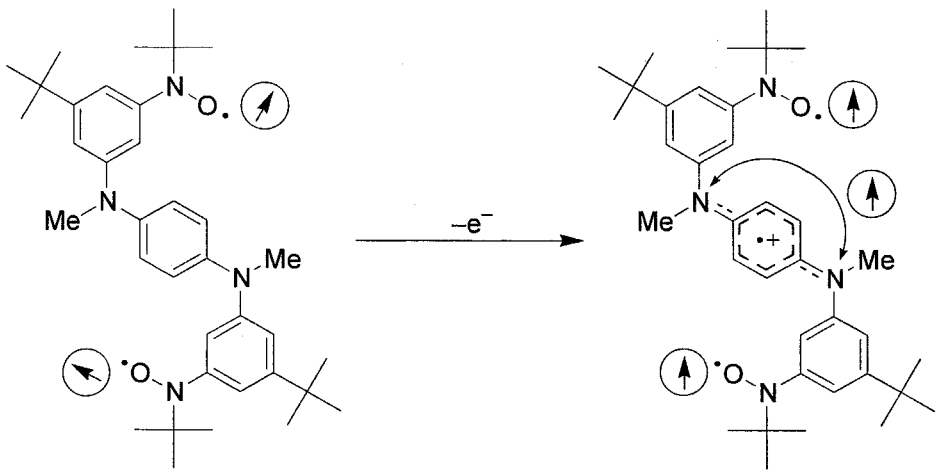

1 1^+

Scheme 1. Spin alignment mediated by mixed-valence state in $\mathbf{1}^+$.

been described in our previous theoretical study [10], the ferromagnetic coupling between the localized multi-spin system and the delocalized electron spin is closely related to the realization of spin-polarized molecular wire. In this chapter, we describe on the first observation of spin alignment mediated by mixed-valence state in multi-spin organic system. We selected *para*-phenylenediamine (PDA) derivative **1** carrying two persistent nitroxide groups (Scheme 1) since radical cations of PDA molecules are widely accepted as important organic mixed-valence systems [7,9].

5.2 Experimental Section

General Methods

^{1}H and ^{13}C spectra were recorded on a JEOL JNM-AL400, a JNM-EX400 or a JNM-AL300 spectrometer, and chemical shifts are given in parts per million (ppm) relative to internal tetramethylsilane (δ 0.00 ppm). Elemental analyses were performed by Center for Organic Elemental Microanalysis, Kyoto University.

Materials

Toluene and *n*-butyronitrile were distilled from CaH_2 under an argon atmosphere, tetrahydrofuran (THF) was distilled from sodium–benzophenone or potassium–benzophenone under an argon atmosphere, *N*,*N*-dimethylformamide (DMF) was dried over molecular sieves 4A, and benzonitrile was dried through alumina (ICN, Alumina N, Akt. I) column with bubbling of argon, just before use. All the other purchased reagents and solvents were used without further purification. Column chromatography was performed using silica gel (Kanto Chemical Co., Inc., Silica gel 60N, spherical neutral) or alumina oxide (Kanto Chemical Co., Inc., Aluminum Oxide, Activated for column chromatography).

N-(3-Bromo-5-*tert*-butylphenyl)-*N*-(*tert*-butyldimethylsiloxy)-*N*-*tert*-butylamine (**3**) were synthesized by the modified method of literature [11].

***N,N'*-Bis[3-*tert*-butyl-5-(*N*-(*tert*-butyldimethylsiloxy)-*N*-*tert*-butylamino)phenyl]-*N,N'*-dimethyl-*p*-phenylenediamine (4).** A mixture of **2** (1.50 g, 11.0 mmol), **3** (10.0g, 24.1 mmol), NaO*t*-Bu (2.50 g, 25.5 mmol), $Pd(OAc)_2$ (150 mg, 0.65 mmol) and 2-(Di-*tert*-butylphosphino)biphenyl (150 mg, 0.50 mmol) in toluene was refluxed for 1 day. The resulting mixture was concentrated by evaporation under reduced pressure. The residue was diluted with Et_2O and water, and the organic layer was separated and dried over $MgSO_4$. After evaporation of the solvent, the crude product was chromatographed on silica gel (CH_2Cl_2:*n*-hexane = 1:4 as eluent) to afford **4** (4.80 g, 54 %) as a white solid: ^{1}H NMR (400MHz, C_6D_6) δ 6.96–6.99 (m, 8H), 6.91 (br-s, 2H), 3.07 (s, 6H), 1.30 (s, 18H), 1.21 (s, 18H), 1.03 (s, 18H), 0.93 (br-s, 12H); ^{13}C NMR (100 MHz, C_6D_6) δ 151.9, 151.0, 148.8, 144.3, 122.7, 115.6, 114.5, 113.6, 61.0, 40.6, 35.0, 31.6, 26.6, 26.5, 18.4, –4.2. Anal. Calcd. for $C_{48}H_{82}N_4O_2Si_2$: C, 71.76; H, 10.29; N, 6.97. Found: C, 71.58; H, 10.44; N, 6.81.

***N,N'*-Bis[3-*tert*-butyl-5-(*N*-*tert*-butyl-*N*-hydroxyamino)phenyl]-*N,N'*-dimethyl-*p*-phenylenediamine (5).** To an ice-cooled solution of **4** (564 mg, 0.70 mmol) in 5 ml of THF was added slowly 7 ml (7 mmol) of 1.0 M solution of tetrabutylammonium fluoride in THF. Stirring was continued for 45 min at 0 °C and for 2 h at room temperature. After addition of water and Et_2O, the organic layer was separated and the aqueous layer was extracted with Et_2O. The organic layers were combined and dried over $MgSO_4$. By evaporation under reduced pressure, slightly reddish brown solid was obtained and washed with *n*-hexane containing a small amount of Et_2O to give **5** (355.4 mg, 88 %) as a white solid: ^{1}H NMR (400MHz, acetone-d_6) δ 7.36 (br-s, 2H), 6.96 (s, 4H), 6.84 (t, J = 1.9 Hz, 2H), 6.79 (t, J = 1.9 Hz, 2H), 6.73 (t, J = 1.9 Hz, 2H), 3.27 (s, 6H), 1.26 (s, 18H), 1.11 (s, 18H); ^{13}C NMR (100 MHz, acetone-d_6) δ 151.8, 151.0, 149.2, 144.4, 122.6, 115.4, 114.0, 113.3, 60.3, 40.8, 35.2, 31.6, 26.6.

***N,N'*-Bis[3-*tert*-butyl-5-(*N*-*tert*-butyl-*N*-oxylamino)phenyl]-*N,N'*-dimethyl-*p*-phenylenediamine (1).** To a solution of **5** (76 mg, 0.13 mmol) in CH_2Cl_2 (10 mL) was added an excess Ag_2O (308 mg, 1.3 mmol), and the mixture was stirred for 2 h. After filtration through celite, the solvent was evaporated under reduced pressure. The residue was chromatographed on silica gel (Et_2O:CH_2Cl_2:*n*-hexane = 1:4:5 as eluent) to afford **1** (63 mg, 83 %) as a red solid: ESR (toluene at room temperature) g = 2.006, $|a_N|$ = 6.3 G; FAB HRMS (*m*-nitrobenzyl alcohol) m/z (relative intensity %) calcd for $C_{36}H_{52}N_4O_2$ $[M]^+$ 572.4090, found 572.4085 (7.4); $C_{36}H_{53}N_4O_2$ $[M+H]^+$ 573.4169, found 573.4162 (6.2); $C_{36}H_{54}N_4O_2$ $[M+2H]^+$ 574.4247, found 574.4208 (7.4); Anal. Calcd. for $C_{36}H_{52}N_4O_2$: C, 75.48; H, 9.15; N, 9.78; O, 5.59. Found: C, 75.36; H, 9.10; N, 9.60; O, 5.58.

Electrochemical Measurement

The cyclic voltammetry (CV) measurements were carried out in benzonitrile solution containing 0.1 M tetrabutylammonium tetrafluoroborate ($TBABF_4$) as a supporting electrolyte (25 °C, scan rate 100 mV/sec) using an ALS/chi Electrochemical Analyzer Model 612A. A three-electrode assembly was used, which was equipped with a platinum disk (2 mm^2), a platinum wire, and Ag/0.01 M $AgNO_3$ (acetonitrile) as the working, the counter, and the reference electrode, respectively. The redox potentials were referenced against ferrocene/ferrocenium (Fc/Fc^+) couple.

UV/Vis/NIR Spectrum Measurement

UV/Vis/NIR spectra were obtained with a Perkin Elmer Lambda 19 spectrometer. Spectroelectrochemical measurements were carried out with self-constructed optically transparent thin-layer electrochemical (OTTLE) cell (light pass length = 1mm) equipped with a platinum mesh, a platinum coil, and a silver wire as the working, the counter, and the pseudo-reference electrode, respectively. The potential was applied

with an ALS/chi Electrochemical Analyzer Model 612A.

ESR Measurement

ESR spectra were recorded on a JEOL JES-SRE2X or a JEOL JES-TE200 X-band spectrometer, in which temperature was controlled by a JEOL DVT2 variable-temperature unit or an Oxford ITC503 temperature controller combined with an ESR 910 continuous flow cryostat, respectively. A Mn^{2+}/MnO solid solution was used as a reference for the determination of *g* values and hyperfine coupling constants. Pulsed ESR measurements were carried out on a Bruker ELEXES E580 X-band FT ESR spectrometer.

Magnetic Susceptibility Measurement

Magnetic susceptibilities of the powder samples were measured by a Quantum Design MPMS-5S system. The raw data were corrected for both the magnetization of sample holder alone and the diamagnetic contribution of the sample itself. The estimation of the diamagnetic contribution was done by using Pascal's constants.

5.3 Results and Discussion

5.3.1 Synthesis

As shown in Scheme 2, the bisnitroxide **1** was prepared in three steps. The coupling reaction of *N,N'*-dimethyl-*p*-phenylenediamine **2** with the protected hydroxylamine **3** in the presence of palladium catalyst affords the precursor **4**. After desilylation of **4** with tetrabutylammonium fluoride, the desired bisnitroxide **1** was obtained as reddish brown solid by oxidation of the bishydroxylamine **5** with Ag_2O.

Scheme 2. Synthetic route for **1**[a].

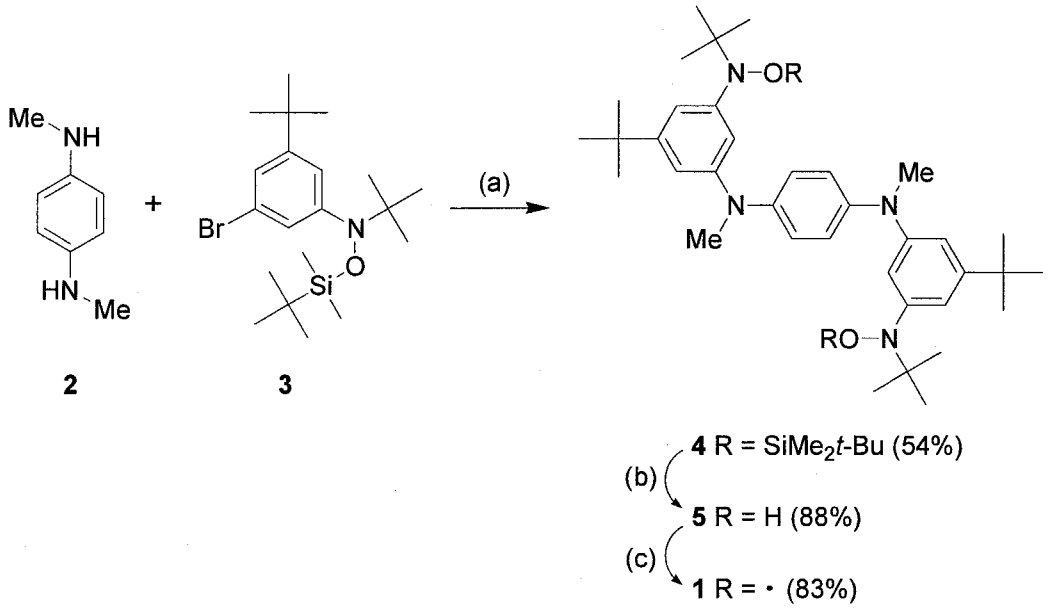

2 **3**

[a]Reagents: (a) (*o*-Biphenyl)P(*t*-Bu)$_2$, Pd(OAc)$_2$, NaO*t*-Bu, toluene; (b) *n*-Bu$_4$F, THF; (c) Ag_2O, CH_2Cl_2.

5.3.2 Electrochemistry

A prerequisite for generating triradical cation of **1** is that the central PDA moiety has lower oxidation potential than those of the two nitroxide groups. The oxidation potentials of **1** were evaluated by cyclic voltammetry in benzonitrile solution at 298 K. The observed voltammogram showed three oxidation waves (Figure 1b). The first oxidation process was found to be reversible by lowering the turn-round potential (Figure 1a). From the comparison of the oxidation potentials for *N*,*N*'-dimethyl-*N*,*N*'-diphenyl-*p*-phenylenediamine (**6**) with that for the *tert*-butylphenyl nitroxide (**7**), the first reversible oxidation wave of **1** can be ascribed to the removal of one-electron from the central PDA moiety (Table 1). The remaining two oxidation peaks probably correspond to the oxidation process of the nitroxide groups and/or the oxidation process from semi-quinone to quinone of the central PDA moiety. It is interesting to note that the difference of the first and second oxidation potentials of PDA derivatives (ΔE) is closely related to the twist angle between the amino group and 1,4-phenylenediyl, which determines the electronic coupling in intramolecular electron transfer [12]. Although the rigorous value of ΔE for **1** is not obtained owing to the overlap of the second and third oxidation processes, the ΔE can be roughly estimated to be 0.52~0.55 V, similar to the value of 0.5 V for **6**. This suggests that the substituting nitroxide groups do not seriously affect the twist angle between the amino group and 1,4-phenylenediyl.

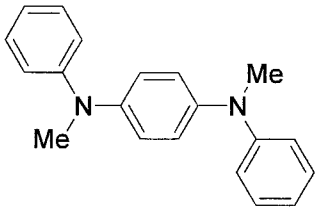

6

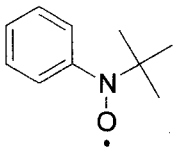

7

Table 1. Redox Potentials of **1** and Related Compounds[a]

	E_1	E_2	E_3
1	0.00	0.52[c]	0.55
6	–0.02	0.48	
7	0.41[c]		

[a]0.1 M *n*-Bu_4NBF_4 in PhCN, potential versus Fc/Fc^+, Pt electrode, 298 K, scan rate 100 mV s^{-1}. [c]Anodic peak potential.

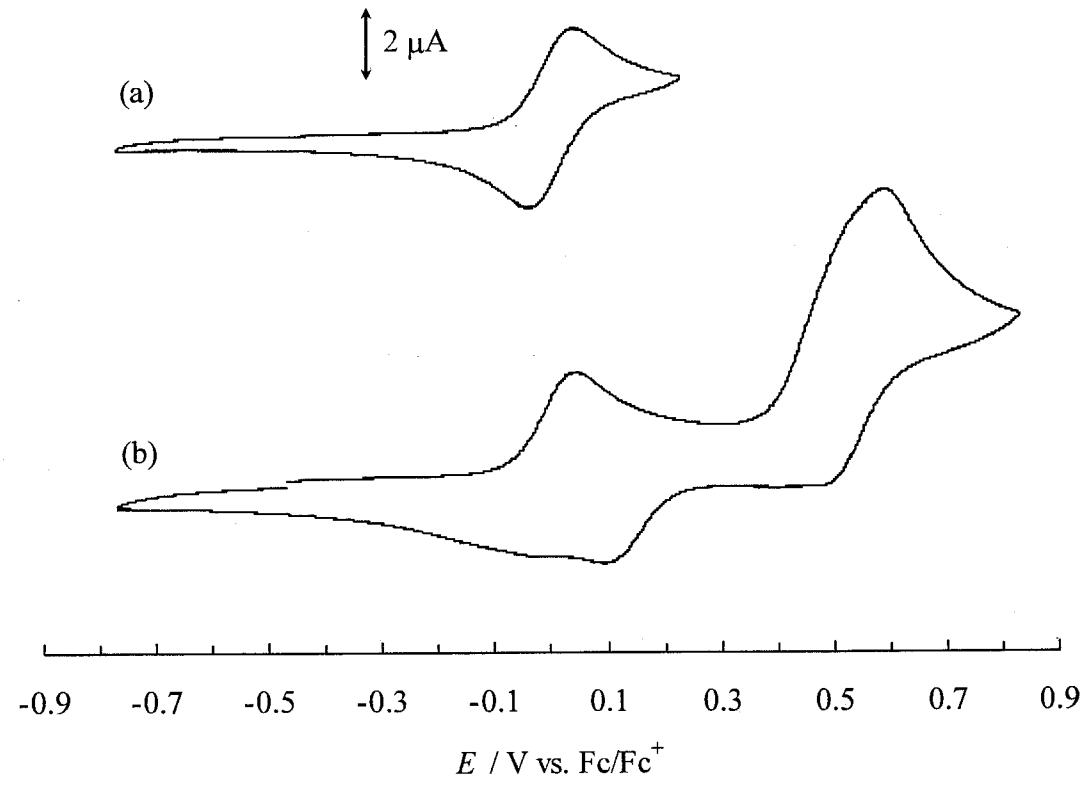

Figure 1. Cyclic voltammograms of **1** in case of (a) low turning potential and (b) high turning potential in benzonitrile containing 0.1 M *n*-Bu_4NBF_4 at 298 K, scan rate 100 mV/s.

5.3.3 UV/Vis/NIR Spectroscopy

In order to confirm the presence of the mixed-valence state in triradical cation of **1**, it is the best way to observe the characteristic intervalence charge transfer (IV-CT) absorption band [13]. Therefore, we have measured the UV/Vis/NIR spectral change during the course of the oxidation of **1** by using an optically transparent thin-layer electrochemical cell. For a reference, the IV-CT band of DMDP-PDA was examined in CH_2Cl_2 at room temperature. The IV-CT band grew at 625 nm upon oxidation to the monoradical cation, and further oxidation to the dication resulted in disappearance of this band and increase in the new band at 558 nm. On the other hand, the increase of the band at 693 nm was observed upon oxidation to $\mathbf{1}^+$ as shown in Figure 2. This absorption band is assignable to the IV-CT band of $\mathbf{1}^+$ in comparison with that of the

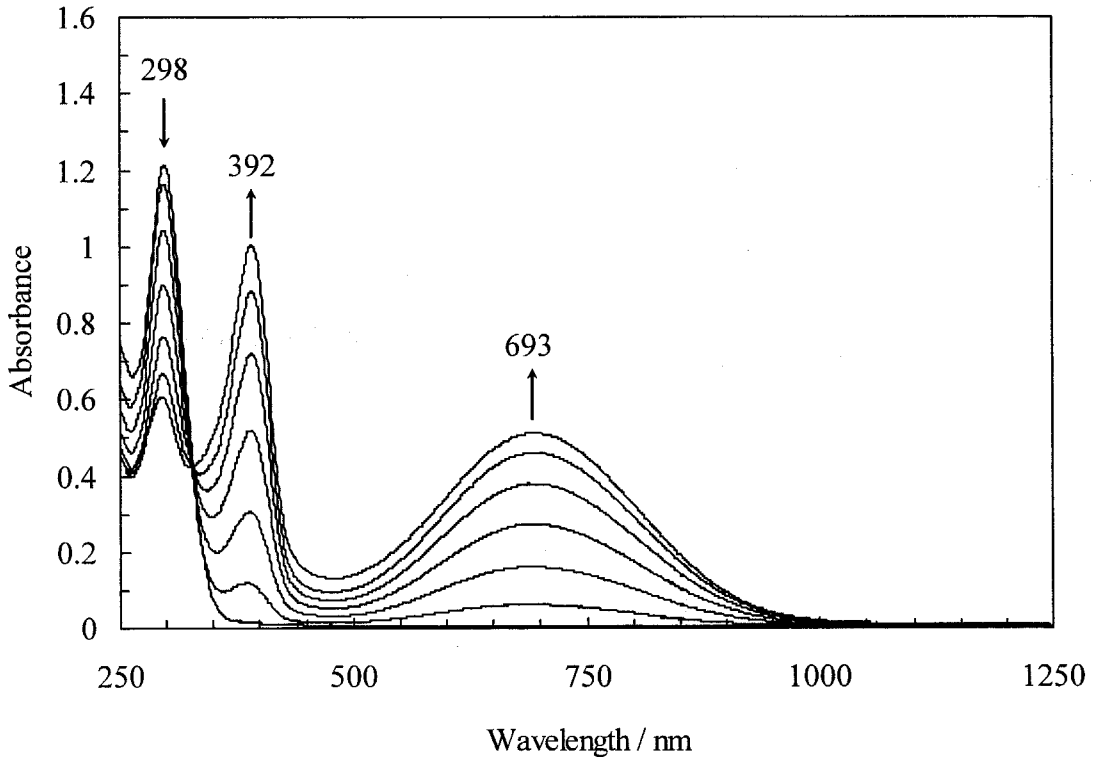

Figure 2. UV/Vis/NIR specrtroelectrogram during sequential oxidation from **1** to $\mathbf{1}^+$ in CH_2Cl_2 containing 0.1 M *n*-Bu_4NBF_4.

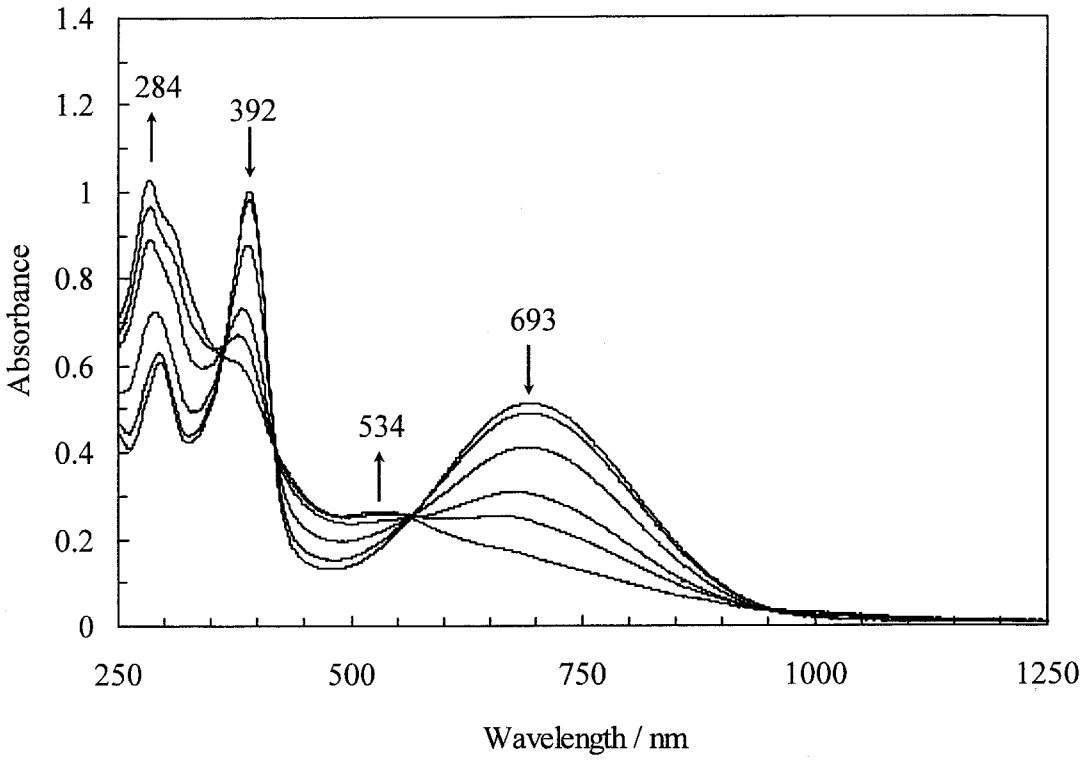

Figure 3. UV/Vis/NIR specrtroelectrogram of further oxidation beyond $\mathbf{1}^+$ in CH_2Cl_2 containing 0.1 M *n*-Bu_4NBF_4

absorption spectrum of further oxidation beyond $\mathbf{1}^+$ showed a disappearance of the IV-CT band and a slight increase in the new band at 534 nm (Figure 3). These spectral changes indicate that the intramolecular electron spin transfer takes place between two amino groups in the central PDA moiety after one-electron oxidation of **1**. Note that the same spectral changes were also seen by the chemical oxidation with $SbCl_5$ in CH_2Cl_2.

The observed IV-CT band showed an overlap with the adjacent bands. Hence we performed the deconvolution of the IV-CT band by using three Gaussian functions (one function for the IV-CT band and two for the adjacent overlapping band) as shown in Figure 4 [14]. Although the Gaussian curve does not fit well to the low-energy side of the IV-CT band, this asymmetry can be explained by the energy cut-off

originating from the smallest energy gap (= $2V$: V stands for the Hush electronic coupling energy) between the ground and excited states [13]. The value of V was estimated 3580 cm^{-1} by using equation (1) [9a].

$$V = \frac{\mu_{eg}}{er} \nu_{max} \tag{1}$$

$$\mu_{eg} = 0.09584 \sqrt{\frac{\int \varepsilon(\nu) d\nu}{\nu_{max}}} \tag{2}$$

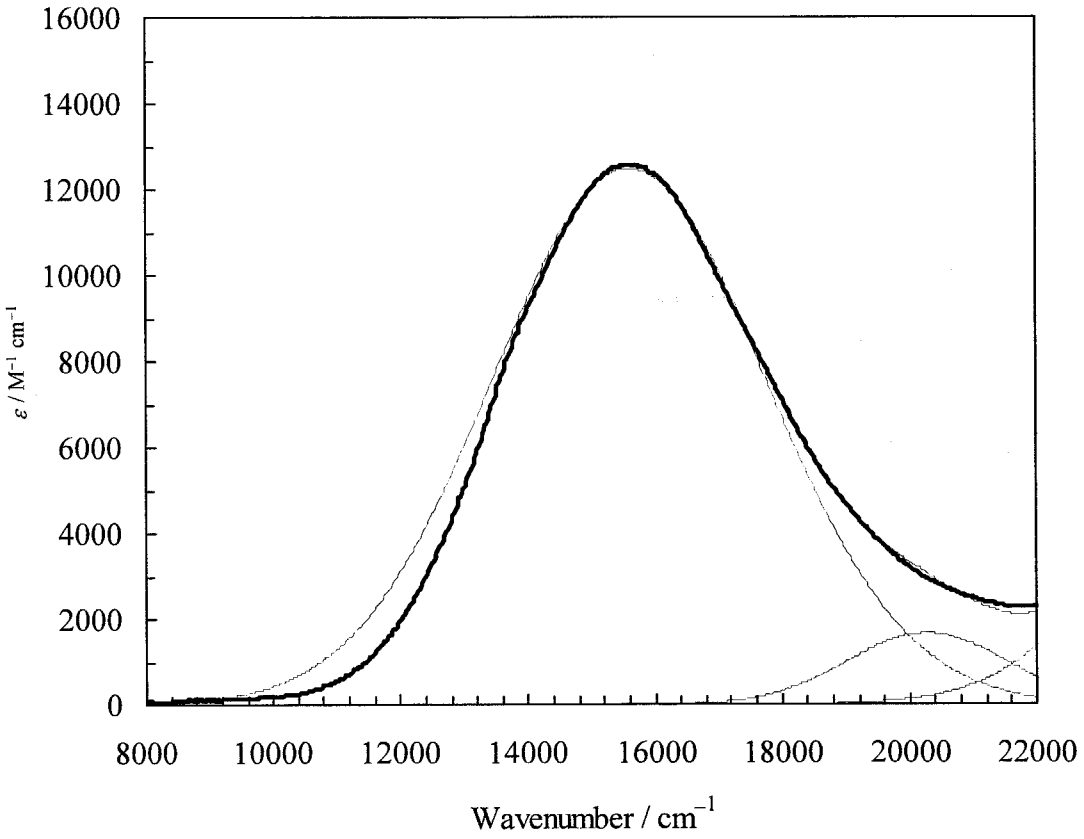

Figure 4. IV-CT band of **1** oxidized with $SbCl_5$ in CH_2Cl_2 (bold line) and Gaussian band fits (fine line).

Here, ν_{max} is the transition energy and, in this case, its value of 1.56×10^4 cm^{-1} is the same as that the Marcus reorganization energy (λ), and e is the elementary charge. For the distance r between the two redox centers, we used the N–N distance (5.589 Å) from the B3LYP/6-31G* optimization of the model compound of $\mathbf{1}^+$, and the transition moment from the ground state to the excited state (μ_{eg}) was evaluated from equation (2). The integration of the IV-CT band was carried out by using the Gaussian fit function. The thermal electron transfer rate constant (k_{th}) was evaluated from the following equation [9a].

$$k_{th} = \nu_n \exp(-\Delta G^*/RT) \tag{3}$$

where the thermal electron transfer barrier ΔG^* is represented by $\lambda/4 - V + V^2/\lambda$. Moreover, the nuclear frequency factor (ν_n) was assumed to be 9×10^{12} s^{-1} according to Ref. 9a. As a result, the k_{th} value was calculated to be 3.6×10^{10} s^{-1} at 298 K. Judging from this analysis, the triradical cation of **1** is found to be classified into Class II intervalence compounds.

5.3.4 Magnetic Property

The temperature dependence of the magnetic susceptibility (χ_M) measured at a constant field of 500 G from 300 to 2 K by a SQUID magnetometer. The plot of $\chi_M T$ versus T for **1** is shown in Figure 5. The $\chi_M T$ value of **1** was close to the theoretical one of 0.75 emu K mol^{-1} for isolated two spins of $S = 1/2$ in the wide temperature range. Below 50 K, the $\chi_M T$ value decreased gradually and reached 0.47 emu K mol^{-1} at 2 K. The observed data was analyzed by the modified Bleaney–Bowers equation for singlet–triplet model [15] (eq. 4) to give the best fit parameters: $f = 0.996\pm0.001$, $J/k_B = 0.6\pm0.2$ K and $\theta = -1.8\pm0.2$ K. This analysis exhibited a very weak ferromagnetic interaction between the two nitroxide groups in **1** ($J/k_B = 0.6$ K), indicating that the two

nitroxide groups are virtually magnetically uncoupled.

$$\chi_m T = f \frac{2N_A g^2 \mu_B^2}{k_B} \frac{1}{3 + \exp(-2J / k_B T)} \frac{T}{T - \theta} \tag{4}$$

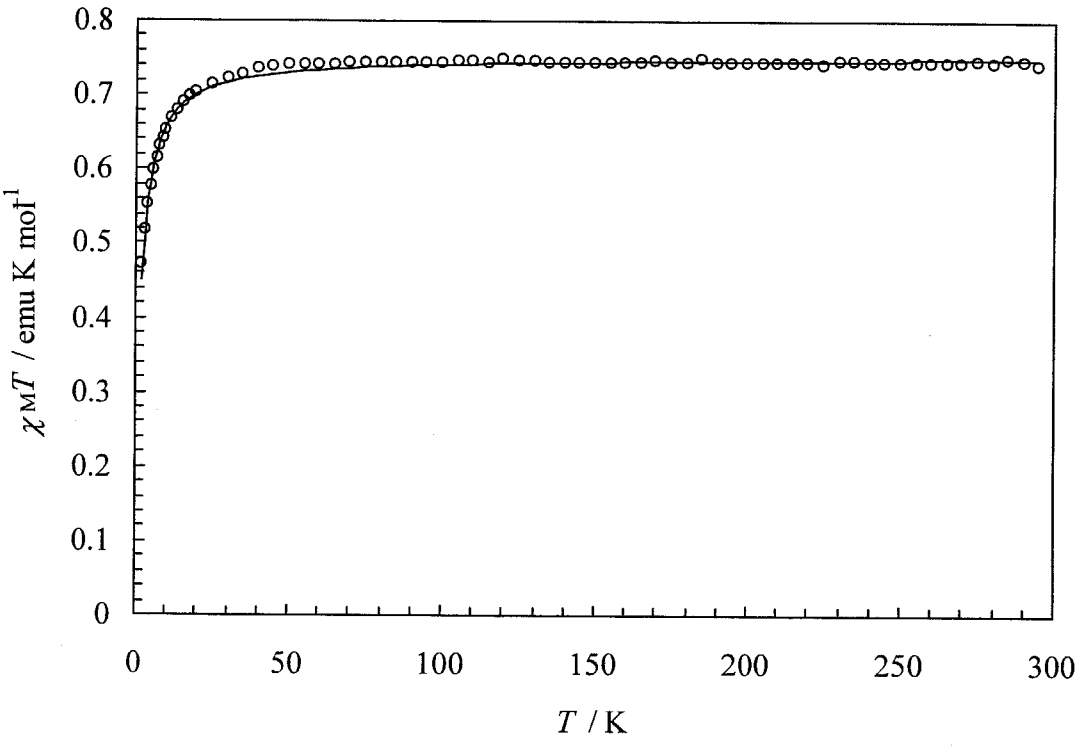

Figure 5. Temperature dependence of $\chi_M T$ of **1** under a field of 500 G. The solid line represents the best theoretical fit to the data (see text).

5.3.5 ESR Spectroscopy

Before turning to the magnetic property of the triradical cation of **1**, we examined the magnetic interaction between the two nitroxide groups of **1** in the neutral state by ESR measurement. The observed EPR spectrum of **1** in frozen *n*-butyronitrile solution consisted of a single signal with unresolved hyperfine- and/or fine-structure at 123 K (Figure 6). In addition, the forbidden $\Delta M_S = \pm 2$ resonance was also observed, suggesting the presence of the triplet species (Figure 6 (inset)).

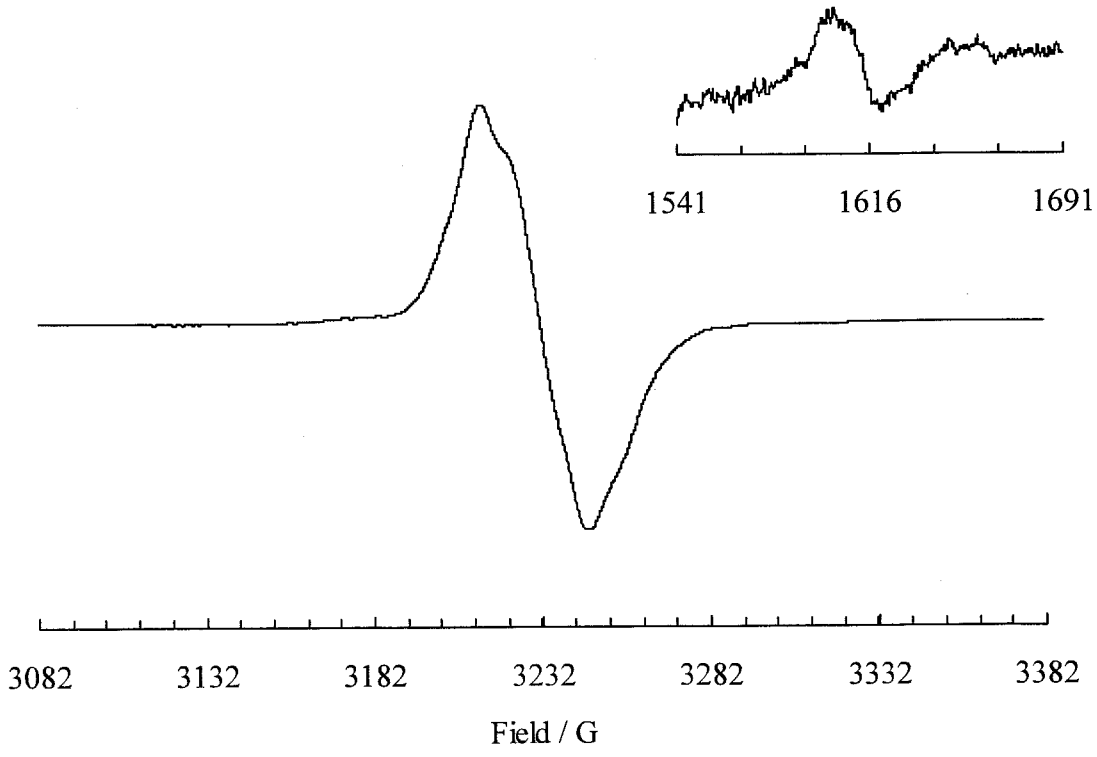

Figure 6. ESR spectrum of **1** in frozen *n*-butyronitrile solution at 123 K and the forbidden $\Delta M_S = \pm 2$ resonance at 123 K (inset).

Finally, the spin preference of triradical cation of **1** is addressed. In the EPR spectrum of the oxidized species of **1** treated with up to 1 molar equivalent of tris(4-bromophenylphenyl)aminium hexachloroantimonate at 195 K, no definite fine-structured spectrum characteristic of the spin quartet state was observed at 123 K, although broad shoulders were seen beside the intense central line (Figure 7). However, the half-field resonance corresponding $\Delta M_S = \pm 2$ transition was detected, and furthermore, the temperature dependence of this forbidden signal obeyed the Curie law (Figure 8), indicating the high possibility of high-spin ground state of the triradical cation $\mathbf{1}^+$.

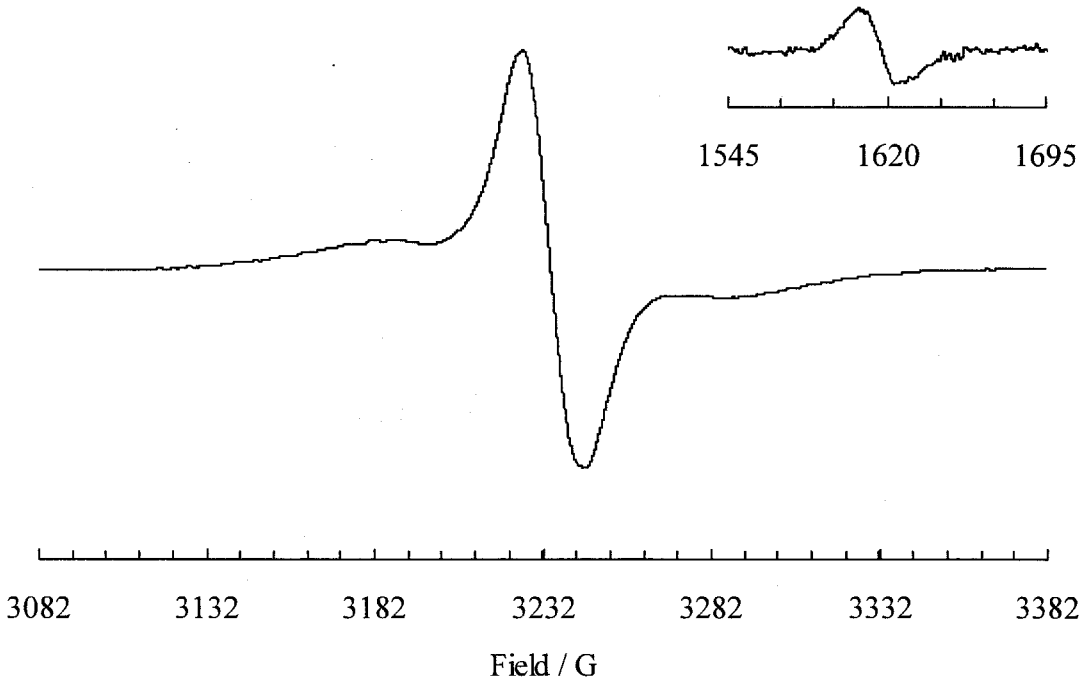

Figure 7. ESR spectrum of $\mathbf{1}^+$ oxidized with tris(4-bromophenyl)aminium hexachloroantimonate in frozen *n*-butyronitrile solution at 123 K and the forbidden $\Delta M_S = \pm 2$ resonance at 123 K (inset).

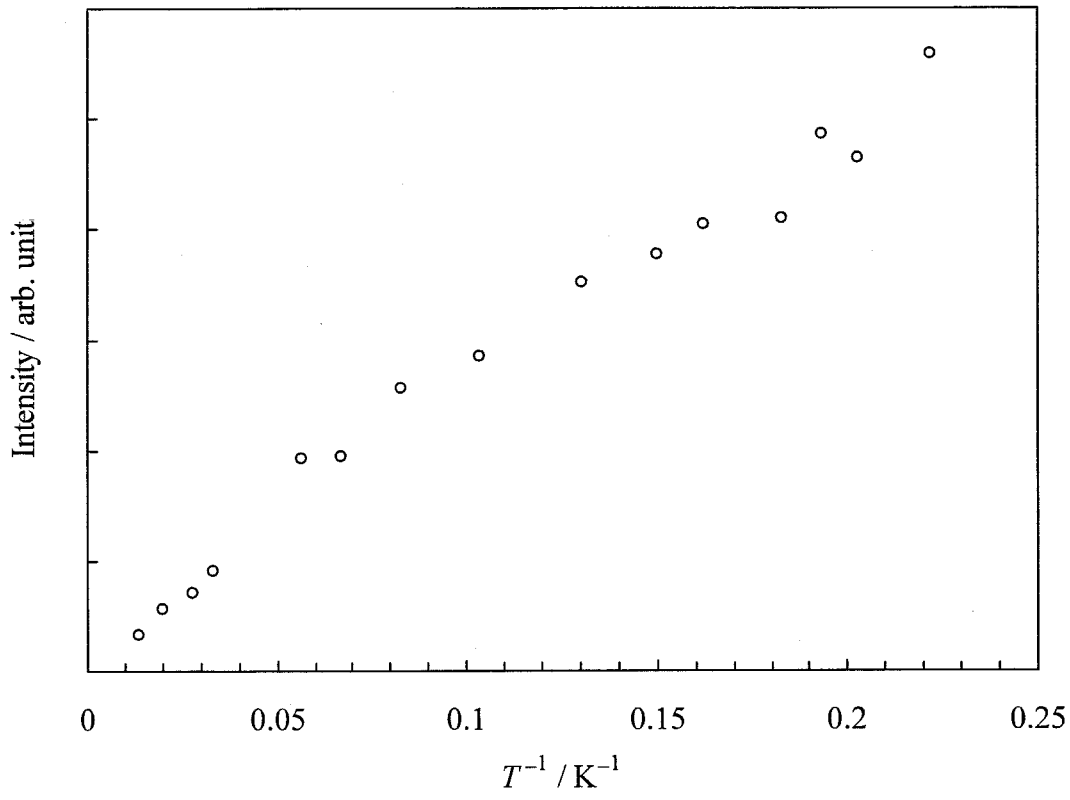

Figure 8. Temperature dependence of the signal intensity for the forbidden $\Delta M_S = \pm 2$ resonance of $\mathbf{1}^+$ oxidized with tris(4-bromophenyl)aminium hexachloroantimonate in frozen *n*-butyronitrile solution.

In order to identify unequivocally spin multiplicity of the main species of the oxidized species of **1** at low temperature, we measured the electron spin transient nutation (ESTN) spectrum based on the pulsed EPR method (Figure 9) [16]. Judging from the ratio [16] between the nutation frequency in question and that for $| S, M_S > = |$ 1/2, +1/2 > ↔ | 1/2, –1/2 > transition (23 MHz), the main nutation signals observed at 39 and 45 MHz were found to be assignable to $| S, M_S > =$ | 3/2, ±3/2 > ↔ | 3/2, ±1/2 > and | 3/2, 1/2 > ↔ |3/2, –1/2 > transitions, respectively. The weak nutation signal at 33 MHz corresponds to | 1, 0 > ↔ | 1, ±1 > transition of the unoxidized **1**.

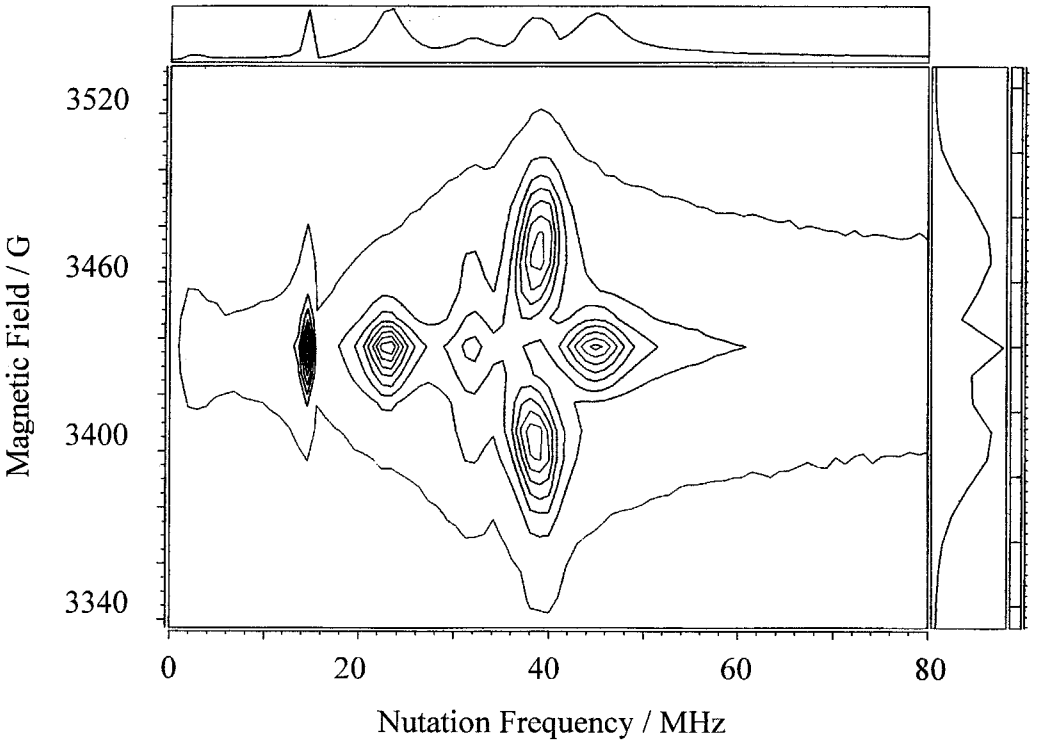

Figure 9. ESTN spectrum of $\mathbf{1}^+$ oxidized with tris(4-bromophenyl)aminium hexachloroantimonate in frozen *n*-butyronitrile solution at 5 K.

5.4 Conclusion

In summary, it was demonstrated the first example of parallel spin alignment mediated by the mixed-valence state for multi-spin organic molecule. The present triradical cation is also considered to be novel in that the localized spin and the delocalized spin coexist in. Currently, the extension of the present molecule to the oligoaniline-based system are undertaken, and the application to the single-molecular devices is also.

References

[1] (a) L. Thomas, Nature 383 (1996) 145; (b) A. Thiaville, J. Miltat, Science 284 (1999) 1939; (c) J.R. Friedman, M.P. Sarachik, J. Tejada, R. Ziolo, Phys. Rev. Lett. 76 (1996) 3830; (d) C. Sangregorio, T. Ohm, C. Paulsen, R. Sessoli, D. Gatteschi, Phys. Rev. Lett. 78 (1997) 4645; (e) W. Wernsdofer, R. Sessoli, A. Caneschi, D. Gatteschi, A. Cornia, Europhys. Lett. 50 (2000) 552.

[2] M.N. Leuenberger, D. Loss, Nature 410 (2001) 789.

[3] J.A. Crayston, J.N. Devine, J.C. Walton, Tetrahedron 56 (2000) 7829.

[4] (a) D.A. Doughherty, Acc. Chem. Res. 24 (1991) 88; (b) H. Iwamura, N. Koga, Acc. Chem. Res. 26 (1993) 346; (c) A. Rajca, Chem. Rev. 94 (1994) 871.

[5] (a) M. Matsushita, T. Nakamura, T. Momose, T. Shida, Y. Teki, T. Takui, T. Kinoshita, K. Itoh, J. Am. Chem. Soc. 114 (1992) 7470; (b) S. Rajca, A. Rajca, J. Am. Chem. Soc. 117 (1995) 9172; (c) T. Nakamura, T. Momose, T. Shida, T. Kinoshita, T. Takui, Y. Teki, K. Itoh, J. Am. Chem. Soc. 117 (1995) 11292; (d) T. Nakamura, T. Momose, T. Shida, K. Sato, S. Nakazawa, T. Kinoshita, T. Takui, K. Itoh, T. Okuno, A. Izuoka, T. Sugawara, J. Am. Chem. Soc. 118 (1996) 8684; (e) J. Sedó, D. Ruiz, J. Vidal-Gancedo, C. Rovira, J. Bonvoisin, J.-P. Launay, J. Veciana, Adv. Mater. 8 (1996) 748.

[6] (a) M. Matsushita, T. Nakamura, T. Momose, T. Shida, Y. Teki, T. Takui, T. Kinoshita, K. Itoh, Bull. Chem. Soc. Jpn. 66 (1993) 1333; (b) A. Izuoka, M. Hiraishi, T. Abe, T. Sugawara, K. Sato, T. Takui, J. Am. Chem. Soc. 122 (2000), 3234; (c) J. Nakazaki, I. Chung, M.M. Matsushita, T. Sugawara, R. Watanabe, A. Izuoka, Y. Kawada, J. Mater. Chem. 13 (2003) 1011; (d) G. Harada, T. Jin, A. Izuoka, M.M. Matsushita, T. Sugawara, Tetrahedron Lett. 44 (2003) 4415.

[7] (a) S.F. Nelsen, Chem. Eur. J. 6 (2000) 581; (b) L.-P. Launay, Chem. Soc. Rev. 30

(2001) 386.

[8] (a) S. Mazur, A.H. Schroeder, J. Am. Chem. Soc. 100 (1978) 7339; (b) S.F. Nelsen, J.A. Thomson-Colon, M. Katfory, J. Am. Chem. Soc. 111 (1989) 2809; (c) J.E. Almlöf, M.W. Feyereisen, T.H. Josefiak, L.L. Miller, J. Am. Chem. Soc. 112 (1990) 1206; (d) P. Maslak, M.P. Augustine, J.D. Burkey, J. Am. Chem. Soc. 112 (1990) 5359; (e) S. Utamapanya, A. Rajca, J. Am. Chem. Soc. 113 (1991) 9242; (f) J.P. Telo, M.C.B.L. Shohoji, B.J. Herold, G. Grampp, J. Chem. Soc., Faraday Trans. 88 (1992) 47; (g) J. Bonvoisin, J.-P. Launay, M. van der Auweraer, F. C. De Schryver, J. Phys. Chem. 98 (1994) 5052; (h) K. Lahil, A. Moradpour, C. Bowlas, F. Menou, P. Cassoux, J. Bonvoisin, J.-P. Launay, G. Dive, D. Dehareng, J. Am. Chem. Soc. 117 (1995) 9995; (i) J. Bonboisin, J.-P. Launay, W. Verbouwe, M. van der Auweraer, F.C. De Schryver, J. Phys. Chem. 100 (1996) 17079; (j) S.F. Nelsen, H.Q. Tran, M.A. Nagy, J. Am. Chem. Soc. 120 (1998) 298; (k) C. Lambert, W. Gaschler, E. Schmälzlin, K. Meerholz, C. Bräuchle, J. Chem. Soc., Perkin Trans 2 (1999) 577; (l) C. Rovira, D. Ruiz-Molina, O. Elsner, J. Vidal-Gancedo, J. Bonvoisin, J.-P. Launay, J. Veciana, Chem. Eur. J. 7 (2001) 240; (m) M. Mayor, M. Büschel, K.M. Fromm, J.-M. Lehn, J. Daub, Chem. Eur. J. 7 (2001) 1266; (n) C. Lambert, G. Nöll, F. Hampel, J. Phys. Chem. A 105 (2001) 7751; (o) S.V. Lindeman, S.V. Rosokha, D. Sun, J.K. Kochi, J. Am. Chem. Soc. 124 (2002) 842; (p) C. Lambert, G. Nöll, Chem. Eur. J. 8 (2002) 3467; (q) F. Dumur, N. Gautier, N. Gallego-Planas, Y. Sahin, E. Levillain, M. Masino, A. Girlando, V. Lloveras, J. Vidal-Gancedo, J. Veciana, C. Rovira, J. Org. Chem. 69 (2004) 2164.

[9] (a) C. Lambert, G. Nöll, J. Am. Chem. Soc. 121 (1999) 8434; (b) C. Lambert, G. Nöll, J. Schelter, Nat. Mater. 1 (2002) 69; (c) C. Lambert, G. Nöll, J. Chem. Soc., Perkin Trans 2 (2002) 2039.

[10] A. Ito, M. Urabe, K. Tanaka, Polyhedron 22 (2003) 1829.

[11] T. Ishida, H. Iwamura, J. Am. Chem. Soc. 113 (1991) 4238.

[12] T. Nishiumi, Y. Nomura, Y. Chimoto, M. Higuchi, K. Yamamoto, J. Phys. Chem. B 108 (2004) 7992.

[13] (a) N.S. Hush, Prog. Inorg. Chem. 8 (1967) 391; (b) N.S. Hush, Electrochem. Acta 13 (1968) 1005; (c) N.S. Hush, Coord. Chem. Rev. 64 (1985) 135.

[14] For the deconvolution procedure, see: A.-C. Ribou, J.-P. Launay, K. Takahashi, T. Nihira, S. Tarutani, C. W. Spangler, Inorg. Chem. 33 (1994) 1325.

[15] B. Bleaney, K.D. Bowers, Proc. R. Soc. London A214 (1952) 451.

[16] The magnetic moments with distinct spin quantum numbers (S) precess with their specific nutation frequency (ω_n) in the presence of a microwave irradiation field and a static magnetic field. The nutation frequency for a transition from $| S, M_S >$ to $| S, M_S +1>$ can be expressed as $\omega_n = [S(S+1) - M_S(M_S+1)]1/2\omega_0$ under certain conditions. This indicates that ω_n can be scaled with the total spin quantum number S and the spin magnetic quantum number M_S in the unit of ω_n (= ω_0) for the doublet species; $\sqrt{2}$ for S =1, $\sqrt{3}$ and 2 for S = 3/2. For determination of spin-multiplicity for high-spin molecules by using the pulsed EPR technique, see: (a) J. Isoya, H. Kanda, J.R. Norris, J. Tang, M.K. Brown, Phys. Rev. B 41 (1990) 3905; (b) A.V. Astashkin, A. Schweiger, Chem. Phys. Lett. 174 (1990) 595; (c) K. Sato, M. Yano, M. Furuichi, D. Shiomi, T. Takui, K. Abe, K. Itoh, A. Higuchi, K. Katsuma, Y. Shirota, J. Am. Chem. Soc. 119 (1997) 6607; (d) A. Ito, H. Ino, Y. Matsui, Y. Hirao, K. Tanaka, K. Kanemoto, T. Kato, J. Phys. Chem. A 108 (2004) 5715.

Chapter 6

Theoretical Study on Radical Substituent's Effect of *p*-Phenylenediamine-Based Spin System

6.1 Introduction

Recently, many organic mixed-valence compounds have been reported, and the intramolecular electron transfer have been examined [1], in which an extra electron hops between the redox sites, that is, the extra electron is somewhat (or completely) delocalized over the redox sites. When the localized spin is added to the mixed-valence system, the double-exchange interaction is expected to work between the localized and delocalized spins, leading to a parallel spin alignment [2]. The stable organic radicals such as nitroxide and nitronyl nitroxide radical are well known as the localized spin source in organic compounds. Therefore, the organic multi-spin systems, including both of the localized and delocalized spins, can be constructed by combining the stable radicals with the organic mixed-valence systems. In Chapter 5, the spin alignment mediated by mixed-valence state in *N*,*N*'-bis[3-*tert*-butyl-5-(*N*-*tert*-butyl-*N*-oxylamino)phenyl]-*N*,*N*'-dimethyl-*p*-phenylenediamine was discussed from the

experimental results. In this chapter, the author theoretically examines the electronic structures of the neutral and cationic forms for the simplified model shown in Figure 1 to clarify the effect of peripherally substituted radical groups, i.e., nitroxide and nitronyl nitroxide radicals.

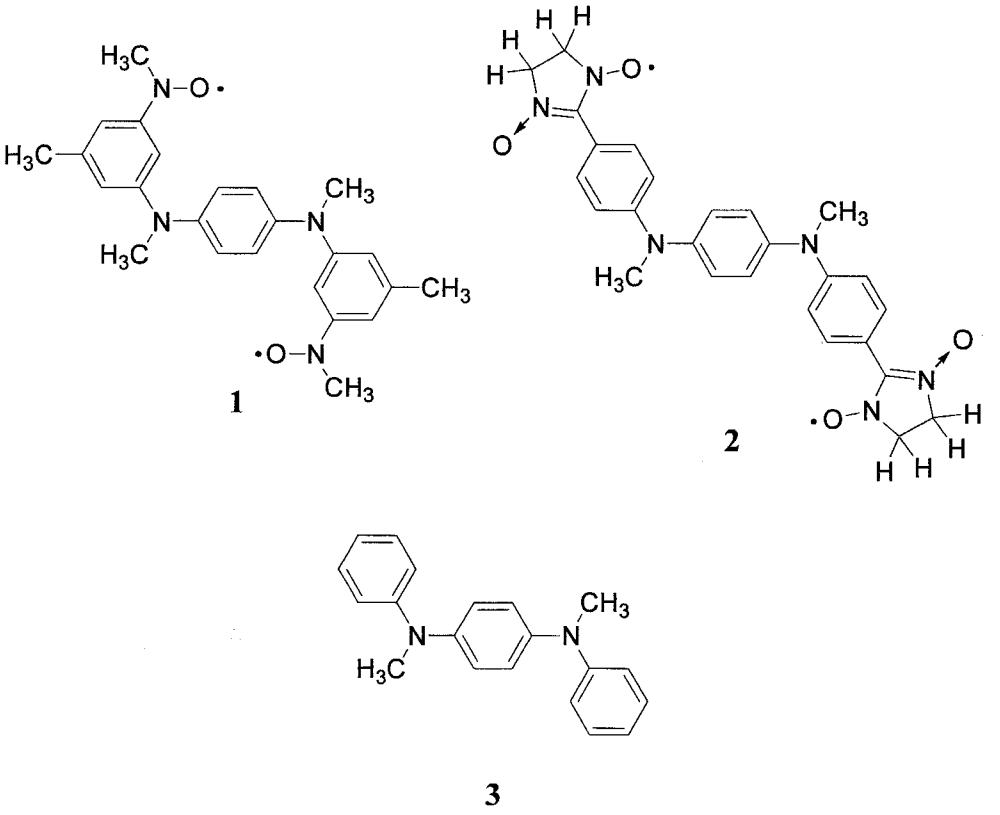

Figure 1. Calculated model compounds studied in this chapter.

6.2 Computational Details

For the neutral and cationic states of **1** and **2**, the hybrid HF/DF (UB3LYP [3]) calculations were performed by using 6-31G* basis sets for C, N and O, and 6-31G

basis sets for H. Full geometry optimizations were carried out under the C_i symmetrical constraint. For the calculation of the open-shell singlet state, the broken-symmetry wavefunction was employed. All of the computations were carried out with Gaussian 98 program package [4].

6.3 Results and Discussion

First of all, the geometry optimization on the singlet and triplet states of **1** and **2**, and the doublet and quartet states of $\mathbf{1}^+$ and $\mathbf{2}^+$ were performed at the UB3LYP/6-31G* level. The calculated total energies and the $<S^2>$ values for the corresponding high-spin and low-spin states of **1**, $\mathbf{1}^+$, **2** and $\mathbf{2}^+$ are summarized in Table 1, and the calculated structural parameters are listed in Tables 2 and 3. Here, the atomic numberings and the torsional angles (φ_1, φ_2, φ_3) are defined as Figure 2, and the quinoidal parameter q (%) was evaluated using eq. (1) (ref. [5]):

$$q = 100 \times \frac{d_1 - d_2}{d_1' - d_2'} \tag{1}$$

where d_1 and d_2 are the optimized bond lengths in the central benzene ring depicted in Figure 3, and d_1' and d_2' are taken from the bond lengths of $\mathbf{3}^+$ optimized at the UB3LYP/6-31G* level (d_1' = 1.428 Å and d_2' = 1.372 Å).

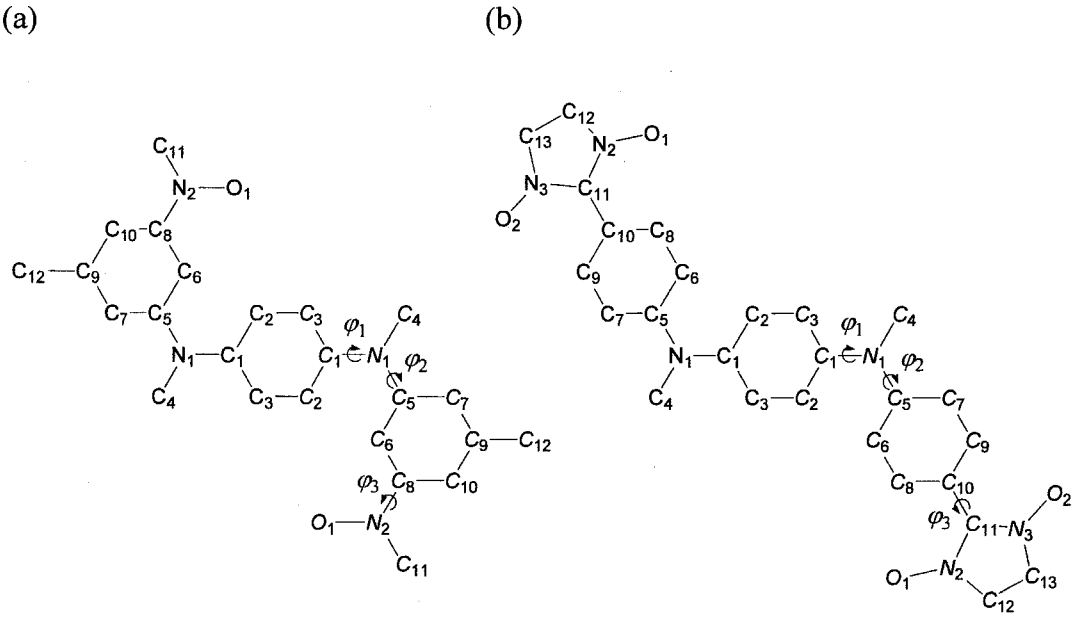

Figure 2. Atomic numberings and dihedral angles of (a) **1** and (b) **2**. Note that the atoms related by C_i symmetry are in italics.

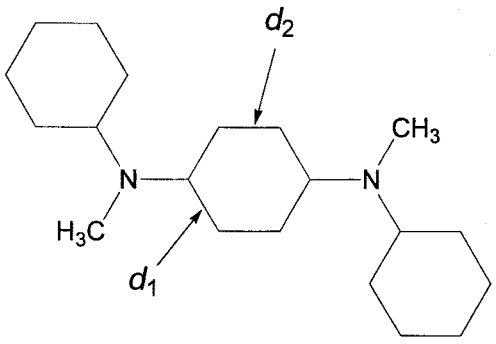

Figure 3. The definition of d_1 and d_2 in the central benzene ring.

6.3.1 Optimized Geometry

In the neutral states of **1** and **2**, the singlet–triplet energy gaps were estimated to be nearly zero, indicating that the singlet and triplet states are virtually degenerated in the neutral state (Table 1). Indeed, the optimized geometries for the singlet states of **1** and **2** are almost the same as those for the corresponding triplet states (Tables 2, 3).

On the other hand, the quartet states of $\mathbf{1}^+$ and $\mathbf{2}^+$ were predicted to be more stable by 0.8 and 2.3 kcal mol^{-1} than the corresponding doublet states, respectively (Table 1). In contrast to the neutral states, the central benzene rings are found to be quinoidally deformed in the cationic $\mathbf{1}^+$ and $\mathbf{2}^+$. Moreover, it should be noted that such a quinoidal deformation accompanies a decrease of φ_1 and an increase of φ_2. Consequently, the optimized structure of the *p*-phenylene moiety in $\mathbf{1}^+$ and $\mathbf{2}^+$ is very similar to that of $\mathbf{3}^+$ in the doublet state. It is noteworthy that only $\mathbf{2}^+$ in the quartet state shows the extremely small q value (84.8 %) in comparison with those of the other cationic species (>97 %). Moreover, the torsional angle φ_1 (φ_2) of the quartet $\mathbf{2}^+$ is larger (smaller) than those in the other cationic state. Since the increasing of the torsional angle φ_1 weakens the π-conjugation between the π-orbital of the central *p*-phenylene moiety and the p-orbitals of the neighboring amino nitrogen atoms, it is expected that the electron transfer between two amino redox sites on the *p*-phenylenediamine moiety is suppressed in the quartet $\mathbf{2}^+$ [6]. This results in the small q value, that is, the low-level quinoidal deformation.

Table 1. Total Energies (E) and $<S^2>$ values[a] for the High-Spin (HS)[b] and Low-Spin (LS)[c] States and Relative Energies (ΔE)[d] of **1**, $\mathbf{1}^+$, **2** and $\mathbf{2}^+$

	E_{HS} (hartree)	$<S^2>_{HS}$	E_{LS} (hartree)	$<S^2>_{LS}$	ΔE (kcal mol^{-1})
1	−1300.7301	2.022	−1300.7301	1.022	~ 0[e]
$\mathbf{1}^+$	−1300.5254	3.788	−1300.5241	1.771	0.8
2	−1635.5588	2.124	−1635.5588	1.124	~ 0[f]
$\mathbf{2}^+$	−1635.3497	3.903	−1635.3461	1.883	2.3

[a]$<S^2>$ values for the pure singlet, doublet, triplet and quartet states are 0, 0.75, 2 and 3.75, respectively. [b]The triplet states for **1** and **2**, and the quartet states for $\mathbf{1}^+$ and $\mathbf{2}^+$. [c]The singlet states for **1** and **2**, and the doublet states for $\mathbf{1}^+$ and $\mathbf{2}^+$. [d]$\Delta E = E_{LS} - E_{HS}$. [e]−0.8 cal mol^{-1}. [f]−2.2 cal mol^{-1}.

Table 2. Optimized Bond lengths (Å) and Structural Parameters, φ_1 (°), φ_2 (°), φ_3 (°) and q (%) for **1** and $\mathbf{1}^+$

	1		$\mathbf{1}^+$	
	Singlet	Triplet	Doublet	Quartet
C_1–$C_2(C_3)$[a]	1.402	1.402	1.428	1.427
C_2–C_3	1.392	1.392	1.371	1.372
N_1–C_1	1.426	1.426	1.363	1.367
N_1–C_4	1.459	1.458	1.470	1.470
N_1–C_5	1.400	1.400	1.441	1.435
C_5–C_6	1.406	1.406	1.390	1.392
C_5–C_7	1.410	1.410	1.401	1.404
C_6–C_8	1.397	1.397	1.406	1.406
C_7–C_9	1.400	1.400	1.400	1.398
C_8–C_{10}	1.408	1.408	1.405	1.405
C_9–C_{10}	1.394	1.394	1.400	1.401
N_2–C_8	1.411	1.411	1.405	1.404
N_2–O_1	1.283	1.283	1.280	1.280
N_2–C_{11}	1.464	1.464	1.467	1.467
C_9–C_{12}	1.513	1.513	1.511	1.511
φ_1	48.3	48.3	13.3	17.0
φ_2	24.7	24.7	59.4	51.8
φ_3	1.5	1.5	2.5	2.6
q	18.0	18.0	102.3	97.7

[a]Average bond length.

Table 3. Optimized Bond lengths (Å) and Structural Parameters, φ_1 (°), φ_2 (°), φ_3 (°) and q (%) for **2** and $\mathbf{2}^+$

	2		$\mathbf{2}^+$	
	Singlet	Triplet	Doublet	Quartet
C_1–$C_2(C_3)$[a]	1.402	1.402	1.427	1.423
C_2–C_3	1.392	1.392	1.372	1.376
N_1–C_1	1.426	1.426	1.366	1.376
N_1–C_4	1.460	1.460	1.470	1.470
N_1–C_5	1.394	1.394	1.436	1.422
C_5–$C_6(C_7)$[a]	1.412	1.412	1.400	1.405
$C_6(C_7)$–$C_8(C_9)$[a]	1.386	1.386	1.390	1.386
$C_8(C_9)$–C_{10}[a]	1.413	1.413	1.412	1.415
C_{10}–C_{11}	1.455	1.455	1.462	1.455
C_{11}–$N_2(N_3)$[a]	1.367	1.367	1.365	1.368
$N_2(N_3)$–$O_1(O_2)$[a]	1.276	1.276	1.271	1.271
$N_2(N_3)$–$C_{12}(C_{13})$[a]	1.482	1.482	1.486	1.486
C_{12}–C_{13}	1.527	1.527	1.529	1.529
φ_1	48.9	48.9	14.8	21.1
φ_2	23.2	23.2	55.7	45.1
φ_3	2.4	2.4	4.4	5.2
q	18.8	18.8	98.8	84.8

[a]Average bond length.

6.3.2 Frontier Orbital

The quartet states of $\mathbf{1}^+$ and $\mathbf{2}^+$ have three singly-occupied molecular orbitals (SOMOs), depicted in Figure 4, where the almost degenerate two SOMOs ($55a_g$ and $54a_u$ for $\mathbf{1}^+$; $65a_g$ and $64a_u$ for $\mathbf{2}^+$) composed of the π-orbitals on the substituting radical moieties are nearly degenerate with the SOMO ($54a_g$ for $\mathbf{1}^+$; $64a_g$ for $\mathbf{2}^+$) composed of the π-orbital on the *p*-phenylenediamine moiety. Apparently, $\mathbf{1}^+$ and $\mathbf{2}^+$ are regarded as *non-disjoint* systems [7], where the same atomic orbitals are shared among the SOMOs. Since the high-spin state is relatively stabilized owing to the exchange interaction in the *non-disjoint* system, the quartet states are expected to be lower in energy than the doublet states in $\mathbf{1}^+$ and $\mathbf{2}^+$. The relatively delocalized $54a_g$ SOMOs for $\mathbf{1}^+$ (the $64a_g$ for $\mathbf{2}^+$) is very similar to that of $\mathbf{3}^+$. In particular, the $64a_g$ SOMO spreads over the nitroxyl oxygen atoms, resulting in the decrease of electron density on the central *p*-phenylene ring. As mentioned in 6.3.1, the quartet $\mathbf{2}^+$ has the larger torsional angle φ_1 along the N_1–C_1 bond and the smaller torsional angle φ_2 along the N_1–C_5 bond than the quartet $\mathbf{1}^+$. This situation causes the decrease of the orbital interaction between the amino redox sites due to the large φ_1, while the p-orbital of the amino nitrogen interacts more with the π-orbital of the peripheral benzene ring. As a result, the electron density on the central *p*-phenylenediamine moiety flows into the benzene rings surrounding the central *p*-phenylenediamine moiety, leading to the more delocalized SOMO. Hence, the delocalized $64a_g$ SOMO strengthens the *non-disjoint* character, resulting in the larger stabilization of the quartet state of $\mathbf{2}^+$.

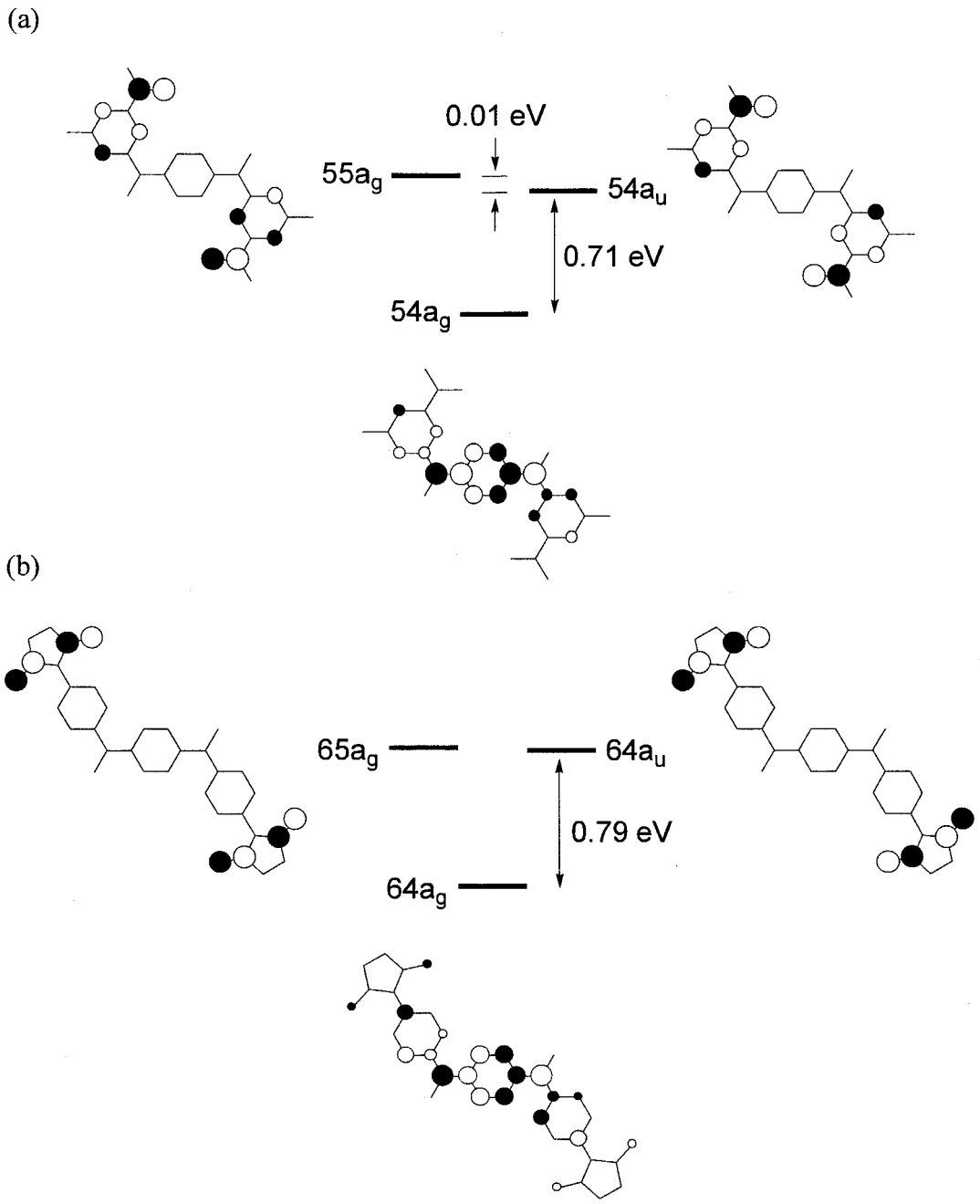

Figure 4. Schematic drawing of the SOMOs for the quartet state of (a) $\mathbf{1}^+$ and (b) $\mathbf{2}^+$ and their relative energy levels.

6.3.3 Natural Orbital Analysis

In order to explore a little further into electron correlations in high-spin molecules, the post-Hartree-Fock calculations are needed, and the complete active space self-consistent field (CASSCF) calculation including all π-orbitals is one of the most reliable methods. However, for the large molecules like $\mathbf{1}^+$ and $\mathbf{2}^+$, it is prohibitively time-consuming to carry out the CASSCF calculations. On the other hand, the natural orbital (NO) analyses for the UHF and UDFT solutions have been often used as an alternative method for the CASSCF calculations, where the orbital overlap (T_i) is related with the occupation numbers of the bonding and antibonding natural orbitals by equation (2).

$$n_i = 1 + T_i,\ n_i^* = 1 - T_i \qquad (2)$$

Herein, $T_i = 1.0$ for the closed-shell pair, that is, the n_i and n_i^* are 2.0 and 0.0, respectively.

Table 4 summarizes the occupation numbers of the NOs calculated at the geometries of the quartet $\mathbf{1}^+$ and $\mathbf{2}^+$. Judging from the occupation numbers of 1.0 for three SOMOs (SO+0 and SO±1), both of the quartet states of $\mathbf{1}^+$ and $\mathbf{2}^+$ show the negligible orbital overlaps between the magnetic orbitals. On the other hand, the occupation numbers of (HO–1), (HO–2), (LU+1), and (LU+2)MOs in $\mathbf{2}^+$ considerably deviates from 2.0 and 0.0 for the pure closed-shell pair. This indicates that these orbitals significantly contribute to the spin polarization effect in $\mathbf{2}^+$.

Table 4. Occupation Numbers[a] of the Natural Orbitals of $\mathbf{1}^+$ and $\mathbf{2}^+$

	$\mathbf{1}^+$		$\mathbf{2}^+$	
	Doublet	Quartet	Doublet	Quartet
LU+3	0.002	0.003	0.003	0.003
LU+2	0.002	0.004	0.027	0.031
LU+1	0.004	0.004	0.031	0.037
SO+1	0.984	1.000	0.934	1.000
SO+0	1.000	1.000	1.000	1.000
SO–1	1.016	1.000	1.066	1.000
HO–1	1.996	1.996	1.969	1.963
HO–2	1.998	1.996	1.973	1.969
HO–3	1.998	1.997	1.997	1.997

[a]Calculated at the geometry of the quartet state.

6.3.4 Spin Density Distribution

It is well-known that the reasonable spin densities are usually obtained by the DFT method. The B3LYP spin densities are listed in Table 5. For both **1** and **2** in the singlet states, the sign of spin density on one atom after the other changes alternately except for the amino nitrogen atoms. On the other hand, for both $\mathbf{1}^+$ and $\mathbf{2}^+$ in the quartet states, the alternation of the sign appear only on the peripheral aryl moieties, whereas the positive spin densities appear on all the atoms in the central *p*-phenylenediamine moiety, indicating the double-exchange interaction works in the systems of $\mathbf{1}^+$ and $\mathbf{2}^+$. Compared with the spin density on the central *p*-phenylenediamine moiety (N_1, C_1, C_2, and C_3) of $\mathbf{3}^+$, the spin densities of $\mathbf{1}^+$ are very similar to those of $\mathbf{3}^+$, while the spin densities of $\mathbf{2}^+$ are smaller than those of $\mathbf{3}^+$. This is consistent with the fact that the SOMO on the central *p*-phenylenediamine moiety delocalizes over the peripheral aryl moieties in $\mathbf{2}^+$ as described in 6.3.2. Moreover, the spin density on the nitroxyl moiety (N_2–O_1) in $\mathbf{1}^+$ decreases from 0.870 to 0.857 as compared with the corresponding spin density in **1**, while the spin density on the nitronyl nitroxide moiety (O_1–N_2–C_{11}–N_3–O_2) increases from 1.038 to 1.080 on going from **2** to $\mathbf{2}^+$. In addition to these changes, the total spin density on the peripheral benzene ring (C_5, C_6, C_7, C_8, C_9, and C_{10}) increases from 0.152 to 0.214 (–0.033 to 0.037) on going from **1**(**2**) to $\mathbf{1}^+(\mathbf{2}^+)$. As a whole, the spin density on the nitroxyl moiety in $\mathbf{1}^+$ delocalizes over the peripheral benzene ring, whereas the spin density on the central *p*-phenylenediamine moiety in $\mathbf{2}^+$ over the peripheral nitronyl nitroxide moieties.

Table 5. Spin Densities for the Ground States of **1**, $\mathbf{1}^+$, **2**, $\mathbf{2}^+$, and $\mathbf{3}^+$

	1 (S)[a, b]	$\mathbf{1}^+$ (Q)[a]	**2** (S)[a, b]	$\mathbf{2}^+$ (Q)[a]	$\mathbf{3}^+$ (D)[a]
N_1	–0.005	0.257	–0.012	0.228	0.261
C_1	0.003	0.096	0.004	0.071	0.098
C_2	–0.003	0.064	–0.004	0.052	0.064
C_3	–0.003	0.025	–0.004	0.019	0.030
C_4	0.001	–0.020	0.001	–0.018	–0.020
C_5	–0.053	–0.083	–0.038	–0.064	–0.022
C_6	0.138	0.165	0.023	0.071	0.034
C_7	0.117	0.150	0.023	0.066	0.028
C_8	–0.100	–0.109	–0.042	–0.075	–0.016
C_9	–0.063	–0.077	–0.048	–0.068	–0.012
C_{10}	0.113	0.168	0.049	0.107	0.032
C_{11}	–0.032	–0.028	–0.209	–0.221	
N_2	0.360	0.333	0.273	0.272	
O_1	0.510	0.524	0.351	0.378	
N_3			0.273	0.271	
O_2			0.350	0.380	
C_{12}			–0.024	–0.024	
C_{13}	0.004	0.005	–0.024	–0.024	

[a]S, D, T, and Q represent the singlet, doublet, triplet, and quartet states, respectively. [b]In the singlet state, the spin densities on two atoms related by C_i symmetry have the same magnitude but the opposite sign.

6.4 Conclusion

The UB3LYP calculations predicted that the cationic states of **1** and **2** have the quartet ground states, i.e., the intramolecular ferromagnetic interaction, while the singlet and triplet states is nearly degenerated in the neutral state. Moreover, it was found that the ferromagnetic interaction can be explained by the *non-disjoint* nature of the SOMOs. In $\mathbf{2}^{+}$, the substitution of the nitronyl nitroxide radical resulted in the more delocalized SOMOs than $\mathbf{1}^{+}$, indicating a strong intramolecular ferromagnetic interaction for $\mathbf{2}^{+}$. However, the large torsional angle along the N_1–C_1 bond in $\mathbf{2}^{+}$ causes a weak overlap between the p-orbitals of the amino redox sites. Therefore, it is expected that the electron hopping between the amino redox sites is suppressed in the case of nitronyl nitroxide substitution ($\mathbf{2}^{+}$).

References

[1] (a) S.F. Nelsen, H. Chang, J.J. Wolff, J. Adamus, J. Am Chem. Soc. 115 (1993) 12276; (b) S.F. Nelsen, R.F. Ismagilov, D.R. Powell, J. Am. Chem. Soc. 118 (1996) 6313; (c) S.F. Nelsen. R.F. Ismagilov, D.R. Powell, J. Am. Chem. Soc. 119 (1997) 10213; (d) C. Lambert, G. Nöll, J. Am. Chem. Soc. 121 (1999) 8434; (e) C. Lambert, W. Gaschler, E. Schmälzlin, K. Meerholz, C. Bräuchle, J. Chem. Soc. Perkin 2 (1999) 577; (f) C. Lambert, G. Nöll, Chem. Eur. J. 8 (2002) 3467.

[2] C. Zener, Phys. Rev. 82 (1951) 403.

[3] A.D. Becke, J. Chem. Phys. 98 (1993) 5648.

[4] M.J. Frisch, G.W. Trucks, H. B. Schlegel, G.E. Scuseria, M.A. Robb, J.R. Cheeseman, V.G. Zakrzewski, J.A. Montgomery, R.E. Jr. Stratmann, J.C. Burant, S. Dapprich, J.M. Millam, A.D. Daniels, K.N. Kudin, M.C. Strain, O. Farkas, J. Tomasi, V. Barone, M. Cossi, R. Cammi, B. Mennucci, C. Pomelli, C. Adamo, S. Clifford, J. Ochterski, G.A. Petersson, P.Y. Ayala, Q. Cui, K. Morokuma, D.K. Malick, A.D. Rabuck, K. Raghavachari, J.B. Foresman, J. Cioslowski, J.V. Ortiz, A. G. Baboul, B.B. Stefanov, G. Liu, A. Liashenko, P. Piskorz, I. Komaromi, R. Gomperts, R.L. Martin, D.J. Fox, T. Keith, M.A. Al-Laham, C.Y. Peng, A. Nanayakkara, M. Challacombe, P.M. W. Gill, B. Johnson, M. Chen, W. Wong, J.L. Andres, C. Gonzalez, M. Head-Gordon, E.S. Replogle, and J.A. Pople, Gaussian 98, Revision A.9; Gaussian Inc.: Pittsburgh, PA, 1998.

[5] R. Rathore, S.V. Lindeman, A.S. Kumar, J.K. Kochi, J. Am. Chem. 120 (1998) 6931.

[6] T. Nishiumi, Y. Nomura, Y. Chimoto, M. Higuchi, K. Yamamoto, J. Phys. Chem. B 108 (2004) 7992.

[7] W.T. Borden, E.R. Davidson, J. Am. Chem. Soc. 99 (1977) 4587.

General Conclusion

In this thesis, the author has studied the properties of organic multi-spin systems by both experimental and theoretical approaches. The new findings in this thesis are summarized as follows.

In Chapter 1, the author studied the redox-switching of tetraarylethylene having two *tert*-butylnitroxide, 1,2-bis[4-(*N*-*tert*-butylaminoxyl)phenyl]-1,2-bis[4-{*N*,*N*-bis(4-methoxyphenyl)amino}phenyl]ethylene, which was successfully synthesized through the McMurry coupling reaction with a low-valent titanium reagent where the separation of *cis*- and *trans*-isomers has been met with failure so far. The magnetic susceptibility measurement revealed that this neutral diradical in the solid state showed antiferromagnetic interaction between radical spins. It was found that the cyclic voltammogram of the diradical showed two resolved one-electron transfer redox waves ascribed to the core tetraphenylethylene moiety and the successive quasi-two-electron transfer corresponding to the two substituted nitroxide moieties. Moreover, it was confirmed by the ESR measurement in frozen solution that the neutral diradical showed the fine-structured spectrum characteristic of the spin triplet species, whereas that the diradical treated with the oxidizing agent the typical anisotropic hyperfine-structured spectrum for the mononitroxide radical, indicating that the intramolecular magnetic interaction changes dramatically. The reversibility was clearly shown from the fact that the ESR spectrum for the neutral diradical was recovered with a chemical reduction,

and the absorption spectrum was spectroelectrochemically reversible for several cycles. These results strongly indicated that the redox-switching of through-bond magnetic interaction of the diradical was successfully achieved.

In Chapter 2, compared with the *para*-nitroxyl-substituted compound in Chapter 1, the tetraarylethylene bearing two *meta*-nitroxyl groups, 1,2-bis[3-(*N*-*tert*-butyl aminoxyl)phenyl]-1,2-bis[4-{*N*,*N*-bis(4-methoxyphenyl)amino}phenyl]ethylene, was studied. This *mata*-nitroxyl-substituted diradical was prepared by the same synthetic method of *para*-nitroxyl-substituted diradical, and the *cis*- and *trans*-mixtures was successfully separated by column chromatography in contrast with the failure of separation in *para*-nitroxyl-substituted diradical. The main product was supposed to be *trans*-isomer by the ESR spectrum in frozen solution. Although the cyclic voltammetry of *meta*-nitroxyl-substituted diradical showed the core tetraphenylethylene moiety has the lower oxidation potential than the substituted nitroxide moiety, the first redox wave ascribed to the tetraarylethylene moiety was unresolved, on the contrary to the observation of two distinct one-electron redox waves in the *para*-nitroxyl-substituted diradical. It was demonstrated by the ESR measurement in frozen solution that the *meta*-nitroxyl-substituted diradical of the neutral state showed the fine-structured spectrum characteristic of the spin triplet species, and that the oxidized one showed the anisotropic hyperfine-structured spectrum typical of the randomly oriented mononitroxide radical, also indicating the drastic change of intramolecular magnetic interaction like the *para*-nitroxyl-substituted compound.

In Chapter 3, the author theoretically investigated the electronic structures of tetraphenylethylene bearing two nitroxyl groups in Chapters 1 and 2. The hybrid Hartree–Fock (HF)/density functional theory (DFT) calculations were carried out for the simplified models of 1,2-bis[*x*-(*N*-*tert*-butylaminoxyl)phenyl]-1,2-bis[4-{*N*,*N*-bis(4-methoxyphenyl)amino}phenyl]ethylene (x = 3 or 4). It was indicated that the change from neutral to dicationic state induces not only the change of molecular structure but

also the intramolecular magnetic interaction for the *para*-nitroxyl substituted tetraphenylethylene and that the electronic structures are different due to the substitution patterns of nitroxyl groups, i.e., the π-conjugated system is more perturbed by *para*-substitution of the nitroxide group than by *meta*-substitution.

In Chapter 4, the syntheses and the electrochemical and the magnetic properties of triphenylamine derivatives with two or three nitronyl nitroxide radicals, i.e., the triradical, tris[4-(1-oxyl-3-oxide-4,4,5,5-tetramethylimidazolin-2-yl)phenyl]amine, and the diradical, *N*,*N*-bis[4-(1-oxyl-3-oxide-4,4,5,5-tetramethylimidazolin-2-yl)phenyl]-4-methoxyphenylamine were investigated. The magnetic susceptibility analyses revealed that each neutral tri- and di-radical in solid state showed weak antiferromagnetic interaction. Unfortunately, the expected high-spin states derived from the cationic species of the above tri- and di-radical were not observed by the ESR spectroscopy since the nitronyl nitroxide moieties had the lower oxidation potentials than the core triphenylamine moieties even in the case of electron-donating methoxy-substitution. The valuable findings were, however, obtained on the electrochemical properties of nitronyl nitroxide-fused triphenylamine systems.

In Chapter 5, the synthesis and the electronic properties of *p*-phenylenediamine having two nitroxyl groups, *N*,*N*'-bis[3-*tert*-butyl-5-(*N*-*tert*-butyl-*N*-oxylamino)phenyl]-*N*,*N*'-dimethyl-*p*-phenylenediamine, were studied from the experimental viewpoint. It was found by cyclic voltammetry that the first oxidation potential was ascribed to the one-electron transfer of *p*-phenylenediamine moiety in comparison with the reference compounds. The cationic triradical generated by the oxidation of *p*-phenylenediamine-based diradical showed the inter valence charge transfer (IVCT) band, and was found to be classified into Class II mixed-valence system by the analysis of IVCT band. Furthermore, the quartet state of the cationic triradical was observed in frozen solution by the continuous wave and the pulsed ESR methods. Therefore, the ferromagnetic spin alignment mediated by the mixed-valence state, in which the

localized spins on nitroxide moiety and the delocalized spin on *p*-phenylenediamine moiety coexist, was experimentally demonstrated in the present cationic triradical for the first time.

In Chapter 6, the author theoretically investigated the models of *p*-phenylenediamine with *tert*-butylnitroxide radicals, *N,N'*-bis[3-*tert*-butyl-5-(*N*-*tert*-butyl-*N*-oxylamino) phenyl]-*N,N'*-dimethyl-*p*-phenylenediamine, and *p*-phenylenediamine with nitronyl nitroxide radicals, *N,N'*-bis[4-(1-oxyl-3-oxide-4,4,5,5-tetramethylimidazolin-2-yl) phenyl]-*N,N'*-dimethyl-*p*-phenylenediamine, on the basis of the hybrid HF/DFT method. It was predicted that both of the cationic *p*-phenylenediamine derivatives with radical substituents had the ground quartet states while the singlet and triplet states were nearly degenerated for those in the neutral state. Moreover, their SOMO patterns had the *non-disjoint* nature, causing the ferromagnetic spin alignments. Considering the substitution effect of the nitronyl nitroxide radical, the SOMO on the central *p*-phenylenediamine moiety was more delocalized to intrude into the outside aryl groups, increasing the torsional angle along the inner N–C bond of the central *p*-phenylenediamine moiety. Therefore, it was expected that the electronic coupling between the aminic redox sites would be suppressed due to the weakened orbital interaction between the p-orbital of aminic nitrogen atom and the π-orbital of p-phenylene in the case of nitronyl nitroxide substitution.

Concluding this thesis, the author has studied the electronic properties of organic multi-spin systems from both experimental and theoretical points of view. In this course of study, the redox-switchable spin systems and the high-spin mixed-valent systems have been demonstrated. These organic molecular systems could also be considered as novel dynamic multi-spin systems, whereas the traditional high-spin systems are static. The author hopes that the present study contributes to the development of science and technology in organic spin systems.

List of Publications

Chapter 1

Tetraarylethylene Having Two Nitroxide Groups: Redox-Switching of Through-Bond Magnetic Interaction by Conformation Change.

A. Ito, Y. Nakano, T. Kato, K. Tanaka.

Chem. Commun. (2005) 403-405.

Chapter 2

Redox-Switching of Intramolecular Magnetic Interaction: Tetraarylethylene Bearing Two *meta*-Nitroxyl Groups.

Y. Nakano, A. Ito, K. Tanaka.

J. Org. Chem., to be submitted.

Chapter 3

Intramolecular Magnetic Interaction Controlled by Redox Reaction of Tetraphenylethylene-Based Spin System.

Y. Nakano, A. Ito, K. Tanaka.

Synth. Met., in press.

Chapter 4

Synthesis and Intramolecular Magnetic Interaction of Triphenylamine Derivatives with Nitronyl Nitroxide Radicals.

Y. Nakano, T. Yagyu, T. Hirayama, A. Ito, K. Tanaka.

Polyhedron, in press.

Chapter 5

Spin Alignment Mediated by Mixed-Valence State: Triradical Cation of *p*-Phenylenediamine Having Two Nitroxide Radicals.

A. Ito, Y. Nakano, M. Urabe, T. Kato, K. Tanaka.

Angew. Chem. Int. Ed. Engl., to be submitted.

Chapter 6

Theoretical Study on Radical Substituent's Effect of *p*-Phenylenediamine-Based Spin System.

Y. Nakano, A. Ito, K. Tanaka.

Chem. Phys. Lett., to be submitted.

The following paper is not included in this thesis:

Synthesis, Structures, and Magnetic Properties of Cu(II) and Zn(II) Coordination Complexes Containing Nitroxide Radicals as Chelating Ligands.

A. Ito, Y. Nakano, M. Urabe, K. Tanaka, M. Shiro.

Eur. J. Inorg. Chem., to be submitted.